SOL-EMULSION-GEL PREPARATION AND PHYSICAL CHARACTERIZATION FOR ZrO_2 AND V/ZrO_2

TANAKORN RATANA

A THESIS SUBMITTED IN PARTIAL FULFILLMENT

OF THE REQUIREMENTS FOR

THE DEGREE OF MASTER OF SCIENCE

(APPLIED ANALYTICAL AND INORGANIC CHEMISTRY)

FACULTY OF GRADUATE STUDIES

MAHIDOL UNIVERSITY

2000

ISBN 974-664-318-5

Thesis
Entitled

SOL-EMULSION-GEL PREPARATION AND PHYSICAL CHARACTERIZATION FOR ZrO_2 AND V/ZrO_2

Tanakorn Ratana
.....
Mr. Tanakorn Ratana
Candidate

Waret Veerasai
.....
Lect. Waret Veerasai, Dr.rer.net.
Major-advisor

Ladda Pdungsap.
.....
Asst. Prof. Laddawan Pdungsap,Ph.D.
Co-advisor

.....
Prof. Liangchai Limlomwongse, Ph. D.
Dean
Faculty of Graduate Studies

Ladda Pdungsap.
.....
Asst. Prof. Laddawan Pdungsap, Ph.D.
Chairman
Master of Science Program in
Applied Analytical and
Inorganic Chemistry
Faculty of Science

Thesis
Entitled

SOL-EMULSION-GEL PREPARATION AND PHYSICAL CHARACTERIZATION FOR ZrO_2 AND V/ZrO_2

was submitted to the Faculty of Graduate Studies, Mahidol University
for the degree of Mater of Science
(Applied Analytical and Inorganic Chemistry)

on
May 29, 2000

Tanakorn Ratana
.....
Mr. Tanakorn Ratana
Canadidate

Waret Veerasai
.....
Lect. Waret Veerasai, Dr.rer.net.
Chairman

.....
Asst. Prof.Laddawan Pdungsap, Ph.D.
Member

Chastbongkoch Sriyawach
.....
Mrs. Chastbongkoch Sriyawach, M. Sc.
Menber

.....
Prof. Liangchai Limlomwongse, Ph.D
Dean
Faculty of Graduate Studies
Mahidol University

.....
Prof. Amaret Bhumiratana, Ph.D.
Dean
Faculty of Science
Mahidol University

ACKNOWLEDGEMENTS

I would like to express my sincere thanks to my advisor, Dr. Waret Veerasai for his valuable advice, interest and encouragement. I wish to thank Asst. Prof. Dr. Laddawan Pdungsap for their comments and suggestions. I wish to thank Mrs. Chastbongkoch Siyawach for her valuable guidance and Thai zircon sand providence.

My thanks are also extended to the Applied Analytical and Inorganic Chemistry graduate students and all staffs of the Department of Chemistry and Central Instrument Faculty (CIF), Faculty of Science, Mahidol University for their help during my research works. I am greatly indebted to the member of the Chemistry and Physics divisions, OAEP for their facilities, especially the XRD data. A grateful acknowledgement is made to the Institute for the Promotion of Teaching Science and Technology for the financial support under the Development and the Promotion for Science and Technology talent (DPST) project. I truly thank Miss Namfon Tongtavee for her great assistance and wonderful friendship.

Finally, a special word of thanks is expressed to my family, especially my parent for their care, love, understanding and endless encouragement.

Tanakorn Ratana

4036374 SCAI/M : MAJOR : APPLIED ANALYTICAL AND INORGANIC CHEMISTRY; M.Sc. (APPLIED ANALYTICAL AND INORGANIC CHEMISTRY)
KEY WORDS : SOL-EMULSION-GEL/ ZIRCONIA/ VANADIUM/ THAI ZIRCON SAND

TANAKORN RATANA: SOL-EMULSION-GEL PREPARATION AND PHYSICAL CHARACTERIZATION FOR ZrO_2 AND V/ZrO_2. THESIS ADVISORS: WARET VEERASAI Dr.rer.nat., LADDAWAN PDUNGSAP Ph.D., 117 p. ISBN 974-664-318-5

The ultrafine zirconia powders were prepared from Thai zircon sand by using a sol-emulsion-gel (SEG) method. This SEG method is a combination of the sol-gel and emulsion processes. Zirconyl nitrate prepared from Thai zircon sand was a precursor in this process. The powder characterization was investigated by using X-ray diffraction (XRD), Differential Scanning Calorimetry (DSC), Fourier Transform Infrared spectrophotometer (FT-IR) and Electron Microscopic techniques (TEM and SEM). The as- prepared zirconia powders are amorphous, then crystallize into the metastable tetragonal structure at higher temperature. The monoclinic state appears completely at 1350 °C. The crystal size obtained by means of XRD increased corresponding with the higher calcine temperatures. The morphology of the aggregate particles were composed of nanometre-size crystals in loose form. The influence of an ultrasonic agitator demonstrates less formation of agglomerate, but it induces the thermal instability of zirconia powder.

Zirconia-supported vanadium oxide was successfully obtained also by the SEG method. The various vanadium contents and calcine temperatures were investigated. Phase transition of zirconia support shifts to lower temperature due to the effect of the interaction between vanadium and zirconia. The surface morphology of V/ZrO_2 exhibits a needle form of V_2O_5 crystals at high calcine temperature. This result was confirmed by infrared spectra when vanadium content exceeds monolayer on zirconia surface.

4036374 SCAI/M : สาขาวิชา : เคมีวิเคราะห์และเคมีอินทรีย์ประยุกต์;
วท.ม. (เคมีวิเคราะห์และเคมีอินทรีย์ประยุกต์)

ธนากร รัตนะ : การเตรียมและศึกษาคุณสมบัติทางฟิสิกส์ของเซอร์โคเนียและวาเนเดียมเปื่อนในเซอร์โคเนีย (SOL-EMULSION-GEL PREPARATION AND PHYSICAL CHARACTERIZATION FOR ZrO_2 AND V/ZrO_2). คณะกรรมการควบคุมวิทยานิพนธ์ : วเรศ วีระสัย Dr.rer.nat., ลัดดาวัลย์ ผดุงทรัพย์ Ph.D., 117 หน้า. ISBN 974-664-318-5

ในงานวิจัยชิ้นนี้ได้ทำการเตรียมผงเซอร์โคเนีย ด้วยวิธี ซอลอิมัลชันเจล โดยมีเซอร์โคนิลไนเตรด ที่เตรียมมาจากแร่เซอร์คอนที่พบในประเทศไทยเป็นสารตั้งต้น สมบัติทางฟิสิกส์ของสารที่เตรียมได้ถูกนำมาศึกษาสมบัติต่างๆ คือ สมบัติการเลี้ยวเบนรังสีเอกซ์ (XRD), สมบัติทางความร้อน (DSC), สมบัติการดูดกลืนรังสีอินฟราเรด (FTIR) และ รูปร่างด้วยกล้องจุลทรรศน์อิเล็กตรอน (Electron Microscopic techniques) ผลการศึกษาแสดงให้เห็นว่า อนุภาคของเซอร์โคเนียที่เตรียมได้เป็นรูปอสัญฐานที่อุณหภูมิห้อง แต่เมื่อนำมาเผาที่อุณหภูมิสูง พบว่าจะเปลี่ยนเป็น รูปทรงเตตระโกนอล และ โมโนคลินิกตามลำดับ ขนาดของผลึกสามารถวัดได้จากวิธีการเลี้ยวเบนรังสีเอกซ์ พบว่าผลึกมีขนาดใหญ่ขึ้นเมื่ออุณหภูมิที่ใช้ในการเผาสูงขึ้น การใช้อัลตราซาวด์ ซึ่งเป็นวิธีที่จะช่วยลดการรวมตัวกันของอนุภาค แต่อย่างไรก็ตามมีผลทำให้ลดความเสถียรของเซอร์โคเนียลงด้วย

ได้ประสบความสำเร็จในการเจือวาเนเดียมบนเซอร์โคเนีย โดยการเตรียมขึ้นด้วยวิธีซอลอิมัลชันเจลเช่นกัน ศึกษาผลของการเผาที่อุณหภูมิต่างๆและปริมาณวาเนเดียมที่เจือลงไป พบว่ามีการเปลี่ยนเฟสเร็วขึ้นเมื่อปริมาณวาเนเดียมเพิ่มมากขึ้น น่าจะเป็นผลมาจากอันตรกิริยาระหว่างวาเนเดียกับเซอร์โคเนีย นอกจากนี้ยังพบว่าเมื่อเพิ่มอุณหภูมิในการเผาให้สูงขึ้นจะส่งผลให้วาเนเดียละลายในเซอร์โคเนียได้น้อยลงอีกด้วย

LIST OF CONTENTS

Page

LIST OF TABLES

LIST OF FIGTURES

LIST OF FIGTURES (cont.)

LIST OF FIGTURES (cont.)

LIST OF FIGTURES (cont.)

LIST OF ABBREVIATIONS

Å	Angstrom unit
°C	degree Celsius
d_{hkl}	The lattice spacing for plane hkl or d-specing
ν	Stretching mode
δ	deformation or bending mode
ρ_r	rocking mode
π	out of plane (OOP) mode
as	asymmetric
s	symmetic
b	broad
d	doublet
m	medium
s	strong
sh	shoulder
sp	sharp
w	weak
SEM	Scanning Electron Microscope
TEM	Transmission Electron Microscope
DSC	Differential Scanning Calorimeter
XRD	X-ray powder diffraction
FT-IR	Fourier Transform Infrared spectrometer
SEG	Sol-Emulsion-Gel

LIST OF ABBREVIATIONS (cont.)

V/ZrO_2	Vanadium doped zirconia support
ZCS	Zirconyl chloride synthesis
ZNS	Zirconyl nitrate synthesis
ZHS	Zirconyl hydroxide synthesis
su-process	magnetic stirrer and ultrasonic agitator processes
u-process	ultrasonic agitator
wt %	weigh percent
$t\text{-}ZrO_2$	tetragonal zirconia phase
$m\text{-}ZrO_2$	monoclinic zirconia phase
nm	nanometer
μm	micrometer
mm	millimeter
W/O	water in oil
O/W	oil in water
O/W/O	oil in water in oil
HLB	Hydrophilic-Lipophilic Balance value
JCPDS	X-ray powder data file of Joint Committee on Powder Diffraction Standards

CHAPTER I

INTRODUCTION

Zirconium oxide (ZrO_2) or zirconia has been widely considered as one of the important materials with a wide range of applications [1, 2] as composite supported materials for catalysts, pigments, glasses, refractories, piezoelectric ceramics and as solid electrolyte in fuel cell or oxygen sensor. These applications of zirconia were summarized in Table 1.1. However, the properties of zirconia related materials depend to a great extent on the size, shape and chemical composition of initial zirconia powder [3]. These important properties are controlled by several preparation processes [4]. In this work, we attempt to develop the preparation processes of ultrafine zirconia powder from Thai zircon sand and to compare their properties with others commercial available products.

According to the exporting data from the department of mineral resources in Thailand [5], Thai zircon sand (is known as a source of zirconia) was exported from Thailand as raw zircon mineral without refinery. The value-added projects to refine and prepare zirconia powder from zircon sand had been explored by many research groups [6-8], especially at the Office of Atomic Energy for Peace (OAEP)[9]. Under the collaboration between AAICP of Mahidol University and the chemistry division of OAEP, this thesis had been preformed to modify the synthesis pathways for zirconia powder from Thai zircon sand by using the sol-emulsion-gel technique [10]. This SEG

method also attempt for synthesizing vanadium doped zirconia (V/ZrO_2) [11-15]. The particle sizes, morphology, phase identification and phase transition of the zirconyl products and zirconia has been intensively investigated in this thesis.

Table 1.1 The major applications of zirconia in various fields [1,2]

Type of applications	Uses and benefits
Electroceramic	Oxygen meter, fuel cells
Ceramic colors	Inexpensive and low toxicity colors and glazes
Filter	The low absorption of visible and near UV wavebands plus high refractivity make certain zirconium oxide beneficial addition to optical glass
Gemstones	Zirconia gemstones, refract like diamond
Thermal barrier coating	To improve aircraft fuel consumption
Refractories	Resist high temperature
Bioceramic	Bioinert ceramic
Catalysis	Catalytic systems for the control and support of several catalyst, especially at high temperature, car engine exhaust emission

1.1 Historical Reviews on Zirconium, Zirconium Minerals and Zirconia

Zirconium minerals have been known since ancient time, but their older names jargon called jacinth and hyacinth. However their were not known that contained a distinctive element until 1789 when Martin Heinrich Klaproth, a German chemist, while analyzing the precious stone jargon, found it contained an earth which he could not identify and which he later called *Zirkonerde.* (from the Arabic 'zargon' meaning gold-coloured) [1,16]

For zirconia, Hussak first discovered the baddeleyite (ZrO_2, monoclinic phase) in 1892, and then he was followed by attempts at its exploitation for refractory application [17]. In 1929, Ruff and Ebert used X-ray diffraction (XRD) to establish the monoclinic symmetry of zirconia at room temperature. Besides, they also studied the monoclinic-tetragonal transformation at the temperature higher than 1000°C by using high temperature XRD. At high temperature XRD above 2370°C, Smith and Cline (1962) found the expected cubic phase of zirconia. The details of tetragonal phase (McCulloough, 1959) and monoclinc phase (Teufer, 1962) structure were studied using single crystal diffraction method [17]. In the decade ago Magnesium Elektron Limited (MEL) became the first company to exploit commercially zirconium, which starting to introduce their oxide for ceramic colors. Research undertaken at MEL's Clifton Junction laboratories, soon discovered a wide range of other applications [1]. Preparation of zirconia powder was developed a long time, summarized in Table 1.2.

Table 1.2 The history of zirconia

	Event	Reference
Ancient	Zircon has been used as a gemstone	[1,16]
1789	Zirconia was firstly identified by Martin Heinrich Klaproth	[1,16]
1892	Discovery of ZrO_2 mineral in monoclinic phase, baddeleyite	[17]
1929s	Polymorphic of zirconia was investigated and crystal zirconia structure was known	[18-30]
1959s	Stabilization studies of zirconia structure	[31]
1965s	Metastable tetragonal was investigated	[18-22]
1965s	Zircon mineral was produced to zirconyl compounds	[6-8]
1969s	Developed preparation of zirconyl compound and zirconia from zircon sand mineral	[6-8]
About 1970	MEL company produced commercially many zirconium compounds	[17]
1981s	The zirconia as a biomaterial was studied	[32]
1985s	Hydrothermal preparation of ultrafine ZrO_2 powder	[33-34]

Table 1.2 (continued) the history of zirconia

	Event	Reference
1985s	Micronized zirconia was prepared by precipitation for industry	[35]
1990 s	The emulsion method was used for preparing of ultrafine zirconia	[10, 36-40]
1995s	Synthesis of zirconia powder by spray pyrolysis	[41-42]
1996s	Used of the sol-gel preparation of zirconia	[43-46]

1.2 Zircon Mineral

Zircon, $ZrSiO_4$ is tetragonal in crystallization, a_o = 6.614, c_o = 6.015 Å [47]. The structure of zircon contains of independent SiO_4 tetrahedral and distorted ZrO_8 cubes four molecules per unit cell (Figure 1.1a). They often occur as well-formed crystals that commonly are square prisms terminated by a low pyramid. (Figure 1.1b) Because of its chemical and physical stability, zircon resists weathering and accumulation in residual deposits in beach and river sands [48-52].

Zircon sand is found and mined in number of countries including Australia, Brazil, India, South Africa and USA [3, 4]. In Thailand, zircon is commonly found in the same areas as tin mines in Puket, Pungnga, Chumphon and also found at the beach of Chun Gadi Bay in Prachuap Khiri Khan [5].

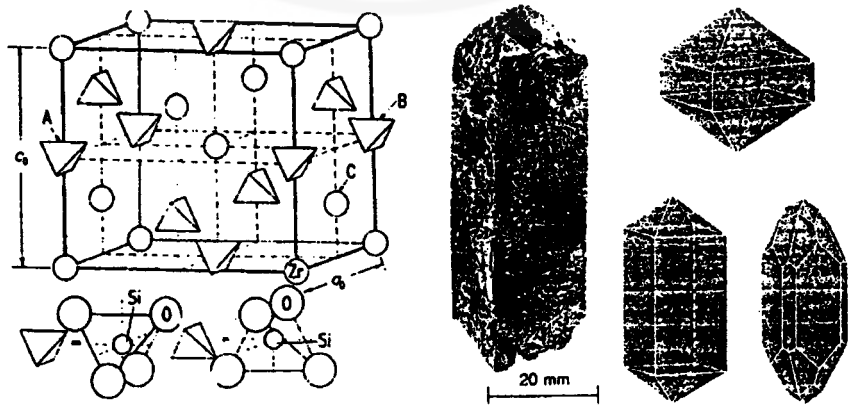

(a) (b)

Figure 1.1 (a) Structure of zircon (b) zircon crystal [50].

1.3 Reviews on Zirconia Powder Preparations

The particle size property of advance ceramic powder is one of the most important, which depends on method of preparation. The smaller powders lead to the lower sintering temperatures and finer grain size distribution [10]. Furthermore the material obtained from sintering small particle affect smaller residual pores, grain sizes and higher density [3]. In case of zirconia powder, many methods have been developed for preparation of small zirconia particles. However, advantage and disadvantage of these methods are reviewed in this section.

1.3.1. Alkaline digestion and heat treatment of zircon sand mineral

Zircon mineral was digested by base and washed by hot water to form frit. Dissolution of frit in acid to zirconyl solution and filtration out of undissolved impurity. Zirconyl hydroxide was precipitated by base then followed by heat treatment at high temperature [6-8].

1.3.2 Thermal decomposition synthesis

Zirconyl salts such as the hydroxide, sulfate, oxychloride, hydroxide, arsenate, acetate, oxalate and nitrate can be thermally decomposed to form zirconium oxide powder. Zirconia obtained as white solid and insoluble in water [53].

1.3.3 Precipitation synthesis

The precipitation process is widely used in many literatures [35,54-55]. Zirconyl salts in aqueous solution were precipitated by changing pH using aqueous ammonium or ammonia gas. Then the precipitated product was separated from the solution by filtration and ignition to form zirconia powder. Furthermore, this technique was modified by using urea as a source of ammonia gas.

1.3.4 Hydrothermal synthesis

Ultrafine powder of single-phase monoclinic ZrO_2 was prepared by hydrothermal treatment of amorphous hydrated zirconia with 8 wt% KF solution under 100 Mpa at 200° to 500°C for 24 hr. The process yielded well-crystallized particles 16 nm and 22 nm in size at 200° and 500°C, respectively [33-34].

1.3.5 Spray pyrolysis

The spray pyrolysis method for zirconia was developed in the 1990 by Shi-Chang Zhang et al. [41]. Zirconyl chloride and zirconyl hydroxychoride were excellent zirconyl salt for solid zirconia particle synthesis and the solid spherical particles were obtained by this method.

1.3.6 Sol-gel techniqus

Ultrafine zirconia particles have been prepared via a sol-gel method. The starting materials for this process are usually zirconium isopropoxide ($Zr(i\text{-}OC_3H_7)_4$), zirconium propoxide ($Zr(n\text{-}OC_2H_7)_4$) and zirconium butoxide ($Zr(n\text{-}OC_4H_9)_4$) [43-44]. However, alkoxide precursor is complicated and difficulty controlled. Furthermore, zirconium alkoxides are generally derived from $ZrCl_4$ and must be kept away from water. Recently, Yugun Xie et al. [45] used zirconyl chloride, $ZrOCl_2$ and ethylene oxide, C_2H_4O as precursors instead of zirconyl alkoxide.

1.3.7 Emulsion synthesis

Recently, The zirconia microparticles and spherical morphology are successfully prepared by precipitation process, which caused by the contact between two emulsion solutions [39]. S. D. Ramamurthi et al. [10] prepared the ultrafine zirconia powder by using $ZrO(NO_3)_2.nH_2O$ as precursor, and Tween 80 as the surfactant in xylene. This method was called sol-emulsion-gel (SEG). The SEG method was adapted to prepare Yttrium doped tetragonal zirconia (YSZ) powder [38]. Furthermore, T. Kannai et al. [30] studied the method to prepared YSZ by SEG technique by various types of surfactant and organic solvent.

Summary for typical protocols for zirconium synthesis.

Alkaline digestion and heat treatment of zircon sand mineral

$$\text{Zircon sand} + \text{NaOH} \xrightarrow{\text{digestion}} ZrO^{2+}(sol^{n}) \xrightarrow{\text{precipitate}} Zr(OH)_4 \xrightarrow{\text{calcination}} ZrO_2$$

Thermal decomposition synthesis

$$ZrOX_2 \xrightarrow{\text{calcination}} ZrO_2$$

Precipitation synthesis

$$ZrOX_2 \xrightarrow{\text{precipitation}} Zr(OH)_4 \xrightarrow{\text{calcination}} ZrO_2$$

Hydrothermal synthesis

$$ZrOX_2 \xrightarrow{\text{growth control agent}} Zr(OH)_x \xrightarrow{\text{hydrothermal (added T\&P)}} ZrO_2 \text{ (crystalline fine)}$$

Spray pyrolysis

$$ZrOX_2 \xrightarrow{\text{spray pyrolysis}} ZrO_2$$

Sol-gel techniques

$$Zr(OR)_4 + R'OH \xrightarrow{\text{hydrolysis}} ZrO^{2+} \xrightarrow{\text{gelation}} ZrO_2 \text{ (gel)} \xrightarrow{\text{calcination}} ZrO_2$$

Emulsion synthesis

$$ZrOX_2 \text{ (aq)} + \text{Organic phase} \xrightarrow{\text{emulsification}} (ZrO^{2+})_n \text{ (colloid)} \xrightarrow{\text{distillation \& reflux}}$$

$$(ZrO)_n \text{ (gel)} \xrightarrow{\text{calcination}} ZrO_2$$

The zircon mineral digestion method is one of the oldest for synthesis zirconia powder. This method consists of the precipitated and thermal decomposition processes. High impurity in zirconia mineral is treated primarily in the filtration steps. The thermal decomposition and precipitation of zirconyl salts are simple techniques for the preparation of zirconia. Both are low costs, but thermal decomposition process gives the particle size correspond with size of starting materials. The precipitation technique is possible to yield particle size about 20-100 nm, but some form large hard agglomerate, which result in longer sintering time and higher sintering temperature. The hydrothermal synthesis and spray pyrolysis methods are the aqueous chemical routes of preparation of nano-crystalline zirconia or nano-particles. However, these methods are high-cost in the synthesis.

The sol-gel method can be controlled and modified in order to obtain a specific material, with better characteristics such as higher surface area, homogeneity and particle size distribution. However, a costly precursor is required. Zirconium alkoxide is expensive because it is generally derived from $ZrCl_4$ and must be kept away from water. Therefore, to overcome these problems, Bowen and co-workers [38] used emulsion method with zirconium salts as precursor for the preparation of ultrafine, unagglomerated and soft powders.

Sol-emulsion-gel (SEG) method [10], which is a combination of sol-gel and emulsion methods, is used for the preparation of ZrO_2 powders. Water droplets containing zirconium ions are suspended and stabilized in an organic nonpolar solvent by addition an appropriate surfactant. The emulsion droplets are gelled by ammonia

gas. These gel droplets are stabilized by elimination of water during heterogeneous distillation. The simplified reaction can be represented as

$$ZrOX_2 + H_2O + 2NH_3 \longrightarrow Zr(OH)_2 + 2NH_4X \longrightarrow ZrO_2$$

In the case of zirconia supported catalysts, the major requirements properties are high interfacial contact area and homogenous of material [57]. Impregnation is the most of common method for V/ZrO_2 preparation [58-59]. However, impregnation results in a relatively low interfacial contact area between the active catalyst and the zirconia support. However, a higher degree of interfacial contact has been generally achieved by co-precipitation or sol-gel methods [57]. The SEG method for ZrO_2 and V/ZrO_2 synthesis is an interesting for investigation in this thesis by two main reasons, firstly as a promising low cost techniques for the value added our Thai zircon and secondly as an alternative pathway for modification of the zirconia products.

1.4 Phase Diagram of Zirconia

A least three polymorphic crystal forms of zirconia [60] are well characterized. The phase transition diagram of ZrO_2 shows its polymorphic phase transition in Figure 1.2. In low temperature regions, a monoclinic crystal is common to the mineral baddeleyite. This monoclinic structure is transformed reversibly to a tetragonal modification at approximately 1170 °C and then to cubic structure at 2300 °C. The cubic crystal is stable up to its melting point at 2715 °C.

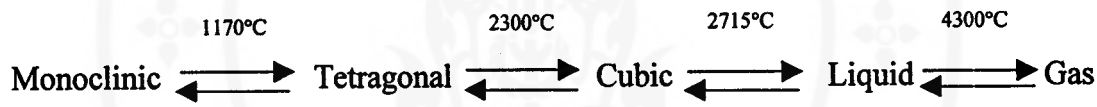

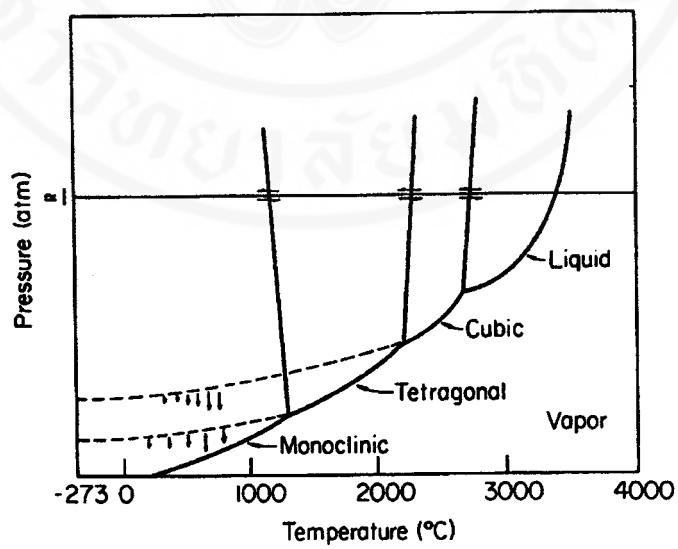

Figure 1.2 Phase diagram for ZrO_2 [60]

The existence of metastable cubic and metastable tetragonal zirconia at low temperature has been reported by several investigators [18-22]. The polymorphic transformation of ZrO_2 may result in cracks in the final products. This property is undesirable phenomena for applications as refractory material. To prevent this polymorphic transform, therefore ZrO_2 is remelted with an electric arc, or small amounts of CaO, Y_2O_3 or MgO are added to the ZrO_2 to promote the greater stability of this cubic or tetragonal form over the entire temperature range. The modified ZrO_2 is known as Partially Stabilized Zirconia (PSZ) [63-63]. According to Figure 1.3, the cubic calcia-stabilized zirconia phase occupies the central range in the diagram and is stable to about 2400°C.

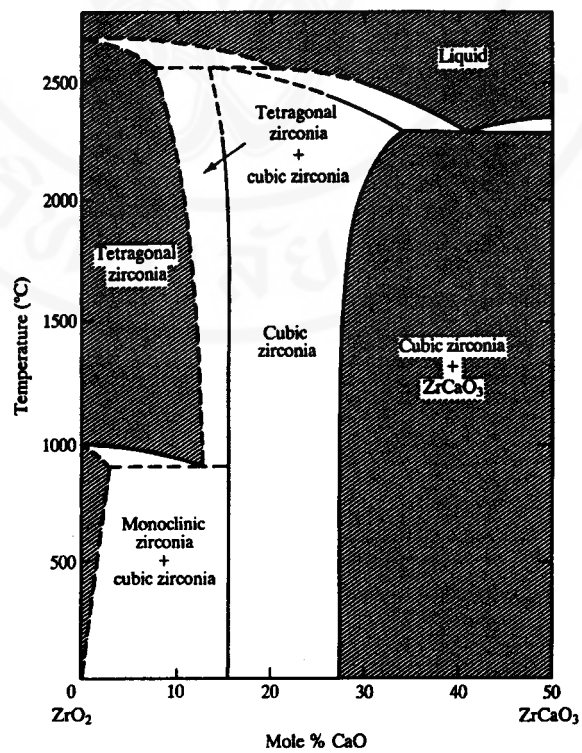

Figure 1.3. Phase diagram for CaO-ZrO_2 system [60]

1.5 Aims and Scope of Thesis

The purpose of this thesis is an attempt to modify the zirconia synthesis partway and to characterize of zirconia and zirconia related products, prepared from Thai zircon sand.

Firstly, to attempt for preparation of zirconyl precursors from Thai zircon sand and compare their properties with others commercial zirconyl compounds.

Secondly, to attempt for preparation of zirconia powder by sol-emulsion-gel (SEG) method from zirconyl compound, prepared from Thai zircon sand. In addition the SEG method was applied to doped vanadium oxide in zirconia support.

The characterization of zirconium mineral samples and the synthesis products, such as crystal size, morphology and phase transition has been investigated by XRD, DSC, FT-IR and EM techniques and interpreted in comparison manners with the properties of existing commercial available compounds.

CHAPTER II

THEORY

2.1 Roles of Particle Size on Material Properties

In general, the average particle sizes in advance materials or ceramic powder range from several tens of angstroms to several microns. A particle is called a "primary particle" if it cannot be subdivided further on any scale of magnification. A primary particle can be either a single crystal or polycrystalline. In the other hand, the particle consists of some subdivisions is called an "aggregate particle" [64]. Many properties of designed materials are influenced not only by size but also by the nature of these primary particles. Therefore, ultrafine particles, which usually, contain submicrometer or nano-particles, are widely investigated to preparation.

The size of particles is the important roles on strength of many ceramic materials. For the smaller particles, the higher adhesion strength among particles was observed [3]. The increase in adhesion strength in fine powder can be understood in terms of the powder's poor flowability.

Likewise, powders, which composed of the smaller particles, the higher surface area, are expected. This property is a requirement for catalysts and other

ceramic materials. According to this property, the total surface area of all cube obtained from breaking up a 1 m^3 cube can be written as [3].

$$S_v = \frac{6}{a}$$

when a is edge length of cubic

The equation assumes particles to be either a perfect cubic or a perfect sphere of equivalent length or dimension. For deviation from spherical or cubic shape, a shape factor is introduced, the value of surface per volume of particle is modified.

$$S_v = \frac{6\alpha}{a}$$

where α is the shape factor

The relation between the specific surface area of a powder and its particle size is obviously shown that the smaller particle size gives the higher specific surface area.

Many advance materials are produced from powder and transformed into solids by compacting or sintering process. The time necessary to produce given fractional shrinkage is proportional to r^3/D, where r is the radius of the particles and D is the diffusion coefficient of solid particle. The decreasing in the particle diameter decreases the required sintering time for threefold. An increase in sintering temperature

decreases the sintering time for a given amount of shrinkage, since the diffusion coefficient increase exponentially according to the relation $D = Ae^{-Ea/RT}$.

This clearly indicates the importance of using smaller fine powders if rapid or low temperature is to be accomplished. The decreasing particle sizes lead to lower sintering temperature. This is reducing costs in production process. Then products, which have smaller residual pores and grain size, obtain after sintering process. Furthermore, the higher density product could be expected as well.

2.2 Sol-Emulsion-Gel (SEG) Method

Although, the sol-gel chemistry has been successfully applied for production of the high quality fine powder with homogeneity [57,66], but this technique is very costly for large-scale preparation of ceramic powder. Zirconium alkoxide precursor is obtained from $ZrCl_4$ via a costly reaction [56].

$$ZrCl_4 + 4ROH + 4NH_3 \longrightarrow Zr(OR)_4 + NH_4Cl$$

To handle metal alkoxide, many precaution are required. Furthermore, zirconium alkoxide is sensitive with water, therefore careful experiment designs are needed. The SEG method has been developed to overcome the disadvantage of sol-gel method [10,38]. This method consists of five major processes, which are sol formation, emulsion and agitator stabilization, gel formation, elimination of unreaction- water and phase inversion.

2.2.1 Sol Formation

Zirconyl nitrate hydrate ($ZrO(NO_3)_2.xH_2O$) was used as a precursor in this work. $ZrO(NO_3)_2.xH_2O$ composes of chains of zirconium atoms which are joined by double bridges of hydroxide ions [67]. The coordination Zr-O is eightfold in shape of a dodecahedron with triangular faces. From the structure, nitrate group may be joined through hydrogen bonds or nitrate coordinate with zirconium atom.

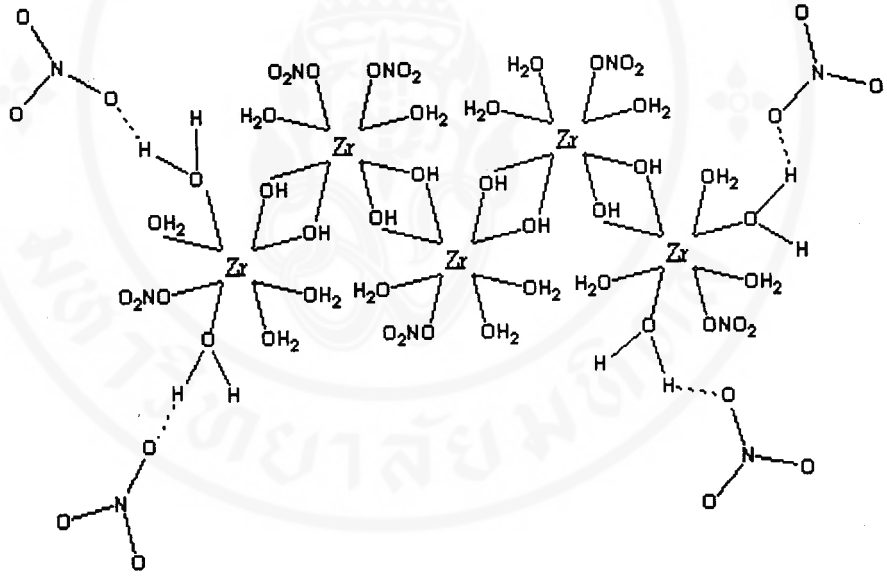

Figure2.1 Model of hydrated zirconium nitrate structure

While hydrated zirconyl nitrate in aqueous solution, form colloid, known as "sol". Furthermore, nitrate group is possibly found as free ion in solution. The stabilization of sol obtained by repulsion force of negative charge.

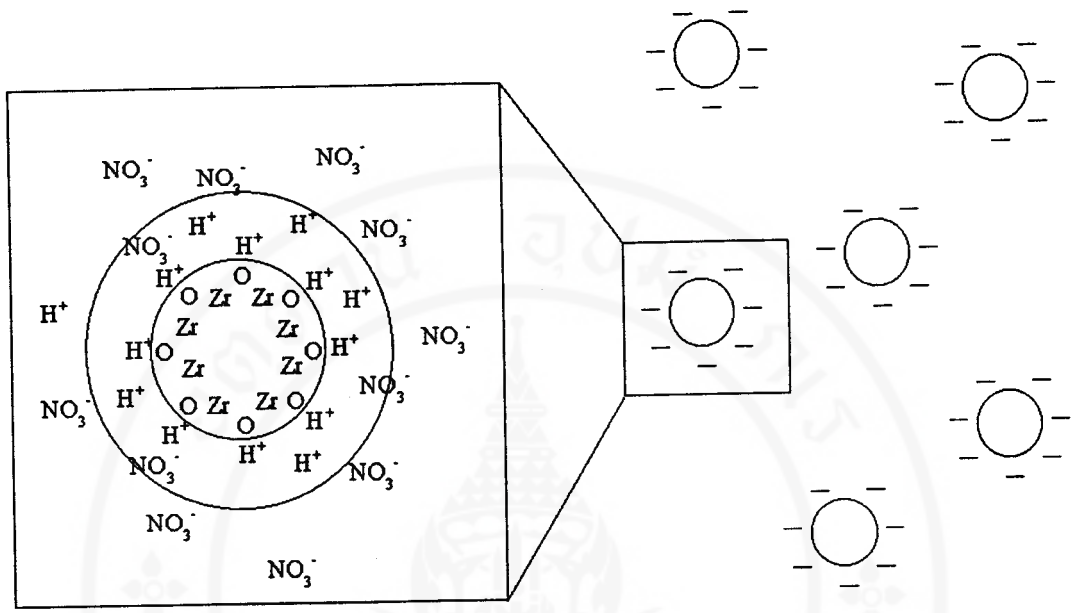

Figure 2.2 The "sol" state for zirconyl nitrate in the solution

2.2.2 Emulsion and Agitator Stabilization

An emulsion in this present work, a colloid state (sol) in aqueous phase is dispersed in the another immisible organic liquid phase (xylene), this colloidal state is stabilized by addition of emulsifying agent. Tween 80 or polyoxyetylene sorbitan mono-oleate is only a non-ionic surfactant that used in this thesis. Non-ionic surfactant is usually classified by "Hydrophilic-Lipophilic Balance" (HLB) value [68-71] which characterizes the interaction energy between aqueous and oil types of phases. The HLB values varies from 0 to 20. The lower HLB value is the more lipophilic liked property and the higher HLB value is the more hydrophilic liked substances. HLB value for Tween 80 is about 15 [71]. It prefers to form a stable oil in water (O/W)

dispersion. Due to small amount of aqueous sol is dispersed in xylene, so water in oil (W/O) is unstable. However, state of oil in water in oil (O/W/O) obtained in solution [70]. To generate well dispersed aqueous droplets in nonaqueous medium and to prevent coalescence effect, the appropriate agitation mechanism and suitable surfactant must be considered. Size and shape of droplet relate many factors such as rate of turbulence (Figure2.3). Furthermore, the ratio of phase volume between oil and water affect shape of droplet formation. (Figure 2.4).

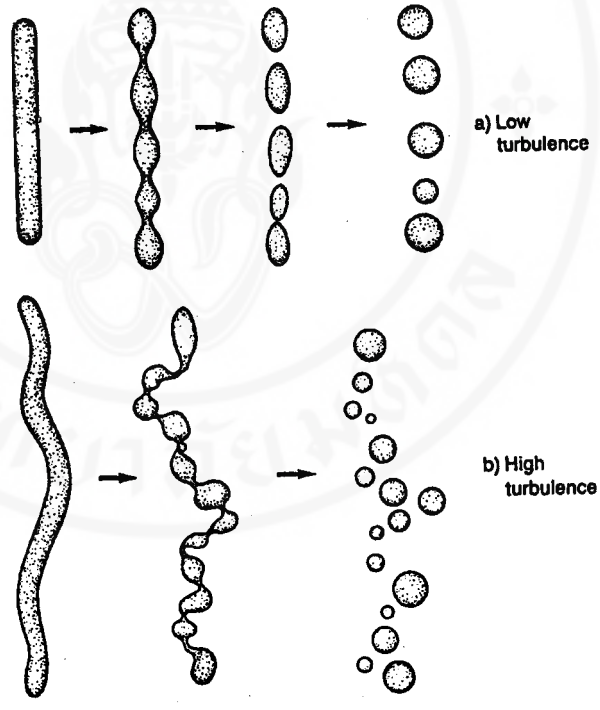

Figure 2.3 The schematic of the break up of a liquid into another immiscible liquid [71]

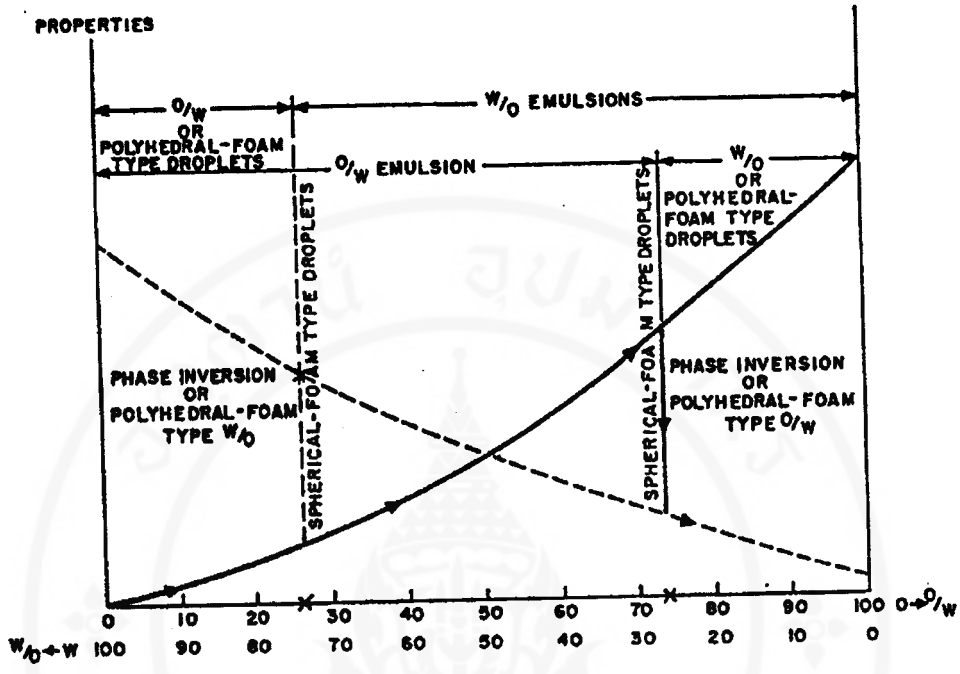

Figure2.4 The relation between phase volume and the droplet or required for emulsion stability [71]

2.2.3 Gel Formation

When ammonia is introduced through aqueous solution, the coordinated water molecules nearby zirconium atom are suspected to lose their protons as in simplified reaction below.

$$Zr)\text{-}^{+}OH_2 + NH_3 \longrightarrow Zr)\text{-}OH + NH_4^{+}$$

The crosslink polymerization is initialized through these hydroxyl groups of $Zr(OH)_4$. This process is known as "gel" formation.

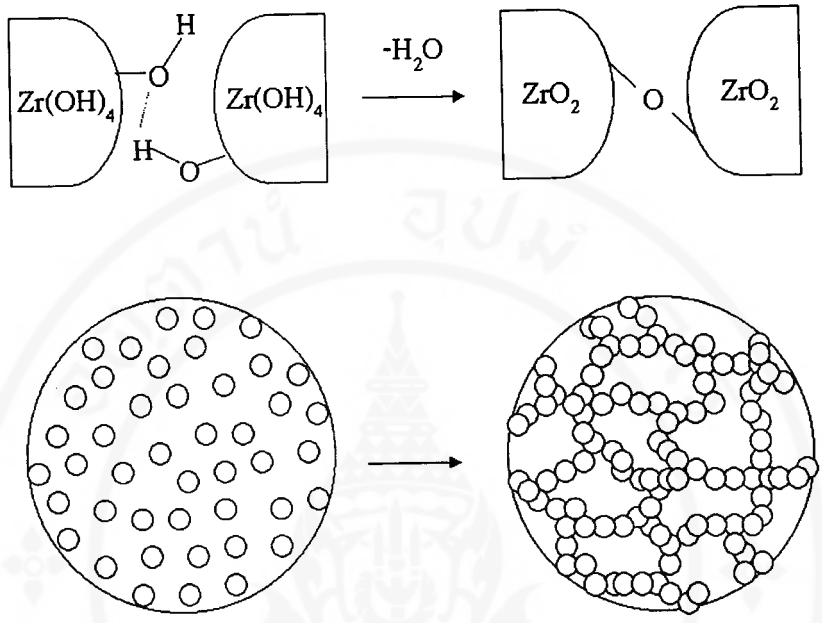

Figure 2.5 The schematic diagram demonstrates gel formation through cross link polymerization process

2.2.4 Elimination of Unreaction - Water

The water is removed from gelation product in distillation step. However, the mixture between water and xylene forms the azeotropic composition [72], so Dean-Stark apparatus is applied to eliminate water residue. The complete water-elimination process is indicated at the constant boiling temperature, 144°C.

2.2.5 Phase Inversion

At about 140 °C is the Phase Inversion Temperature (PIT) for Tween 80. Hydrophilic property of surfactant changes to hydrophobic property, accordingly W/O is stable above 140 °C. Figure2.6 presents phase inversion map, in region B^-, an unstable W/O emulsion is expected. When increase temperature from (1) to (2), the system is changed to more stable region B^+. Along the transition from B^- to B^+, the turbid dispersion is observed at some characteristic temperature and clearly solution will be presented again at higher temperature. This transition temperature is known as cloud point [68].

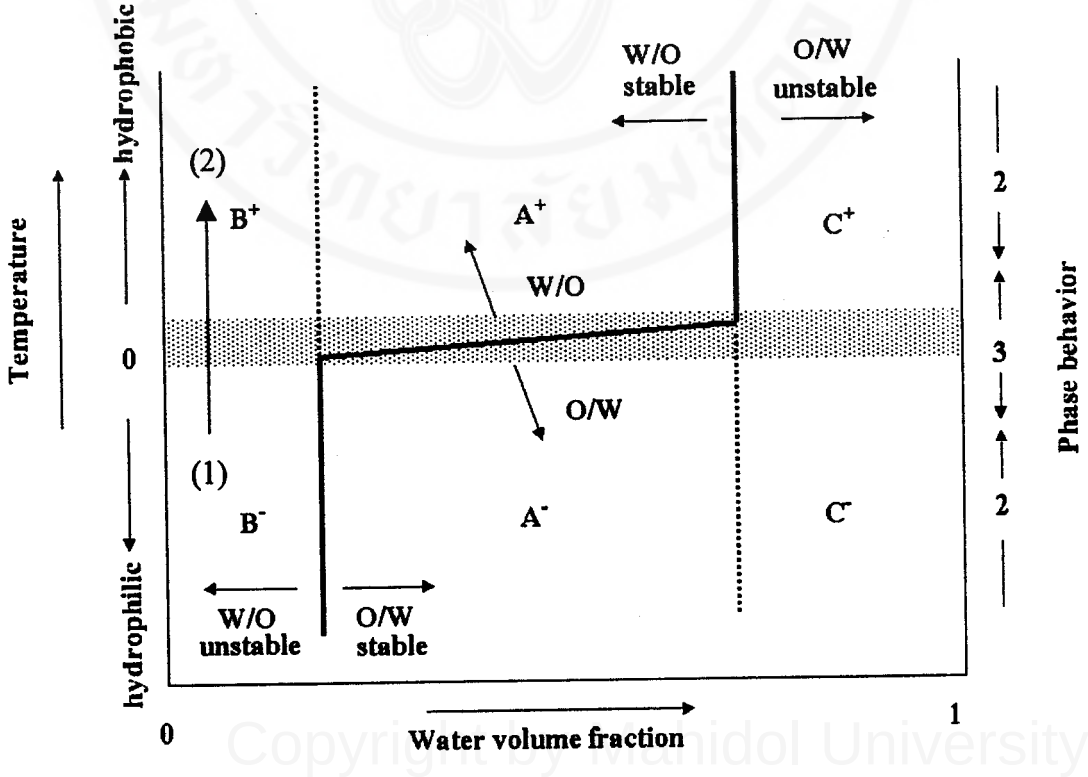

Figure 2.6 Applied phase inversion map of Salager and Brooks [68]

The sol-emulsion-gel process or SEG method can be demonstrated by the schematic diagram in Figure 2.7.

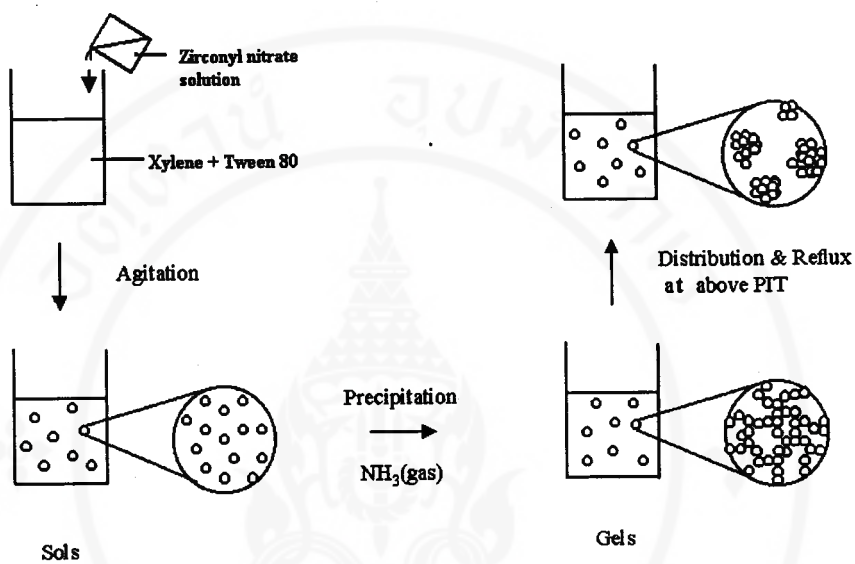

Figure 2.7 The schematic diagram of SEG method

2.3 Characterization

2.3.1 Phase Identification and Crystal Size Determination

X-ray diffraction technique is usually used to identify phase of samples. The standard XRD patterns of zirconia, obtained from the Power Diffraction Databases (JCPDS file) [47] and the three phase crystal structures of zirconia polymorphs, are presented in Figure 2.8 and 2.9, respectively.

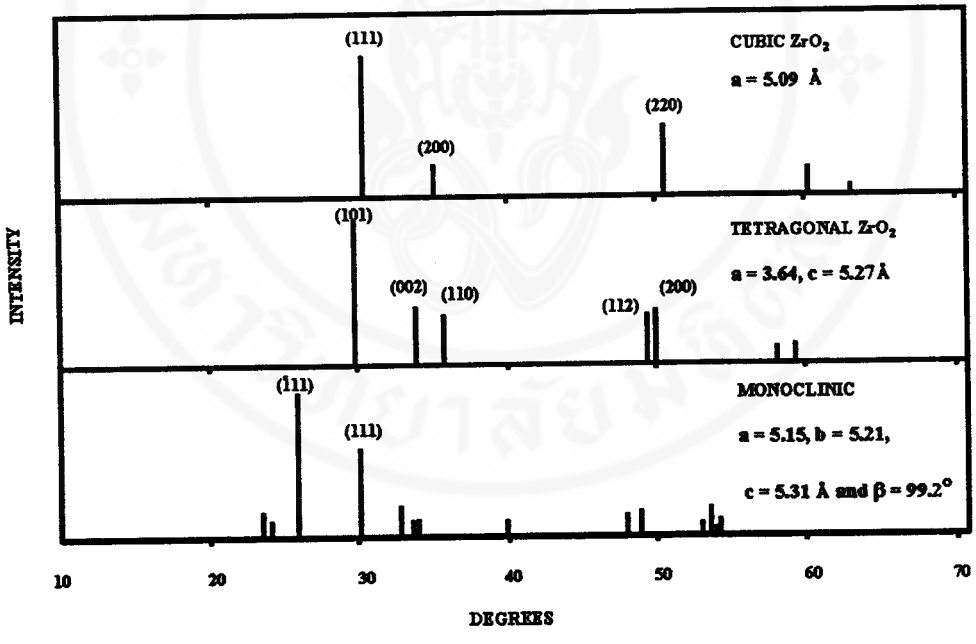

Figure 2.8 XRD patterns for zirconia [47]

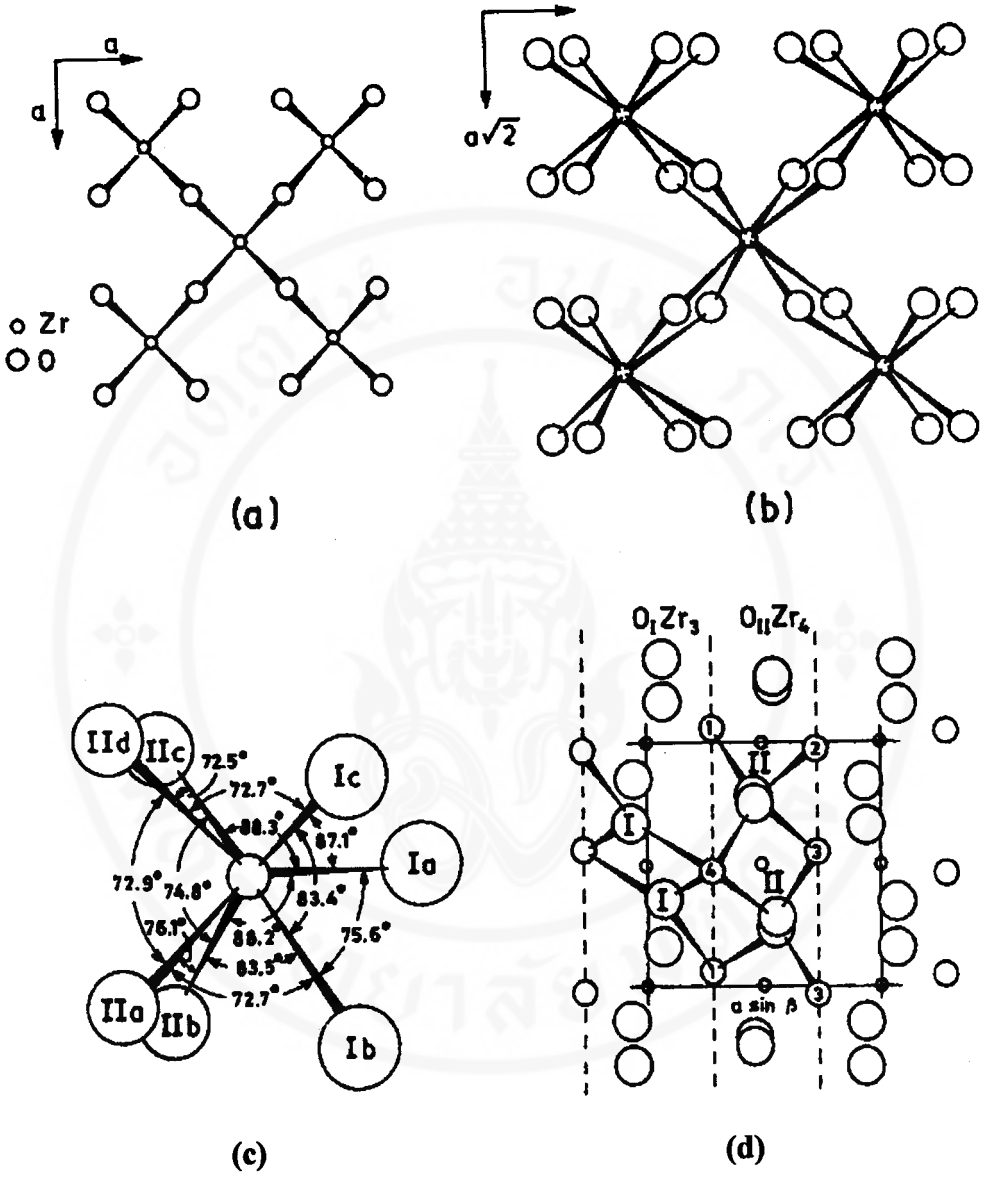

Figure 2.9 Crystal structure of zirconia polymorphs (a) projection of layer of ZrO_8 groups in the cubic ZrO_2 on the (100) plane (b) projection of layer of ZrO_8 groups on the (001) plane of tetragonal ZrO_2 (c) angles and interatomic distance in the ZrO_7 coordination polyhedron of monoclinic ZrO_2 (d) projection of the crystal structure of monoclinic ZrO_2 along the c_m-axis showing layers of $O|Zr_3$ and $O|| ZrO_4$ polyhedral [17].

FT-IR spectroscopic technique is also applicable for zirconia phase identification [74]. The vibration modes of polymorphic zirconia (Zr-O mode) appear at wavenumbers lower than 800 cm^{-1} and the characteristic absorption band as demonstrated in Figure 2.10. Tetragonal and cubic phase present a broad band about 500 cm^{-1}, and monoclinic phase presents several characteristics bands, mainly at 740, 520 and 450 cm^{-1}. Raman spectrum is more distinct for interpreting bands of zirconia polymorphs. This technique can identify each phases of zirconia as shown in Table 2.1. Unfortunately, Raman spectrophotometer is non-available during my work. Therefore information on phase identification is considered by means of XRD patterns only.

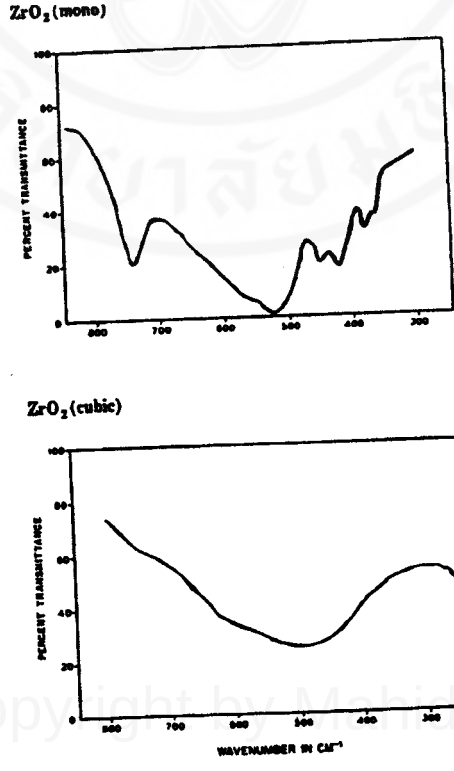

(a)

(b)

Figure 2.10 Infrared spectra for zirconia (a) monoclinic phase and (b) cubic phase [74]

Table 2.1 Raman frequencies for zirconia polymorphs (cm^{-1})

Metastable cubic [74]	Tetragonal Y_2O_3 stabilized [74]	Monoclinic [75]	Monoclinic [76]
490 vb	575 w, b	740 s	745 m
	510 w, b	610 w	620 sh
	435 w, b	528 s	530 sh
	365 w, b	445 + 410 d	450 w
		373 + 360 d	420 w
		278 s, sp	375 w
		237 s, sp	360 sh

The XRD diffraction patterns are so sensitive with amount of water content in zirconyl structures. Therefore the crystal water in molecules determinate via XRD patterns of $ZrOCl_2.xH_2O$ as show in Figure 2.11.

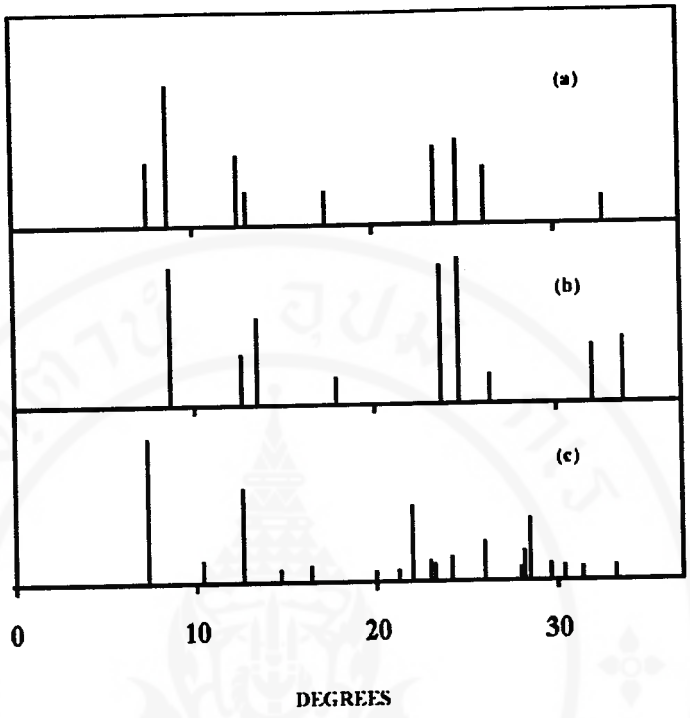

Figure 2.11 XRD patterns for (a) $ZrOCl_2.H_2O$ (b) $ZrOCl_2.6H_2O$ and (c) $ZrOCl_2.8H_2O$ [47]

From XRD pattern, the line positions are measured and assigned with Miller indices (h, k, l). The cell parameters are estimated by using the standard relation for each crystal structure as below. The unit cell or lattice parameters are used as phase identification. The relative intensities of the experimental diffraction pattern are used for quantitative phase analysis [77].

Cubic

$$\frac{1}{d^2} = \frac{h^2 + k^2 + l^2}{a^2}$$

Tetragonal

$$\frac{1}{d^2} = \frac{h^2 + k^2}{a^2} + \frac{l^2}{c^2}$$

Monoclinic

$$\frac{1}{d^2} = \frac{h^2}{a^2} + \frac{l^2}{c^2} - \frac{2hl\cos\beta}{ac} + \frac{k^2}{b^2}$$

The quantitative volume fractions of tetragonal phase in the mixtures of both monoclinic and tetragonal phases is estimated by using the formula below [78, 79, 81].

$$X_t = \frac{I(101)_t}{[I(111)_m + I(\bar{1}11)_m + I(101)_t}$$

$$\upsilon_t = \frac{1.311X_t}{1 + 0.311X_t}$$

$$\upsilon_m = 1 - \upsilon_t$$

Where the subscript m and t refer the monoclinic and tetragonal phase and I refers the X-ray intensity of the corresponding peaks.

The effect of decreasing crystal size serve to increase the observed with broad peaks. X-ray line broadening provides information on the average size of crystal (D_x) by using the Scherrer formula [77].

$$D_x = \frac{k\lambda}{B\cos\theta}$$

Where D_x is the thickness of the crystal (in Angstroms), θ is the diffraction angle, λ is the wavelength of radiation and k is a constant, which is nearly equal to unity (k = 0.9 for this work). This method is limited to crystalline sizes of less than 2000Å, depended on the resolution of XRD instrument. The line broadening, B is measured from full width of the diffraction line at half the maximum intensity (FWHM). The values of B are found by correction equation of the Warren formula [80].

$$B^2 = B_M^2 - B_S^2$$

Where B_M is the measured peak width in radians at half peak height and B_S is the corresponding width of a peak of standard material.

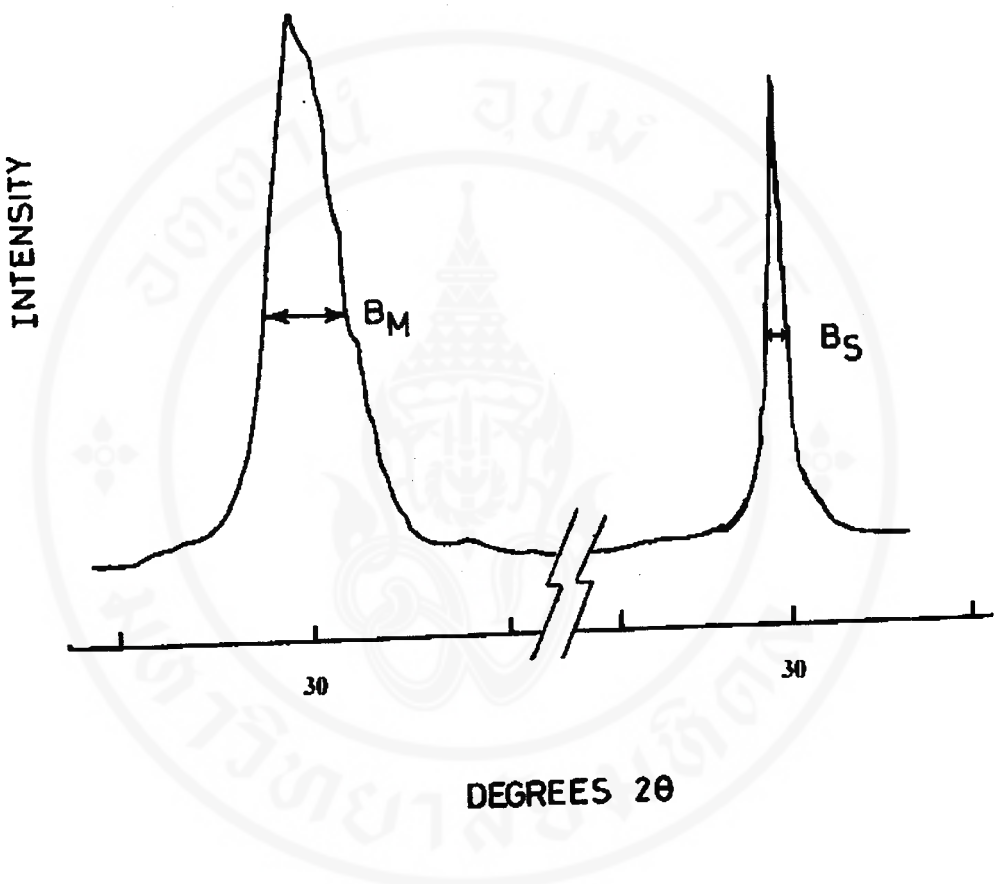

Figure 2.12 Measurement of crystal size from XRD peak

The diffraction line of ZrO_2 at 1500°C calcine temperature is used as reference line of standard in this work. Furthermore, TEM micrographs is also applied for crystal size determination

2.3.2 Vibration Spectra of Zirconyl Compounds and Related Functional Groups

The nitrate group [81, 82] is an importance index for identifying zirconyl nitrate. Two types of nitrate group are existing in zirconyl nitrate, namely nitrate ion, NO_3^- and coordinated nitrato-groups. The symmetry of nitrate ion is presented the point group D_{3h}, according to the vibrational frequencies, as shown in Table 2.2.

Table 2.2 Infrared vibration frequencies for the NO_3^- ion [81]

Type	Infrared	NO_3^-	cm^{-1}	Assigment
A_1'	IA	ν_1	1050	N-O stretching
A_2''	A	ν_2	831	NO_2 deformation
E'	A	ν_3	1390	NO_2 asymmetrical stretching
E'	A	ν_4	720	Planar rocking

The NO_3^- ion coordinates to a metal (nitrato-group) is increasingly strong interaction between NO_3^- ion and metal. The coordinated nitrato-group shows less symmetry than nitrate ion therefore, the changes in the vibration frequencies are considered as in Table 2.3 [81,83].

Table 2.3 Infrared vibration frequencies for the nitrato complex [81].

Type	Infrared	NO_3^-	unidentate cm^{-1}	bidentate cm^{-1}(bridge)	Assignment
A_1	A	ν_3	739	747	NO_2 deformation
A_2	A	ν_1	1253-1290	1350-1280	NO_2 symmetrical stretching N-O
A_1	A	ν_2	970-1034	1040-1030	stretching
B_2	A	ν_6	781-800	802	Nonplanar rocking
B_1	A	ν_4	1481-1531	1610-1413	Asymmetrical stretching
B_1	A	ν_5	713	723	Planar rocking

In general, water vibrational mode appears commonly in many samples, $ZrOCl_2.xH_2O$ and $ZrO(NO_3)_2.xH_2O$. The lattice water absorbs at 3550-3200 cm^{-1} (antisymetric and symmetric OH stretching), at 1630-1600 cm^{-1} (HOH bending) and lower 700 cm^{-1} is rocking, twisting and wagging modes [87].

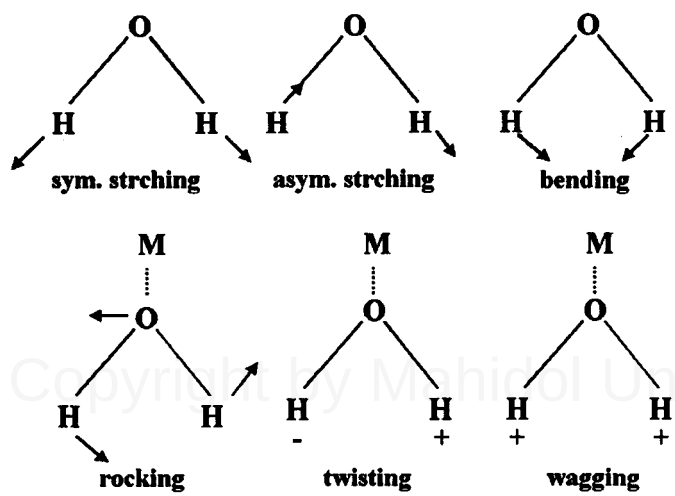

Figure 2.13 The vibrational modes of the water molecule

The hydroxo group can be distinguished from the aqua group, since the former lacks the HOH bending mode near 1600 cm^{-1} [84,85], Furthermore the hydroxo complex exhibits the broad band of MOH bending mode below 1200 cm^{-1} [2, 11].

The FT-IR spectrum of a nonpolar surfactant Tween 80 and its bands assignment [86] are presented in Figure 2.14.

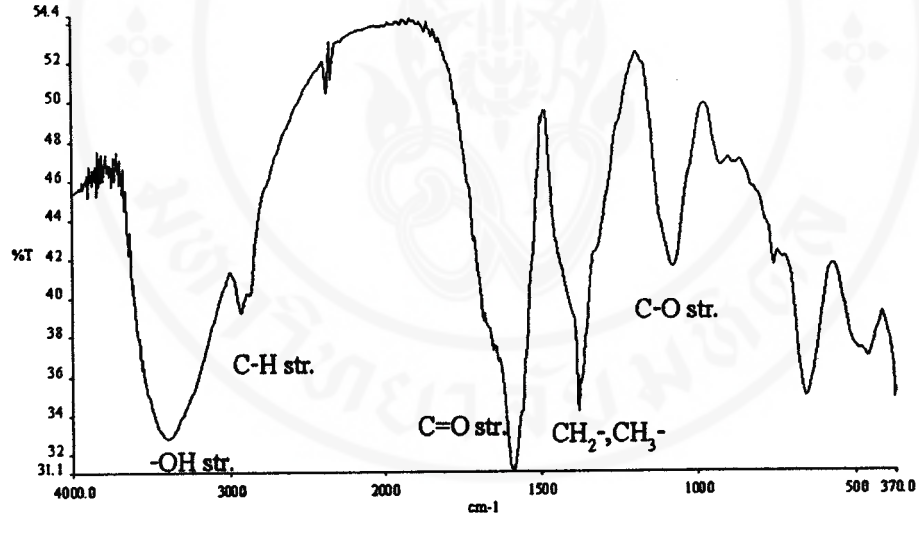

Figure 2.14 Infrared spectrum for Tween 80

Vanadium oxide doped in supported zirconia can be seen by infrared spectrum in Figure 2.15. It presents two distinguished bands at ~ 1000 (V=O mode) and ~800 cm^{-1} (V-O-V mode) [87].

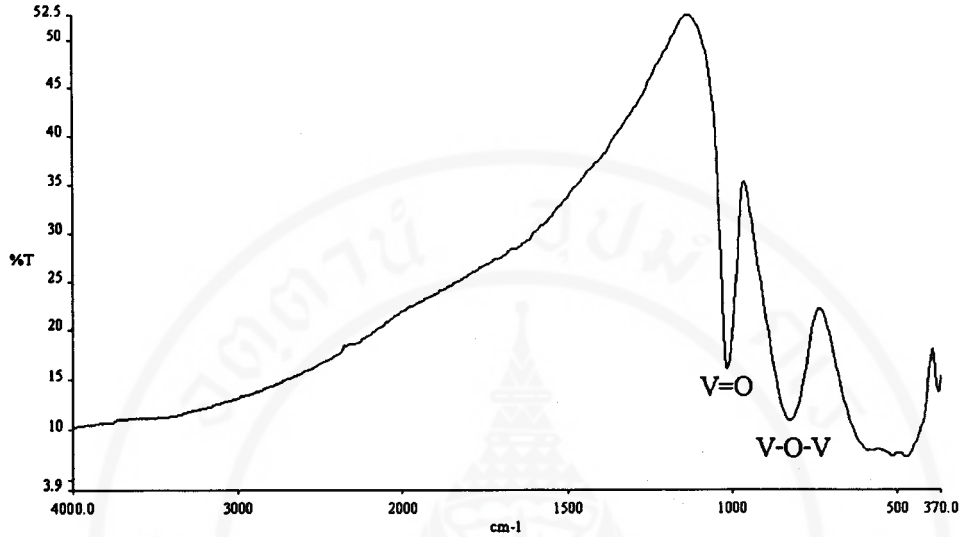

Figure 2.15 Infrared spectra for vanadium oxide

2.3.3 Thermal Analysis

Thermal analysis may be defined as the measurement of physical and chemical properties of materials as a function of temperature. The Power Compensation DSC is used in this study. The appeared bands due to maintain temperature constant ($\Delta T = 0$) when compared with reference. Thus monitoring peak is a difference in powder supplied the heats (ΔH). The thermal changes in the sample understand as positive peak is corresponding with endothermic reaction and the negative peak is exothermic reaction. Figure 2.16 shows a DSC thermogram of ZrO_2, prepared by SEG method [10]. The DSC data indicate organic burnout and nitrate decomposition between 400° C with crystallization at ~500°C.

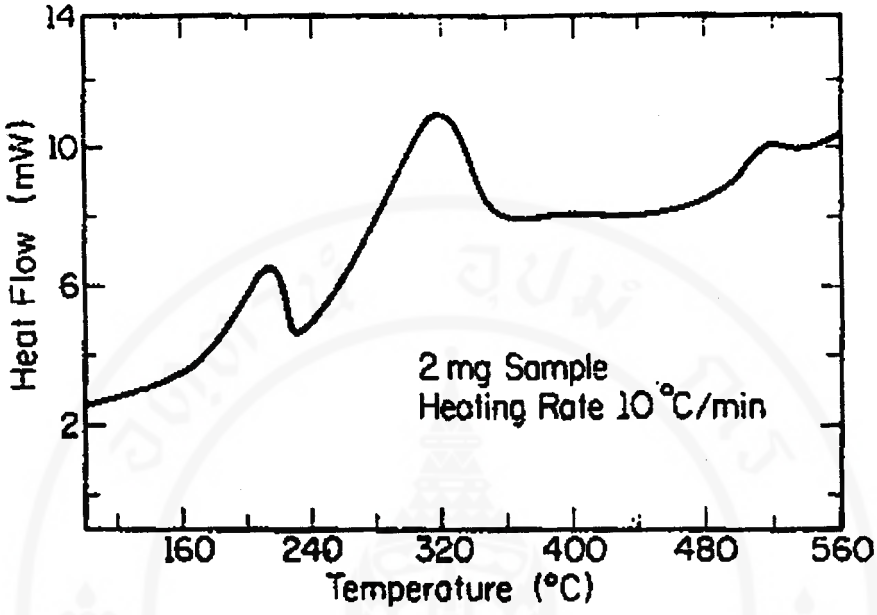

Figure 2.16 DSC thermogram for ZrO_2 powder prepared by the SEG method [10]

2.3.4 Morphology

The Scanning Electron Microscope (SEM) provides the complementary information of geometry, surface and size of particle. In addition, TEM image is also helpful for observation of aggregate structure of powder and crystal size [88].

CHAPTER III

EXPERIMENTS

3.1 Chemicals

Table 3.1 List of chemicals

Chemicals	Suppliers	Grade
$ZrO(NO_3)_2.xH_2O$	Jahnson Matthen Electronics, JM	Purum
$ZrO(NO_3)_2.6H_2O$	Fluka	Purum
$ZrOCl_2.8H_2O$	Fluka	Purum
Xylene	Merck	Analytical
Tween 80	Fluka	Analytical
Hydrochloric acid, 37%	Merck	Analytical
Nitric acid, 65%	Merck	Analytical
Ammonium hydroxide, 25%	Merck	Analytical
Ammonium metavanadate	Merck	Purism
Iso-butyl alcohol	J.T. Baker	Analytical
NaOH	Merck	Analytical
Silver chloride	Merck	Analytical
Nitrogen gas	TIG	99%

3.2 Instruments and Equipment

- Scanning Electron Microscope[1] (Hitachi S-2500)
- Transmission Electron Microscope[1] (Hitachi H-300)
- X-ray diffractometer[2] (Philips PW 1830/40, Single Pen Recorder PM 8203)
- Differential Scanning Calorimeter[1] (Perkin Elmer DSC7)
- Fourier Transform Infrared Spectrophotometer (Perkin Elmer System 2000 FTIR)
- Laser Particle size analysis (Malvern Mastersizer)[2]
- Inductively Coupled Plasma Mass Spectrometry (Perkin Elmer ELAN 6000)[1]
- Stirring Hot Plate (Patterson Scientific Model B292)
- Hot-Air Oven (Lindberg Model 51524)
- Ultrasonic Cleaner (Bransonic Model B2200 E-3)
- Analytical Balance (Precisa Model 240A)

[1] Central Instrument Faculty (CIF), Mahidol University

[2] Office of Atomic Energy for Peace (OAEP)

3.3 Preparation of Zirconyl Compounds from Zircon Sand

Raw zircon sand that contains silicate was fused at 550°C with an approximately 1.5-fold of sodium hydroxide in a nickel crucible. The fusion product or frit is a mixture of sodium zirconate and sodium silicate [6-8].

$$ZrSiO_4 + 4NaOH \rightarrow Na_2ZrO_3 + Na_2SiO_3 + 2H_2O$$

To remove soluble sodium silicate and hydrolyzing impurity, the frit was washed with hot water and then dissolved in hot concentrated hydrochloric acid. The insoluble residue was filtered from the solution by using a sinter glass. The acid-hydrolysis solution was evaporated and cooled to room temperature. The crystallized zirconyl chloride was separated by suction filtering, using a No. 42 Whatman filter paper, then washed several times with acetone and air-dried. The recrystallization procedure was repeated [7]. The product denotes as zirconyl chloride synthesis, ZCS.

Zirconyl hydroxide synthesis or ZHS was prepared by precipitation from ZCS solution with NH_4OH and dried at 100°C for 2 hr. The resulting gel was washed repeatedly with portions of water followed by settling in a centrifuge until the test with $AgNO_3$ for chloride ions was negative.

The white powder of zirconyl nitrate, ZNS obtained by adding hot concentrated nitric acid to ZHS, stirred, slowly evaporated to dryness [7].

All zirconyl products, ZCS, ZHS, ZNS have been characterized by X-ray diffraction, DSC and FT-IR, likewise the information on the geometry of particles were observed by SEM. The results have been confirmed with the obtained results from related commercial available compounds. Then zirconyl compounds were used as precursors for synthesis of ZrO_2 and V/ZrO_2 in SEG procedure. The preparation diagram of zirconyl compounds shown in Figure 3.1.

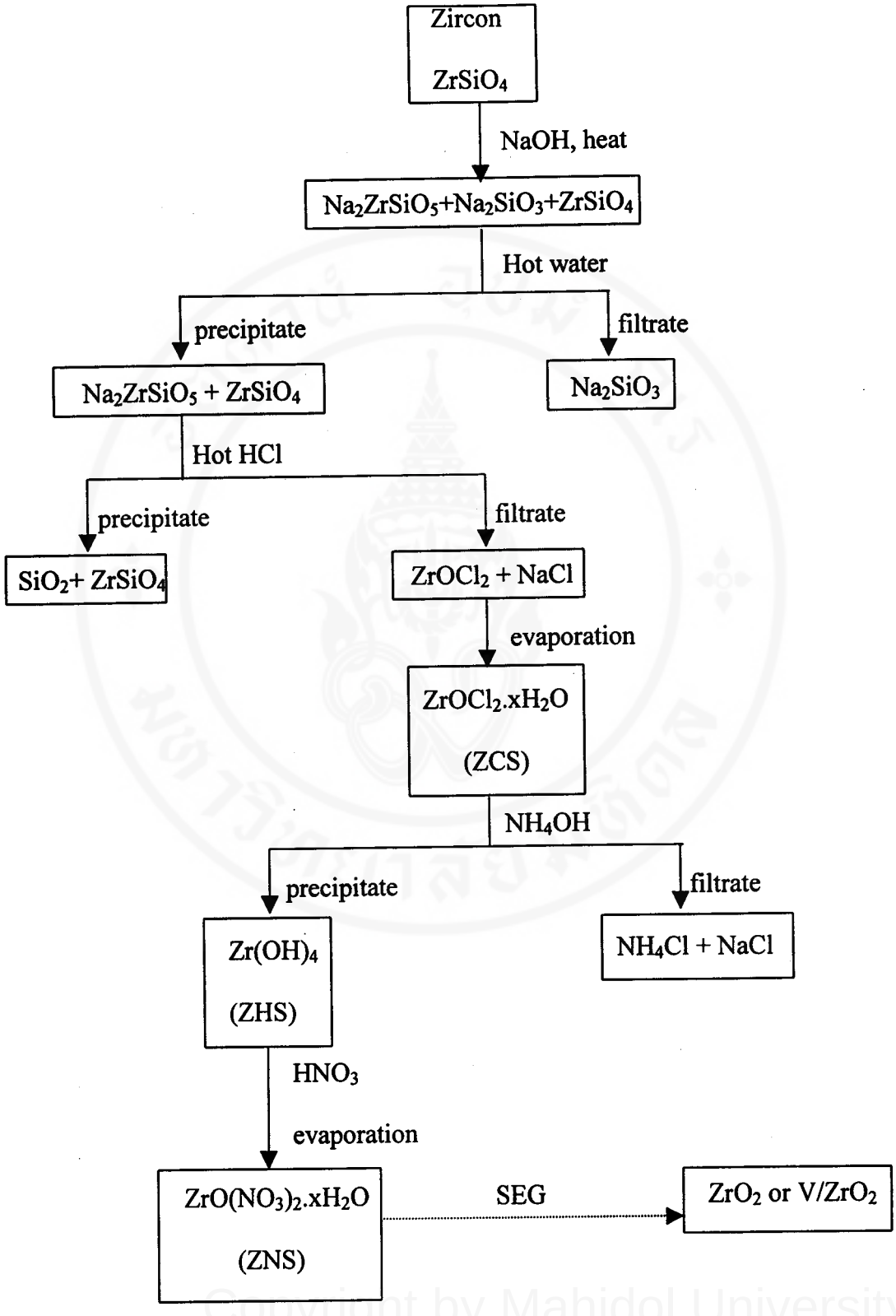

Figure 3.1 Preparation diagram for zirconyl compounds from zircon sand

3.4 Sol-Emulsion-Gel Procedure

3.4.1 Zirconia

A "sol" was prepared from 1 g. of ZNS and 5 ml of deionized water. The sol was heated and stirred at ~90°C until solids was suspended homogeneously as fine colloidal particles. Then filled with 1.08 g of the surfactant, Tween 80 (polyoxethylene sorbitan mono-oleate) and 200 ml xylene, then stirred for 5 min. at room temperature. The sol was added to the stirred xylene solution, and small emulsion droplets developed in the reaction mixture, which were stabilized by the surfactant present. The suspension was ultrasonically agitated for 8 min. Ammonia gas (Figure 3.2) was bubbled through the suspension using a glass tube for 4 to 5 min for gelation zirconyl compound in the emulsion droplets. To prevent agglomeration during gelation, sonication was further required for 3 minutes. The suspension was then transferred to a round-bottom flask for reflux and distillation using a water trap Dean Stark apparatus (Figure 3.3). By heating the reaction mixture to ~95°C, the unreacted water was removed and trapped in the aforemention. The temperature of the suspension was increased and maintained about 144°C, which is the boiling point of xylene. The distillation treatment was finished after the temperature had stabilized at 140°C for 45 min. The powder was isolated by filtering, dried at 140°C for 16 hr [10]. Then powder was calcined in a box furnace at different temperatures. The temperature program shown in Figure 3.4.

The effect of ultrasonic agitation was investigated. Anyhow, after ultrasonic agitation did not demonstrate any significant effect, only stirrer was required for

mixing heterogeneous solution in the other experiments, The results of the phase transition and crystallized size were discussed. The products, which obtained from both procedures, were denoted in Table 3.2.

Ammonia gas was generated from ammonium hydroxide, NH_4OH, as shown in the Figure 3.2. Ammonia gas was introduced to the reaction vessel by passing N_2 gas as a carrier gas through ammonium hydroxide solution at an appropriate concentration and flow rate.

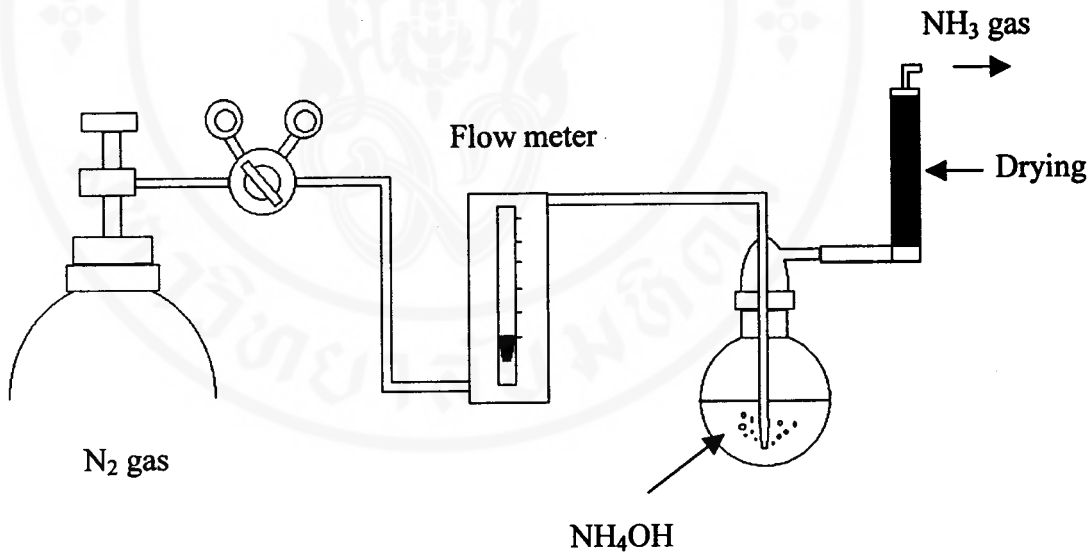

Figure 3.2 The flow system for ammonia gas

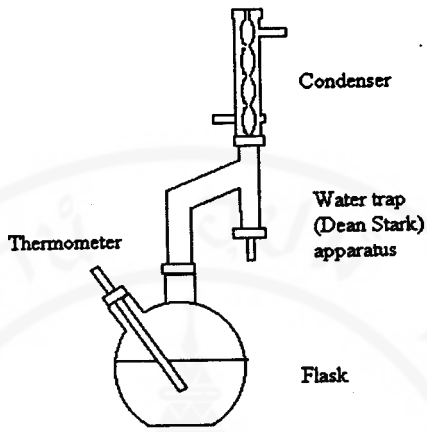

Figure 3.3 Water trap Dean Stark Apparatus used to remove water

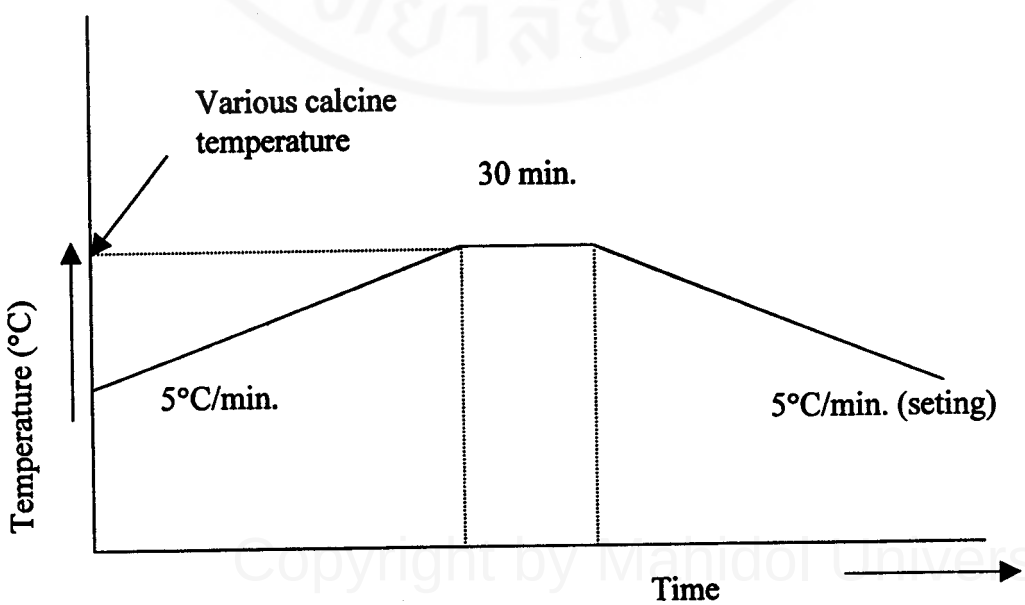

Figure 3.4 A typical temperature program for calcination of samples

Table 3.2 List of zirconia sample identification

Sample code	Calcine temperature (°C)	Agitation
Zr-140-su	140*	Stirrer and ultrasonic
Zr-300-su	300	Stirrer and ultrasonic
Zr-400-su	400	Stirrer and ultrasonic
Zr-500-su	500	Stirrer and ultrasonic
Zr-600-su	600	Stirrer and ultrasonic
Zr-800-su	800	Stirrer and ultrasonic
Zr-1000-su	1000	Stirrer and ultrasonic
Zr-1200-su	1200	Stirrer and ultrasonic
Zr-1350-su	1350	Stirrer and ultrasonic
Zr-140-s	140*	Stirrer
Zr-400-s	400	Stirrer
Zr-600-s	600	Stirrer
Zr-800-s	800	Stirrer
Zr-1000-s	1000	Stirrer

* drying temperature

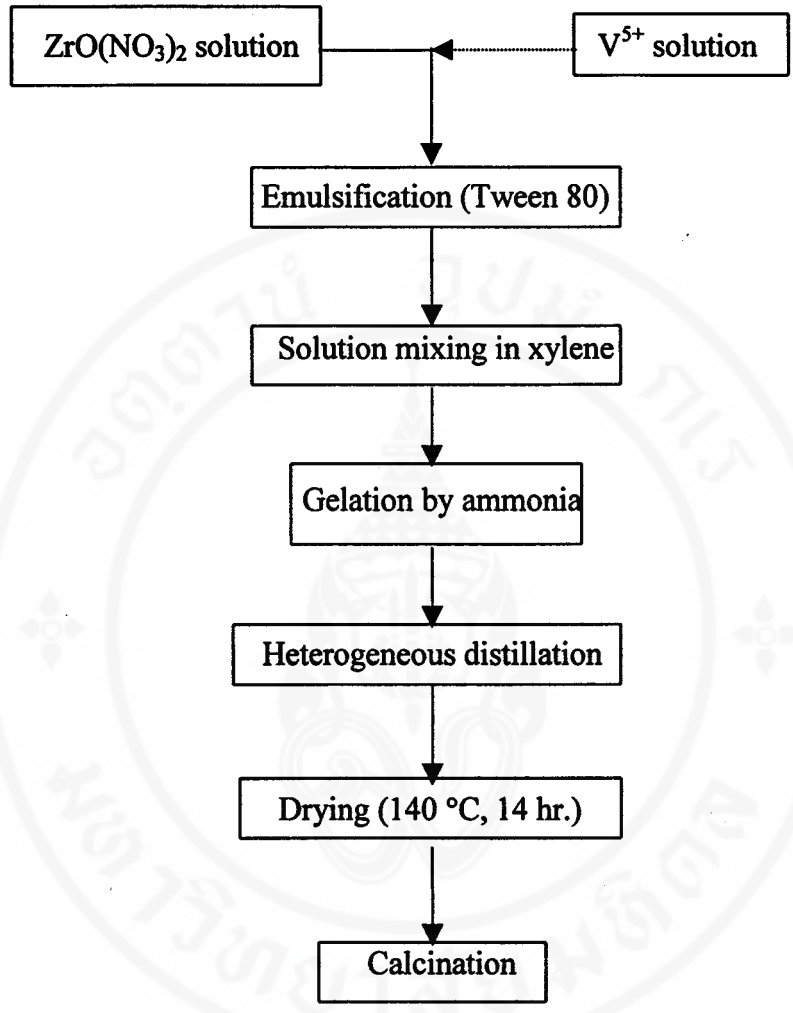

Figure 3.5 The sol emulsion gel processing diagram or SEG method

3.4.2 V/ZrO_2

This section is adapted from section 3.4.1. Ammonium (meta)vanadate, NH_4VO_3 was selected for the preparation of V/ZrO_2 powder. The solution of NH_4VO_3 was prepared from NH_4VO_3 2 g dissolved in nitric acid and then diluted with deionized water to 100 ml. Both NH_4VO_3 and ZNS were dissolved in deionized water. This process is also summarized in Figure 3.5

The powder samples obtained after preparation by SEG method were calcined at different temperatures from 400 to1000 °C as shown in Table 3.3.

Table 3.3 List of V/ZrO_2 identification

Sample code	Calcine temperature (°C)	% weight of vanadium
1V-Zr-140	140*	1
5V-Zr-140	140*	5
10V-Zr-140	140*	10
15V-Zr-140	140*	15
1V-Zr-400	400	1
5V-Zr-400	400	5
10V-Zr-400	400	10
15V-Zr-400	400	15
1V-Zr-600	600	1
5V-Zr-600	600	5

* drying temperature

Table 3.3 (continues) List of V/ZrO_2 identification

Sample code	Calcine temperature (°C)	% weight of vanadium
10V-Zr-600	600	10
15V-Zr-600	600	15
1V-Zr-800	800	1
5V-Zr-800	800	5
10V-Zr-800	800	10
15V-Zr-800	800	15
1V-Zr-1000	1000	1
5V-Zr-1000	1000	5
10V-Zr-1000	1000	10
15V-Zr-1000	1000	15

3.5 Method of Characterizations

3.5.1 Powder X-ray Diffraction

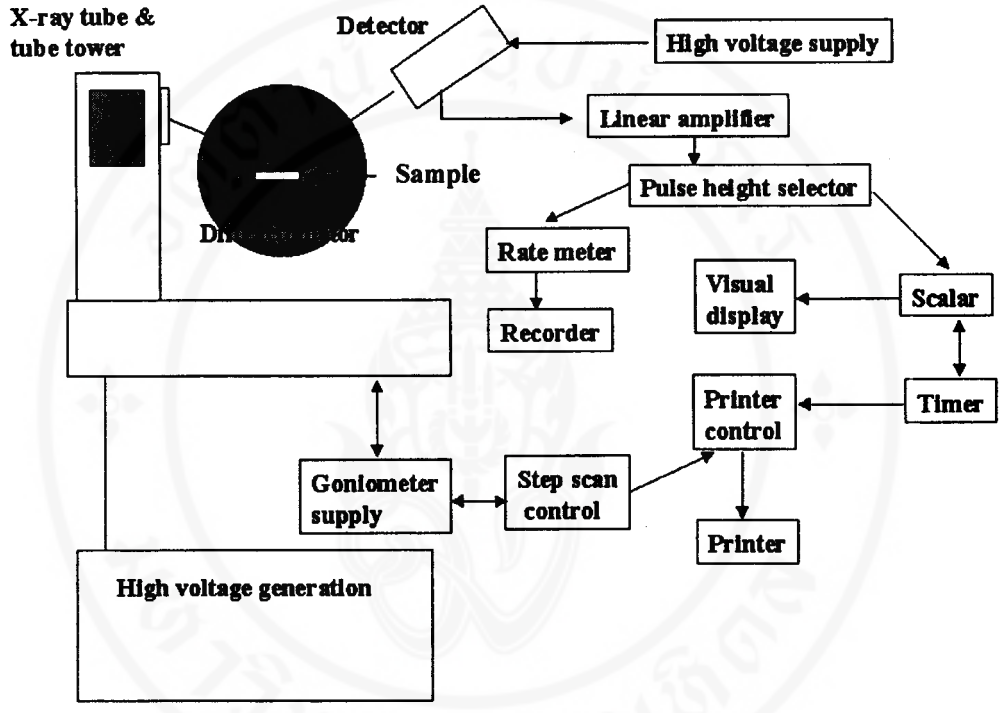

Figure 3.6 Diagram of Philip X-ray diffraction system

X-ray diffraction data in this study were obtained from a Philips PW 1710 instrument using CuKα and Ni filter at 40 kV and 30 mA. The rate was 0.050° degrees per second over a 2θ range from 4 to 70 degrees. Diffraction patterns were plotted between 2θ and counts per second. The d spacing parameter and lattice constant were calculated using Bragg 's equation.

$$n\lambda = 2d\sin\theta$$

When d is d spacing, θ is Bragg angular and λ is wavelength of the CuKα X-ray which is 1.542 Å. A small amount of dried powder sample was packed into an aluminum holder, and the surface was the smoothed flattered by using a spatula.

3.5.2 Fourier Transform Infrared Spectrometry

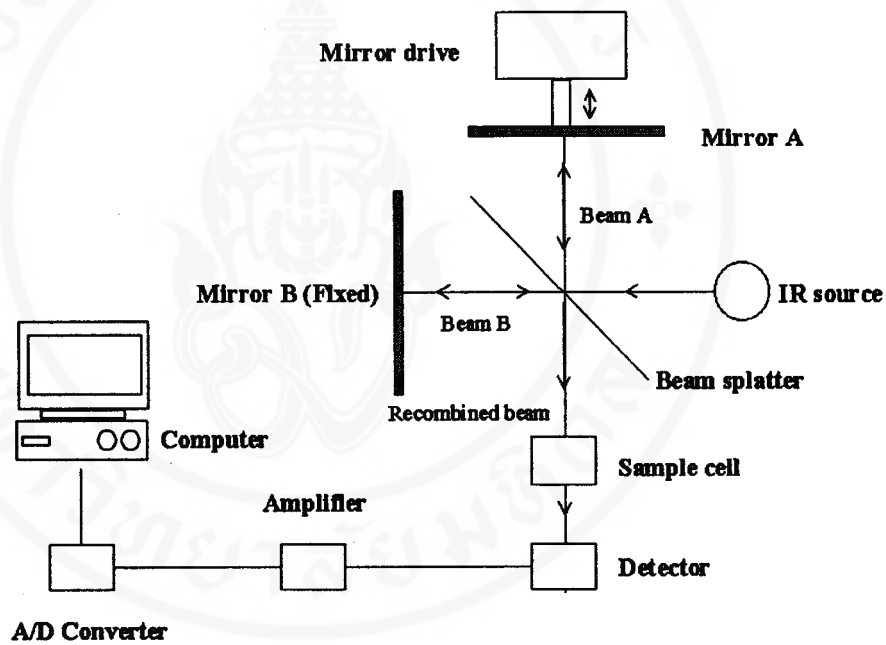

Figure 3.7 Block diagram of an interferometer and associated electronics typically used in a FT-IR instrument

FT-IR spectra were obtained from a Perkin Elmer System 2000 spectrophotometer. The range of frequency from 4000 to 370 cm^{-1} was typically average of 16 scans with 1 cm^{-1} resolution. Each measured spectrum was a record of frequency (cm^{-1}) versus percentage transmittance.

The sample (ca. 1-2 mg) was mixed with 100-200 mg KBr in an agate mortar and grinded until homogeneous. The mixture was then placed in the die (13-mm diameter) and pressed under a pressure of 10 tones of 1 minute to obtain a pellet.

3.5.3 Image Analysis by Using Electron Microscope

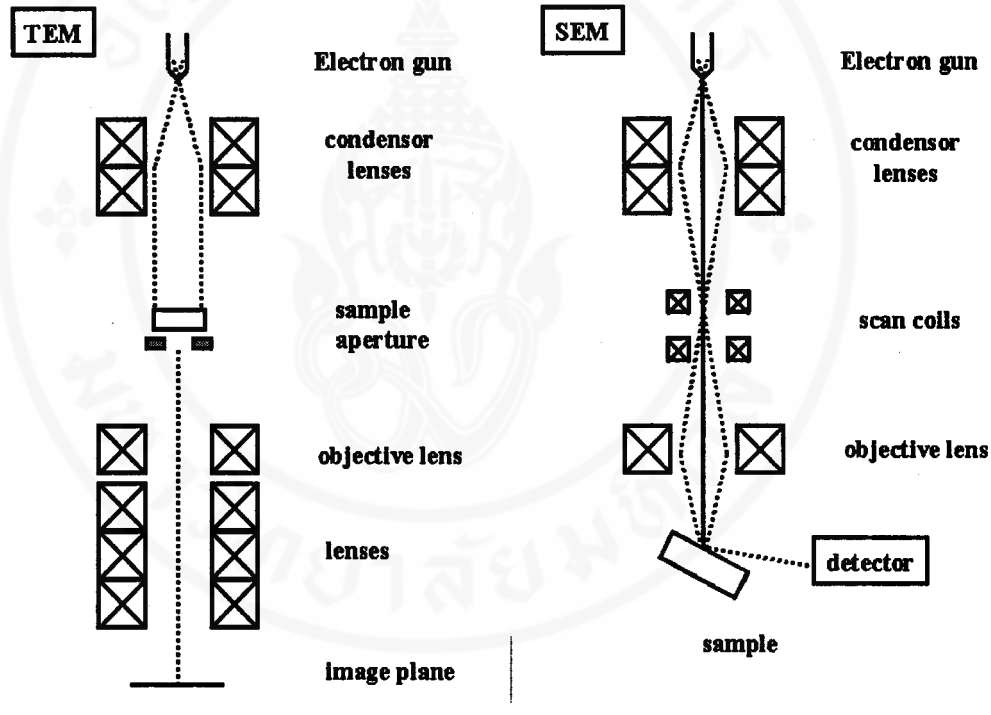

Figure 3.8 TEM and SEM diagrams

The shape, size and surface of all zirconyl products, ZrO_2 and V/ZrO_2 were examined by Scanning Electron Microscope, SEM (HITACHI model 2500) using 15 kV. It was equipped with 35-mm camera and used conventional black-and-white film for image recording. The powder sample was put on a gluey tape. Then sample was

coated with Pt-Pd in Hitachi E-102 Ion Sputter for 2 minutes before being examined with SEM. The TEM (Hitachi model H-300) used W filament at 75 kV. The dry powder sample was dispersed in 2-propanol with the aid of an ultrasonic bath and then introduced onto a formvar grid of the sample holder.

3.5.4 Themal Analysis

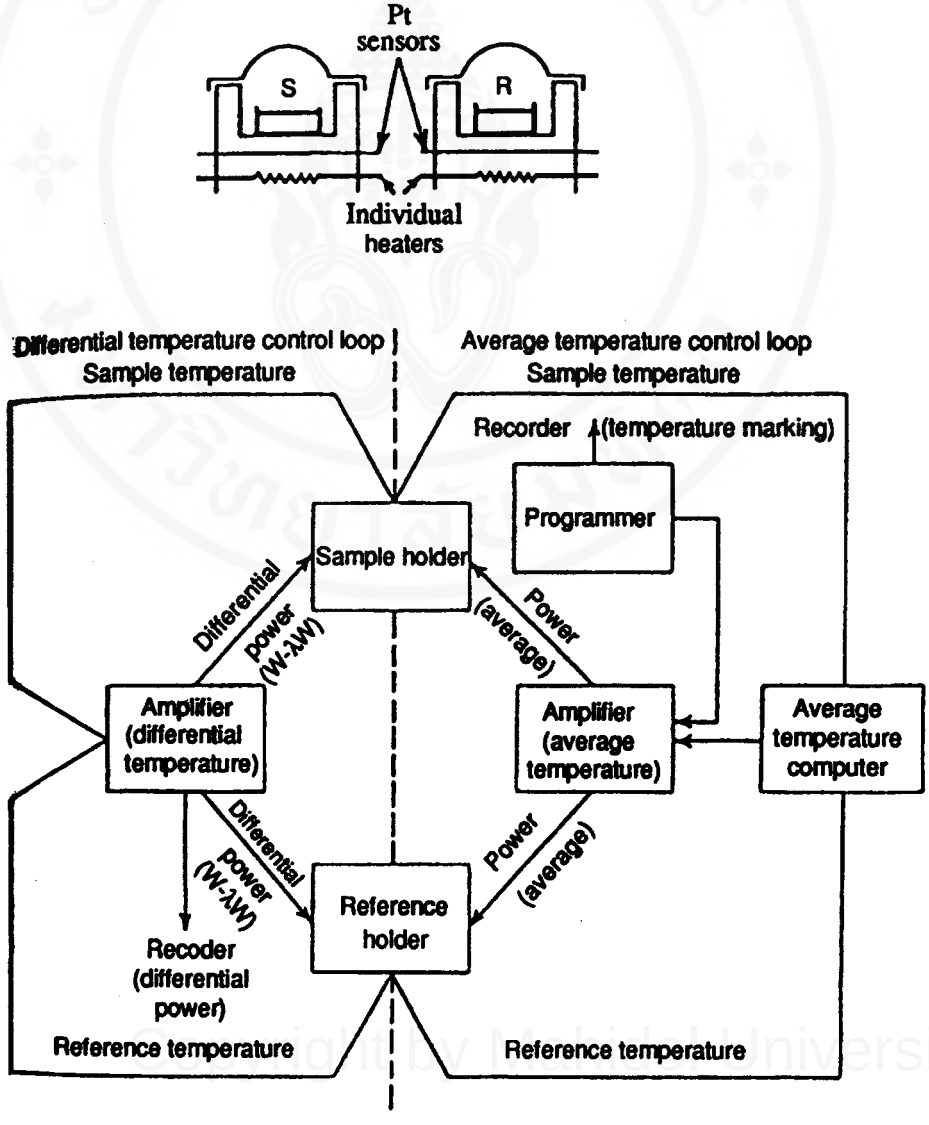

Figure 3.9 Schematic diagram of Perkin-Elmer DSC instrument

DSC measurements were performed by a Perkin Elmer Model DSC over the temperature range of 80–480°C. The investigated temperature was limited at 480°C, according to the available facility at Chemistry Department. Heating rate of 20°C per $min^{-1}$was used. The powder samples (ca. 5 mg.) were placed in an aluminum pan.

CHAPTER IV

RESULTS AND DISCUSSION

The raw material, Thai zircon sand was investigated and characterized in this chapter. Besides, zirconyl compounds, ZCS and ZNS prepared from zircon were characterized by several techniques. The results were compared with many literatures and commercial compounds: $ZrOCl_2.8H_2O$ (Fluka), $ZrO(NO_3)_2.6H_2O$ (Fluka) and $ZrO(NO_3)_2.xH_2O$(JM). ZCS and ZNS used as precursors for zirconia preparation by sol-emulsion-gel technique. Furthermore, morphology, crystal sizes, phase transition and agitation effect of zirconia were studied. Finally, the SEG method was applied to prepare V/ZrO_2.

4.1 The Characterizations Thai Zircon Sand, a Raw Material for Zirconia

Thai zircon sand obtained from the Office of Energy Atomic for Peace is used in this thesis. The chemical compositions consist of mainly ZrO_2, SiO_2 and 1-5% HfO_2. The minor elements consist of uranium, thorium, aluminum, iron and yttrium that they were detected by qualitative ICP-MS. The morphology of Thai zircon sand was characterized by Scanning Electron Microscope. Figure 4.1 shows the particle profiles of ditetragonal dipyramid crystal forms. The average crystal size was about 746 μm in length and 82 μm in width.

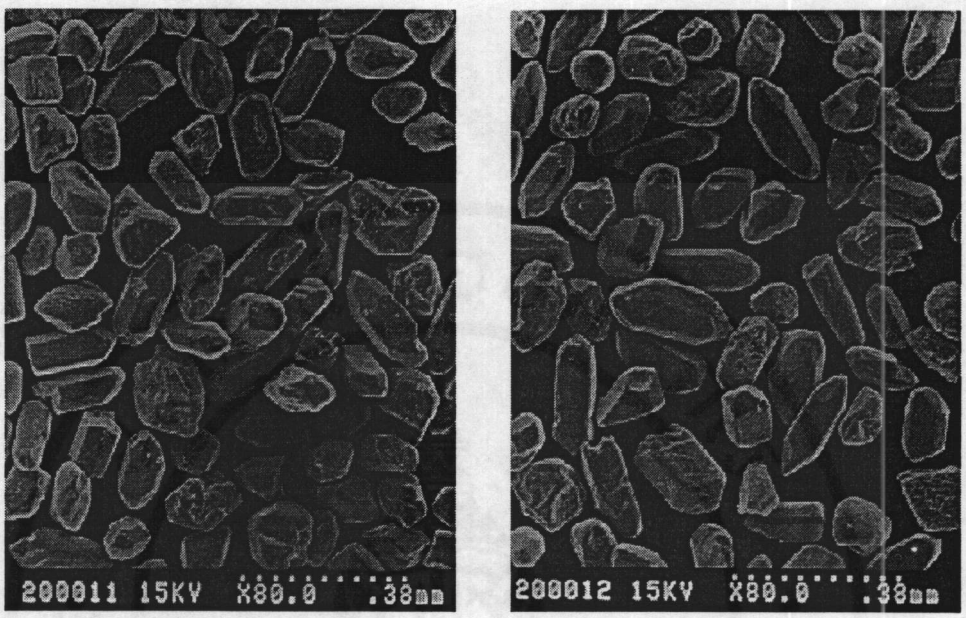

Figure 4.1 Scanning electron micrographs for Thai zircon sand

The infrared spectrum assignment of zircon, was interpreted on the site symmetries of the silicate groups, SiO_4 groups. The free silicate ion is usually tetrahedral symmetry and belongs to point group T_d. Its 9 normal modes of vibration are noted as ν_1(non degenerate), ν_2 (doubly degenerate), ν_3 and ν_4 (each triply degenerate). In the zircon lattice, the silicate ions occupy sites of symmetry, D_{2d}, are lower than the T_d symmetry of the free ion, and hence some of the degeneracies of the free ion frequencies may be splitted [89,90]. Furthermore, symmetry of zircon space group, D_{4h} affects shift of energy level that is summarized in Figure 4.2a

The infrared frequencies of Thai zircon sand were investigated and compared with those results from the several literatures [89-90] as shown in Table 4.1

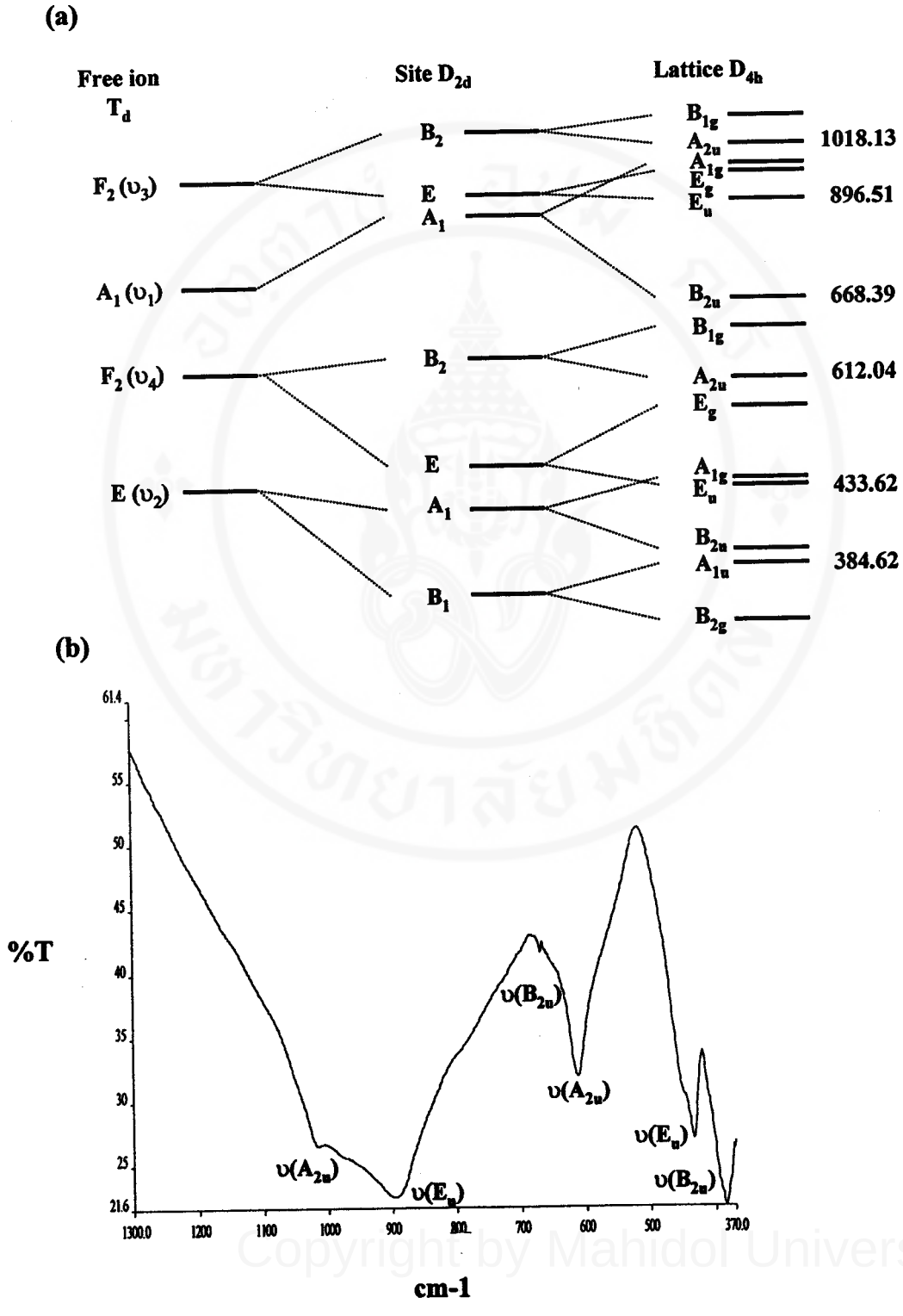

Figure 4.2 (a) Energy diagram for the internal modes of the SiO_4^{4-}complex in zircon (b) The infrared spectrum for Thai zircon sand with band assignment.

Table 4.1 Infrared spectra data and band assignment for zircon sand

Frequency, cm^{-1}			Assignment
Reference [89]	Reference[90]	Thai zircon sand	
1040 –950	989	1018.13	A_{2u}
895	885	896.51	E_u
		668.39	B_{2u}
	608	612.01	A_{2u}
455			
438	430	433.62	E_u
		384.30	A_{1u} and B_{2u}

The X-ray diffraction pattern of Thai zircon sand shown similarity with zircon mineral from JCPDS pattern file [47] (Figure 4.3). Analysis of the data indicates that the unit cell of the Thai zircon sand is the larger than in the JCPDS files. This expected result is due to the co-existence of some hafnium oxide (HfO_2) and other impurities in the raw zircon mineral lattice. Besides, it is possibly an imperfect or defect in crystal lattice [49].

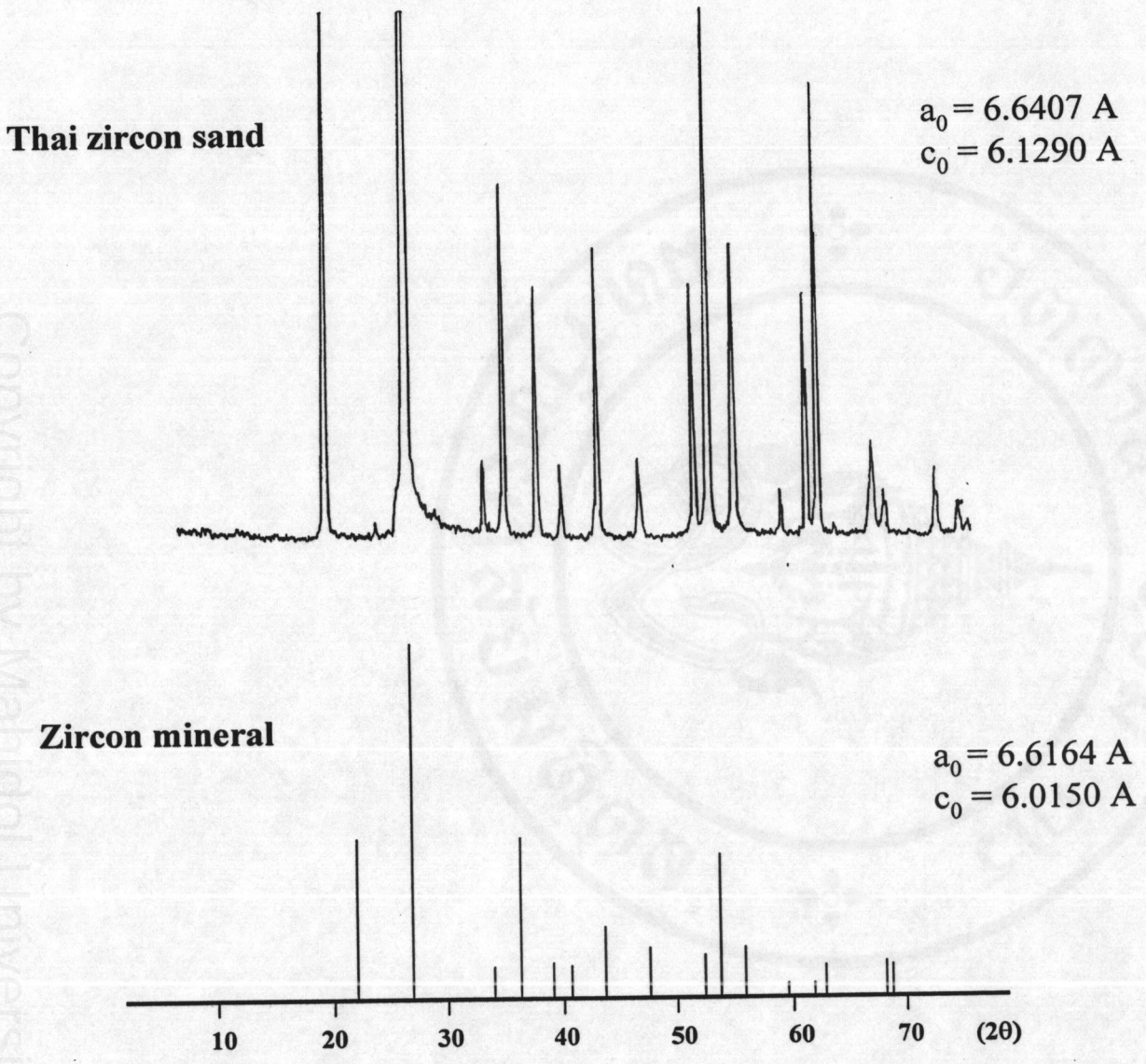

Figure 4.3 XRD patterns for Thai zircon sand compared with zircon mineral from JCPDS database[47]

Table 4.2 XRD parameters of Thai zircon sand compare with zircon sand form JCPDS [47]

JCPDS data base	Thai zircon sand
4.03(45)	4.51
3.30(100)	3.34
2.65(8)	2.68
2.52(45)	2.55
2.34(10)	2.36
2.22(8)	2.24
2.07(20)	2.08
1.91(14)	1.93
1.75(12)	1.77
1.71(40)	1.72
1.65(14)	1.66
1.55(4)	1.56
1.50(4)	1.51
1.48(8)	1.49
1.38(10)	1.39
1.36(8)	1.36
1.29(6)	1.30
a = 6.6164 Å	a = 6.6407 Å
c = 6.0150 Å	c = 6.1290Å

4.2 The Characterizations of Zirconyl Compounds, Prepared from Thai Zircon Sand

Zirconyl compounds, ZCS and ZNS obtained from zircon mineral digestion process were investigated and characterized in this section.

4.2.1 Zirconyl Chloride Synthesis, ZCS

The crystal structure of zirconyl chloride hydrate was firstly explained by Clearfield and Vaughan [91] and was refined by Mak [92]. The zirconyl chloride octahydrate, $ZrOCl_2.8H_2O$, assumed the existence of a polymeric species involving hydroxo bridges, $[Zr_4(OH)_8.16H_2O]^{8+}$. In the tetrameric complex cation the four Zr (IV) atoms form a slightly distorted square arrangement that hold together by dihydroxo bridges. Four H_2O molecules bind with each Zr(IV) to complete a distorted dodecahedral, eight-coordinate geometry. However, some H_2O molecules may disappear from the lattice. Existence of many zirconyl chloride hydrate correspond to a number of water in lattice that alternative between 4 and 10 molecules ($ZrOCl_2.xH_2O$, x=4-10) [93,94].

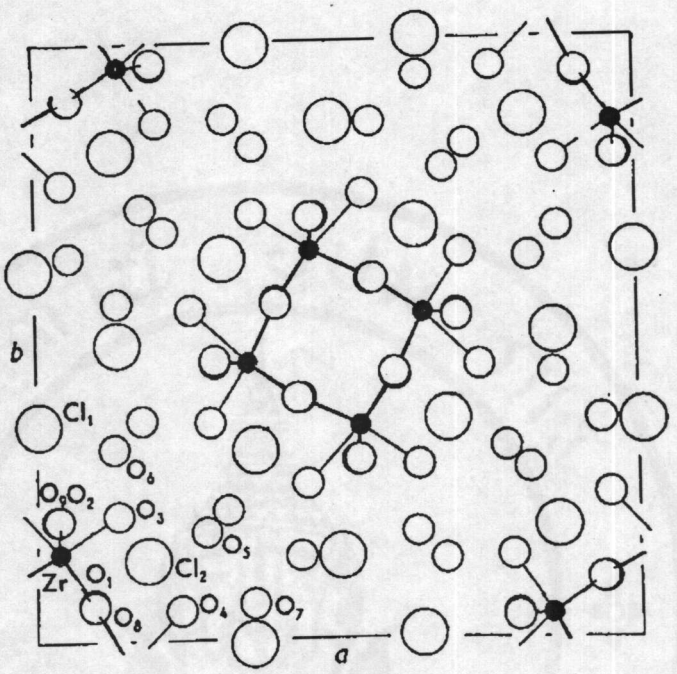

Figure 4.4 Projection of one unit cell of $ZrOCl_8.8H_2O$ on (001) direction [92]

Infrared spectra of zirconyl chloride synthesis, ZCS and $ZrOCl_2.8H_2O$ (Fluka) are compared as shown in Figure 4.5. Besides, band assignment of ZCS compared with the results obtained by Powers et al. [75] is presented in Table 4.3.

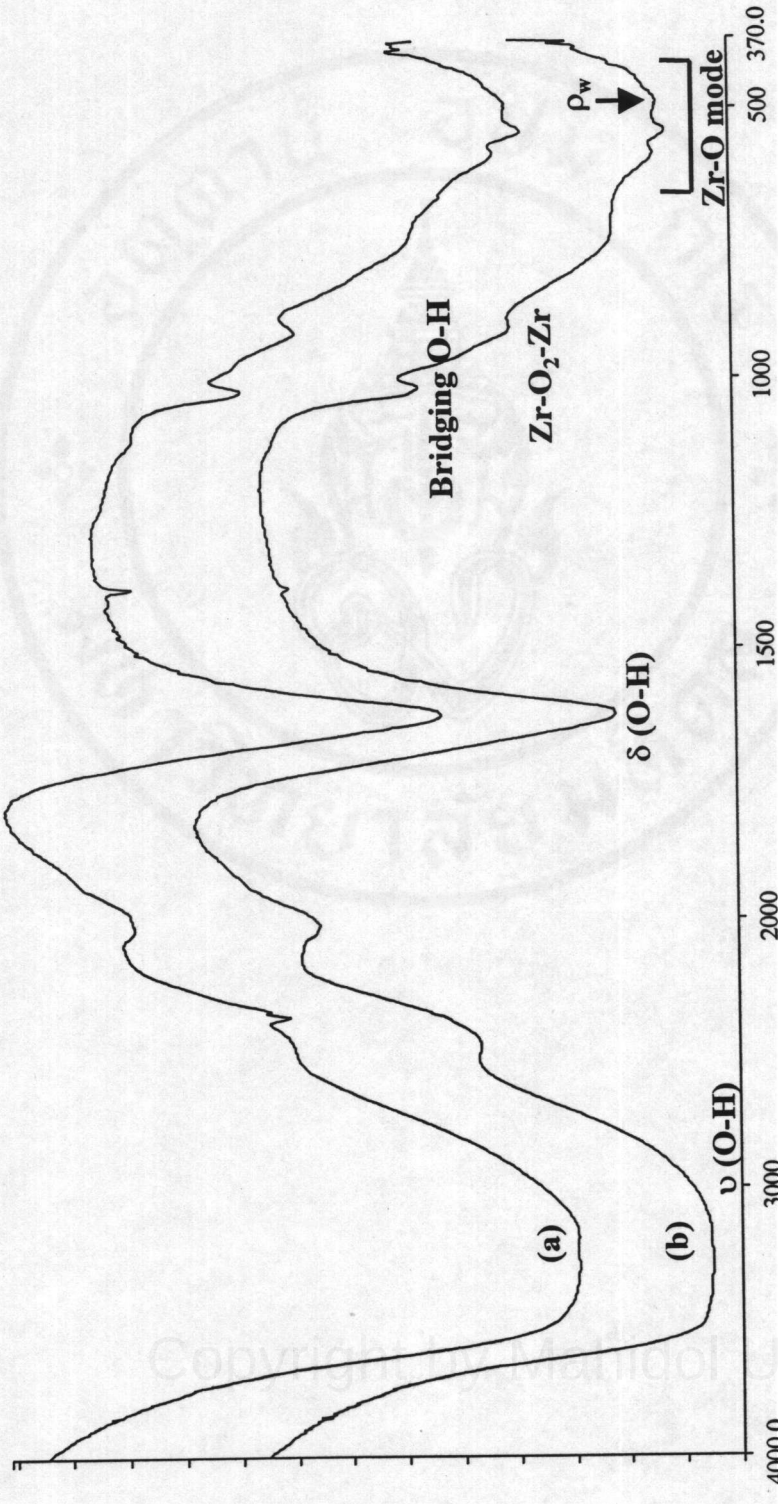

Figure 4.5 Infrared spectra for (a) ZCS and (b) $ZrOCl_3.8H_2O$ (Fluka)

Table 4.3. Infrared Spectra data and band assignment for zirconyl chloride hydrate

Assignment [75]	Frequency, cm^{-1} [75]			ZCS
	$ZrOCl_2.8H_2O$	$ZrOCl_2.6H_2O$	$ZrOCl_2.4H_2O$	
OH str	3520 s, sp		3515 s, sp	
HOH str	3470 s		3410 s	
	3400 s		3350 s	
	3330 s	3300 s, b	3220 s	
	3270 s		3120 s	~ 3295 s, b
HOH def	1640 s	1640 sh		1626 s
	1625 s	1620 s	1610 s	
Bridging OH	1028 m	1020 m	1020 m, sp	1019 m
Def	945 m	950 sh	945 m	
	914 m	910 w	912 m	913 w
Coordinated	835 w, b	850 w	845 w, sp	
Water"rock"				
Zr-O_2-Zr	765 m, b	745 m	735 b	~ 750 b
Asym str				
Zr-O modes	585 s	585 s	615 w	586 w
	545 s	548 s	520 s	546 w
Coordinated	510 s	490 m	470 s	490 w
Water"wag"				
Zr-O modes	445 m	450 s	(Obscured)	445 w
	285 s	278 s, sp	275 s, sp	
	228 s	240 s, sp	249 s, sp	

The region 3700-3000 cm^{-1} was assigned to the symmetric and asymmetric O-H stretching of coordinated and lattices water. Narrow band of medium intensity at 1626 cm^{-1}, was the H_2O deformation vibration. Hydrogen bonding interactions in the crystals appeared at relatively lower energy than the O-H stretching. The band at 1019 cm^{-1} was assigned to the bridging hydroxide deformation. The weak broad band at 490 was expected for a wagging mode of coordinated water.

The absorption in the ~750 cm^{-1} region suggested the presence in the structure of Zr-O_2-Zr chain, the 600-400cm^{-1} region of the spectrum of ZCS comprised of three strong bands which were assigned to zirconium-oxygen modes.

According to the infrared spectra result in Table 4.3 were not clearly to specifically identified type of zirconyl chloride hydrate. The ZCS is probably $ZrOCl_2.8H_2O$ and $ZrOCl_2.6H_2O$ more than $ZrOCl_2.4H_2O$.

The XRD pattern of ZCS powder compared with $ZrOCl_2.8H_2O$ (Fluka), the results were not the distinct identification. However XRD pattern for $ZrOCl_2.6H_2O$ was the best similarity with XRD patterns of ZCS as shown in Figure 4.6.

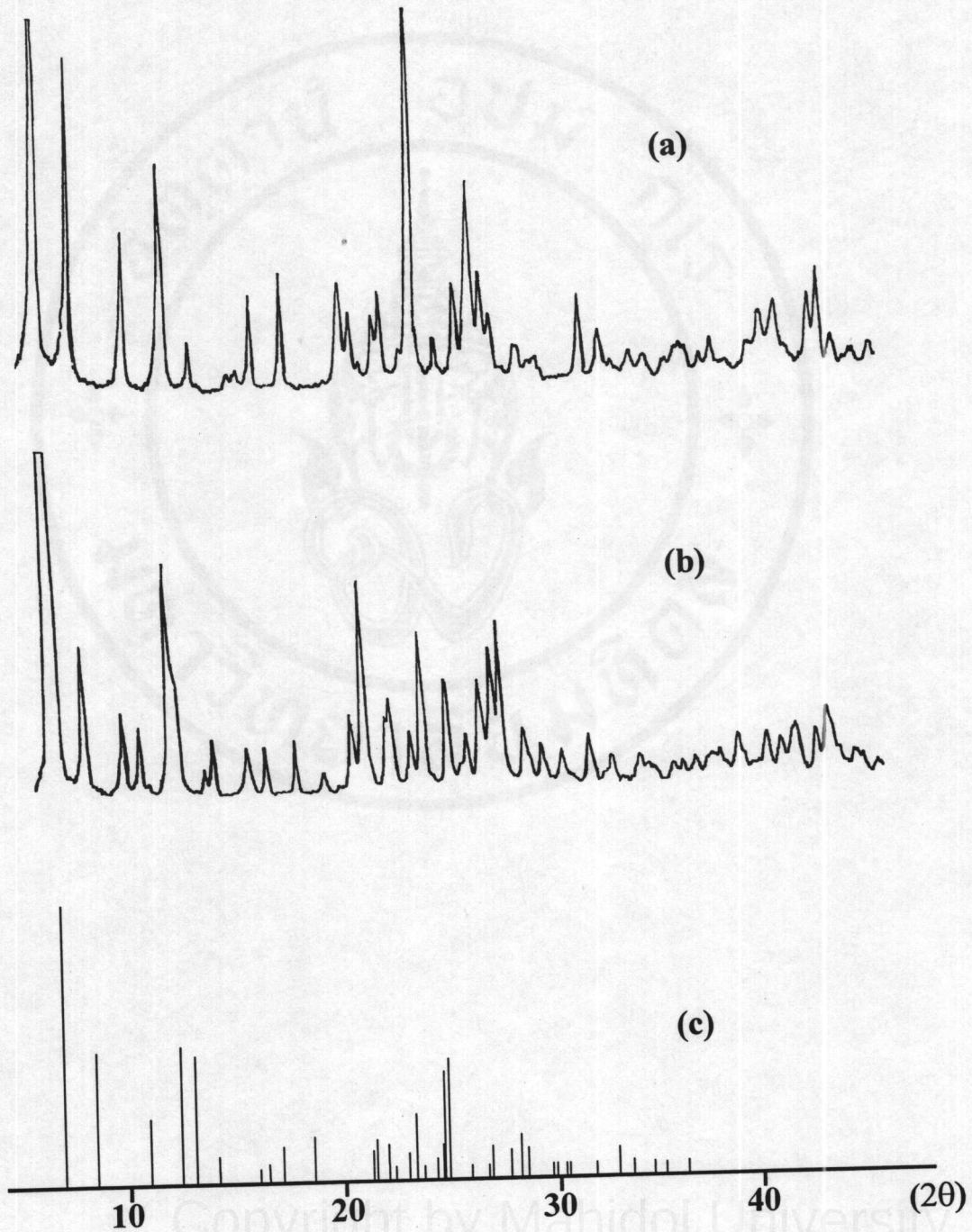

Figure 4.6 XRD patterns for (a) ZCS (b) $ZrOCl_2.8H_2O$ (Fluka) and (c) $ZrOCl_2.6H_2O$ from JCPDS database[47]

The DSC thermogram of ZCS shows in Figure 4.7. Endothermic bands in the range 80 - 200 °C involved the simultaneous loss of water and hydrogen chloride. Different pattern of the DSC thermogram of ZCS and $ZrOCl_2.8H_2O$ (Fluka) attributed the effect of a number of water molecules in the crystal. Above 200°C no significant bands could be detected [75]. The exothermic peak at about 467°C seemed to be the crystallization of ZrO_2 [21].

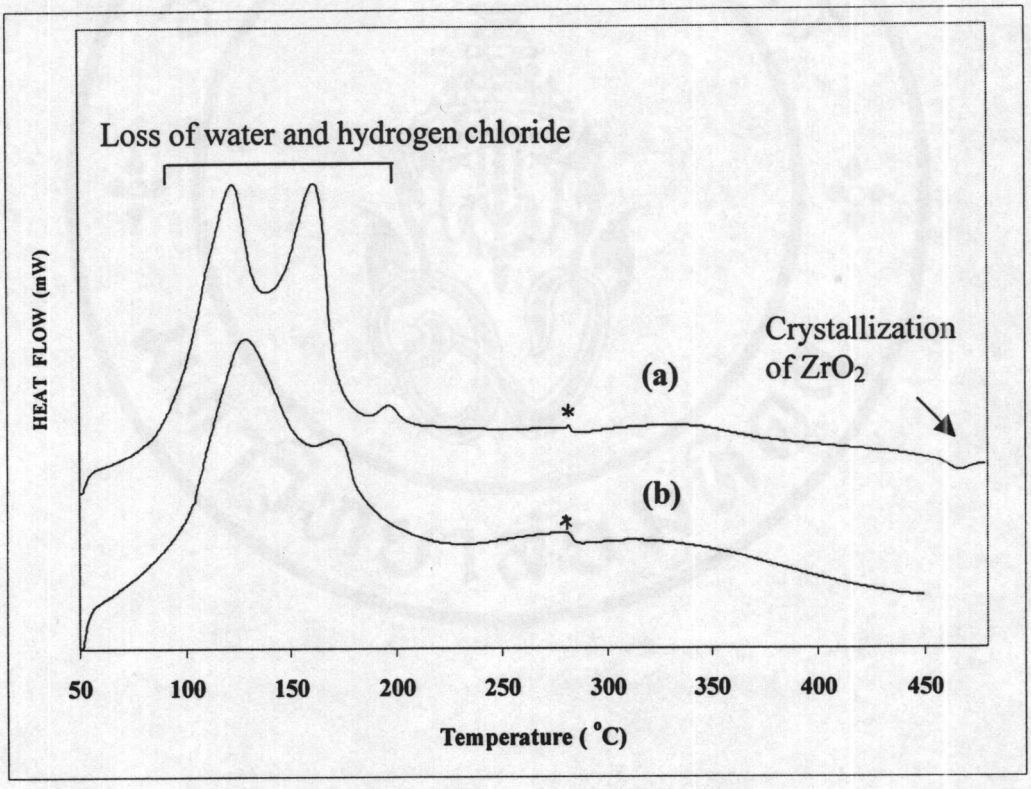

* instrumental defect

Figure 4.7 DSC thermograms for (a) ZCS and (b) $ZrOCl_2.8H_2O$ (Fluka)

The microstructure of ZCS in Figure 4.8 shows the crystals, which appear the needle form. The sample crystal size is approximately of 80 μm in length.

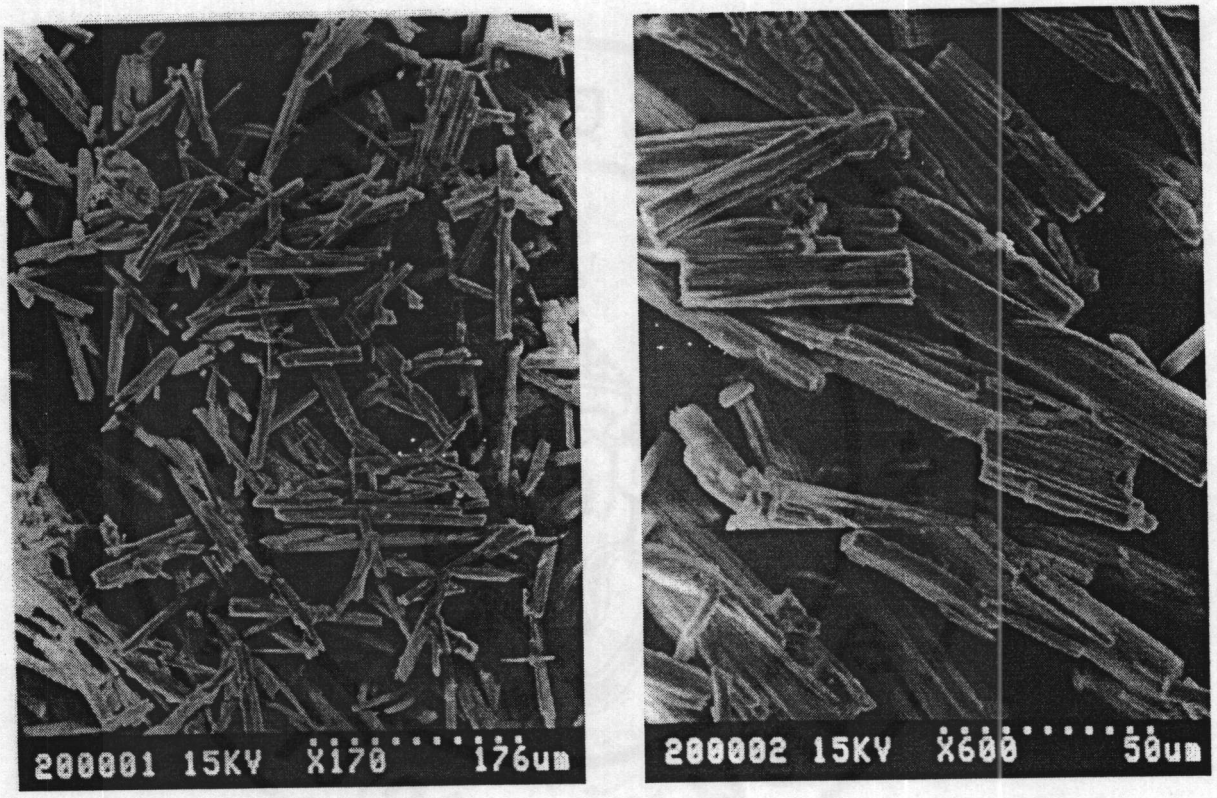

Figure 4.8 Scanning electron micrographs for ZCS

4.2.2 Zirconyl Nitrate Synthesis, ZNS

The structure of zirconyl nitrate hydrate structure was suggested by McWhan and Lundgren [67] to be $Zr(OH)_2(NO_3)_2(H_2O)_4$ structure in 1963 (Figure 2.1). It consists of chains of zirconium atoms, which are joined by double bridges of hydroxide ions. The coordination Zr-O can alternative depend on a number of coordinating groups, which either H_2O or NO_3^-.

The infrared spectra of zirconyl nitrate hydrate were presented in Figure 4.9. The spectrum of ZNS is very similar to each zirconyl nitrate hydrate compounds. There are 1582 - 1514, 1045 - 1012 and 1299 - 1279 cm^{-1}, which are usually assigned to the coordinate unidentate nitrato group (ν_4, ν_2, ν_1 respectively). Besides at 1380 cm^{-1} is interpreted only as the stretching vibration of nitrate ion. In the 3000-3500 cm^{-1} range is a broad band in the spectra of the stretching vibrations of water. The sharp band at 3538 cm^{-1} is attributed to the O-H stretching of bridging hydroxide. The broad intense absorption at about 3400 cm^{-1} is assigned to the symmetic and asymmestic O-H stretching of coordinated and lattices water. There are also the bands of the deformation vibration of water with frequency about 1610 cm^{-1}. The weak band at 868 cm^{-1} is assigned to the rocking mode of coordinated water. The band at 800 - 500 cm^{-1}, can be assigned to the frequencies of the $Zr\text{-}O_2\text{-}Zr$ chains. Besides, the bands characterizing the Zr-O are usually located in 445-425 cm^{-1} range. The infrared spectra results were summarized in Table 4.4. These results are not clear in the distinct identified type of zirconyl nitrate hydrate.

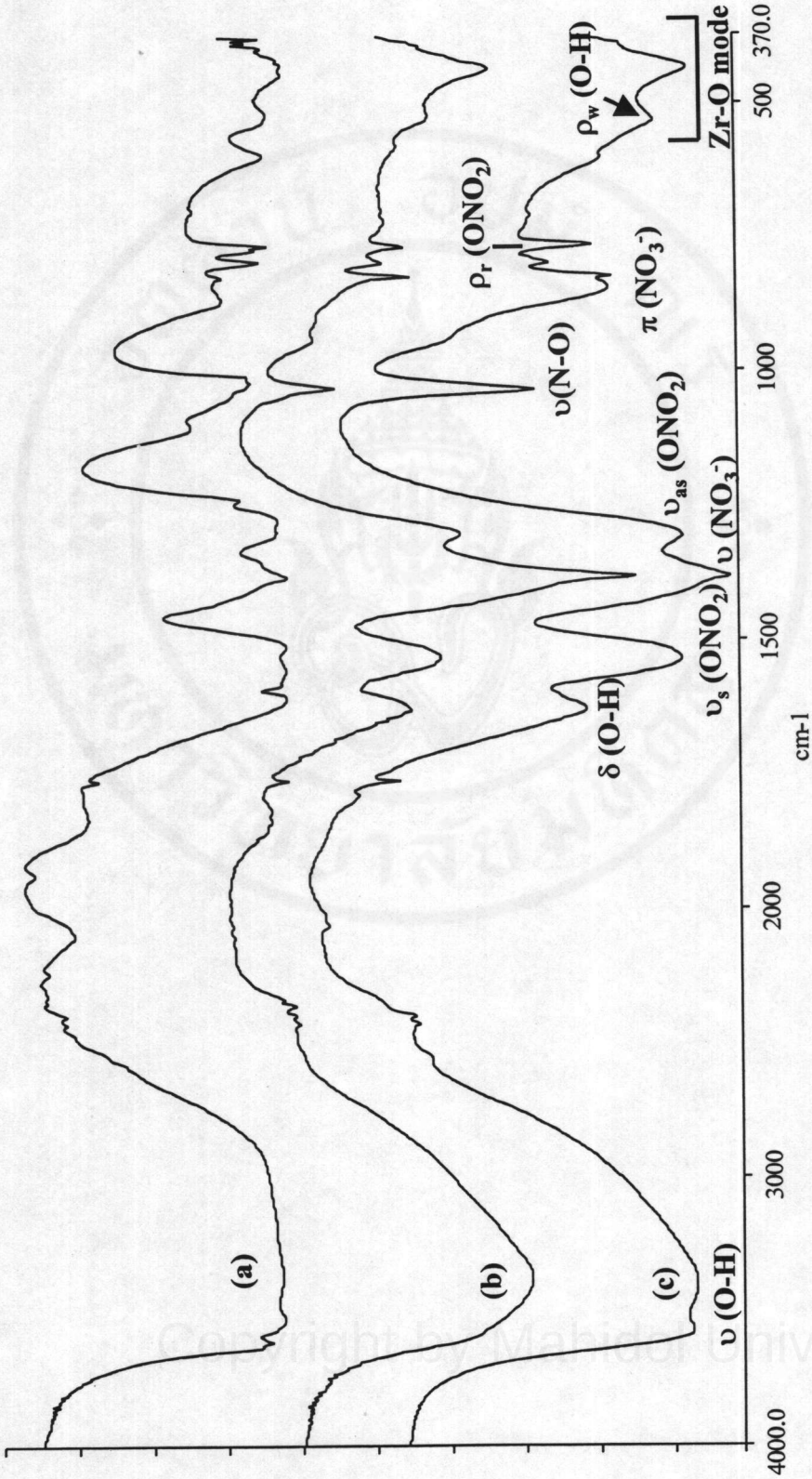

Figure 4.9 Infrared spectra for (a) ZNS, (b) $ZrO(NO_3)_2.6H_2O$ (Fluka) and (c) $ZrO(NO_3)_2.xH_2O$ (JM)

Table 4.4 Infrared spectra and band assignment for $ZrO(NO_3)_2.6H_2O$ (Fluka), $ZrO(NO_3)_2.6H_2O$ (JM) and ZNS

Assignment [75,83]	Frequency, cm^{-1}		
	$ZrO(NO_3)_2.6H_2O$ (Fluka)	$ZrO(NO_3)_2.xH_2O$ (JM)	ZNS
HOH str			3616 sp
		3561.72	3535 s
	3378.03	3401.14	~3381 b
HOH def	1632.46	1630.02	1610 s
	1537.49	1538.87	1582 w
Asy str(ONO_2)			1557 s
			1514 s
NO_2 asy str (NO_3^-)	1384.29	1384.20	1384 s
NO_2 asy str(ONO_2)	1304.05	1307.63	1299 s
	1032.24		1279 s
			1237 m
			1103 m
N-O str (ONO_2)		1036.74	~1045 sh
			1023 m
	940.68	936.95	1012 m
Rocking (H_2O)	907.12	848.83	868 m
NO_2 def (NO_3^-)	825.06	825.93	826 m
Nonplanar rocking (ONO_2)	799.77	800.54	797 s
Zr-O_2-Zr, ν_3 and ν_5 and	769.02, 721.00	766.86, 711.75	775 s, 767s
Zr-O mode	668.398, 582.60	601.25, 533.41	698 w, 599 s
	519.19, 433.80	432.83	523 s, 445 s
			425 s

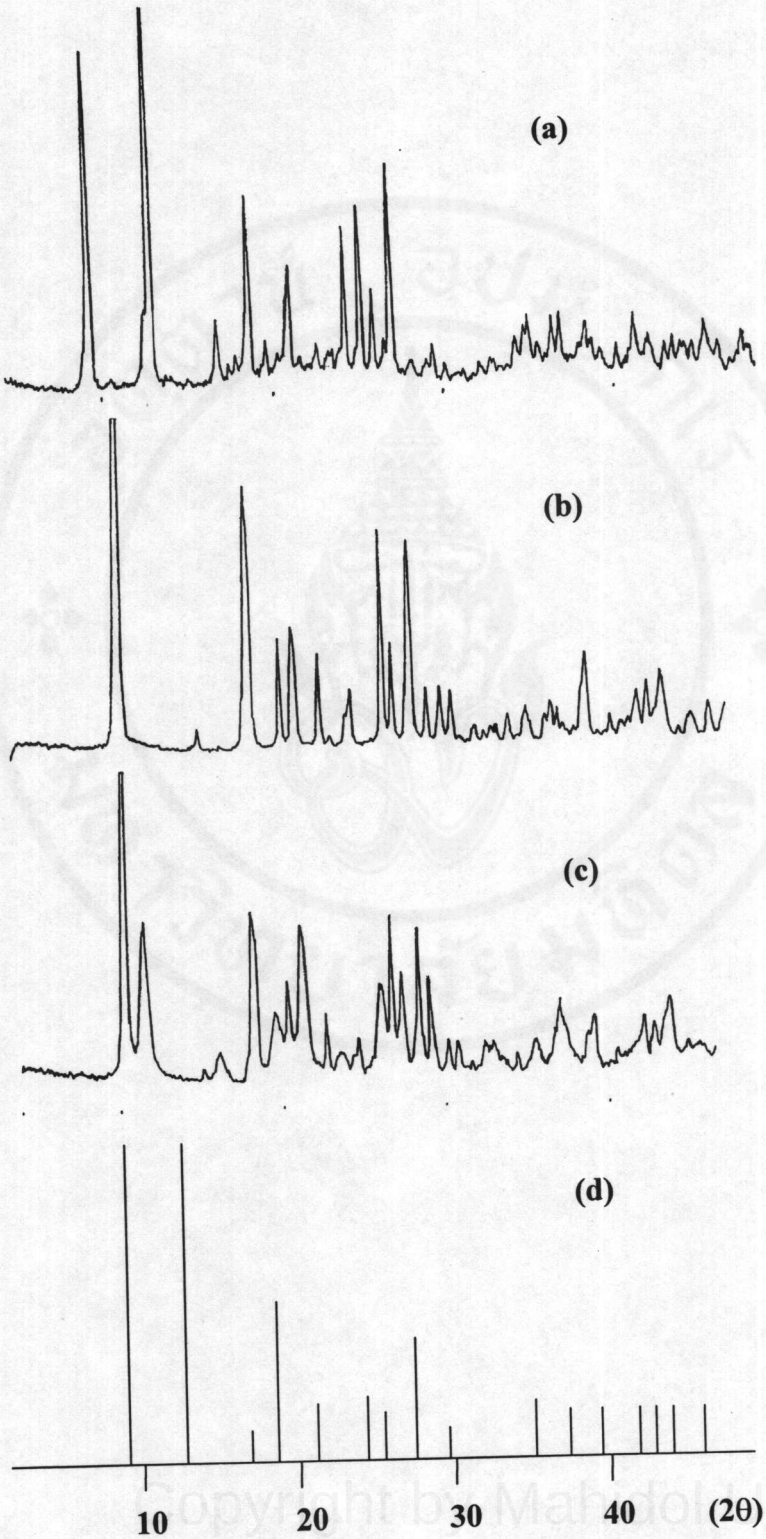

Figure 4.10 XRD patterns for (a) ZNS (b) $ZrO(NO_3).6H_2O$ (Fluka) (c) $ZrO(NO_3).xH_2O$ (JM) and (d) $ZrO(NO_3)_2.2H_2O$ from JCPDS database [47]

The XRD patterns for $ZrO(NO_3)_2.xH_2O$ (JM) and $ZrO(NO_3)_2.6H_2O$ (Fluka) are not similarly with ZNS. The XRD patterns of ZNS compared with $ZrO(NO_3)_2.2H_2O$ that show similarly pattern peak as shown in Figure 4.10. The different of XRD patterns may be the effects from water contain in lattice.

DSC thermograms range 80 - 270°C corresponds to the evaporation of water and nitric acid, which affected from each different nitrate group. The crystallization of zirconia occurs at about 474°C as shown in Figure 4.11.

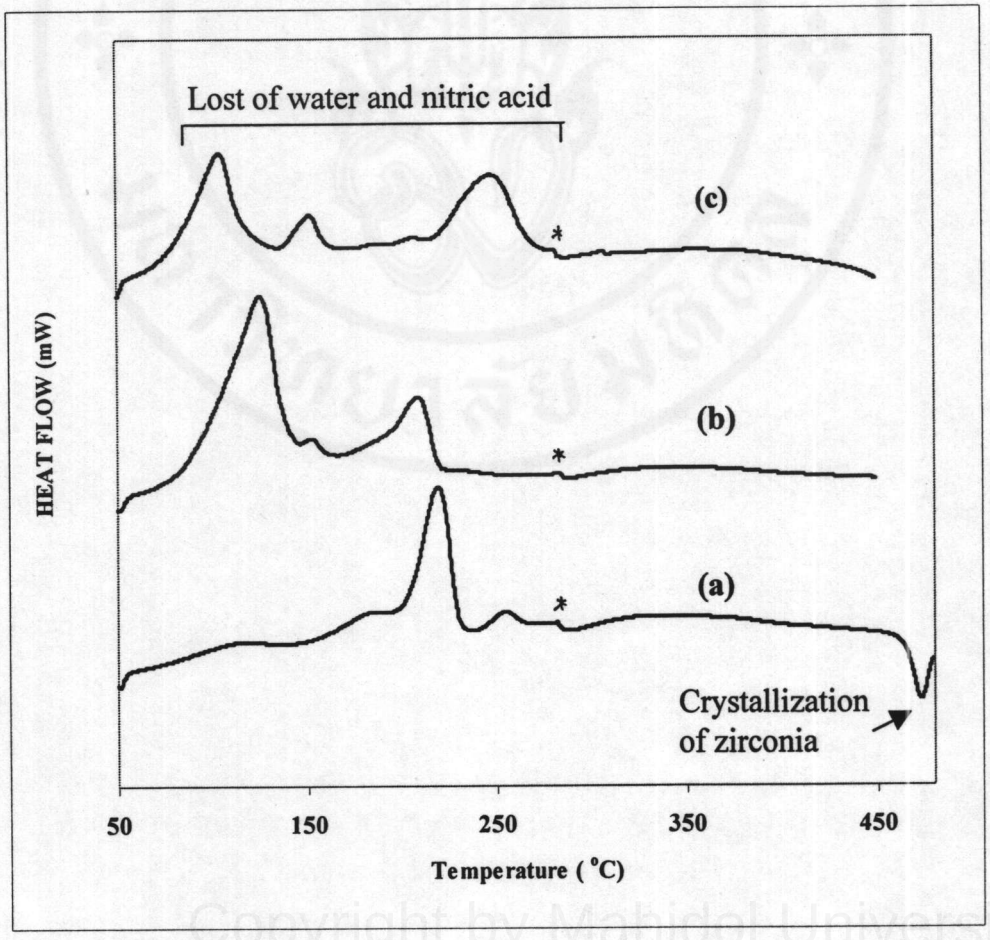

* is instrument defect

Figure 4.11 DSC thermograms for (a) ZNS (b) $ZrO(NO_3)_2.6H_2O$ (JM) and (c) $ZrO(NO_3)_2.xH_2O$ (Fluka)

The morphology of ZNS was investigated by using SEM. The Scanning electron micrographs show an agglomerate small particle as presented in Figure 4.12.

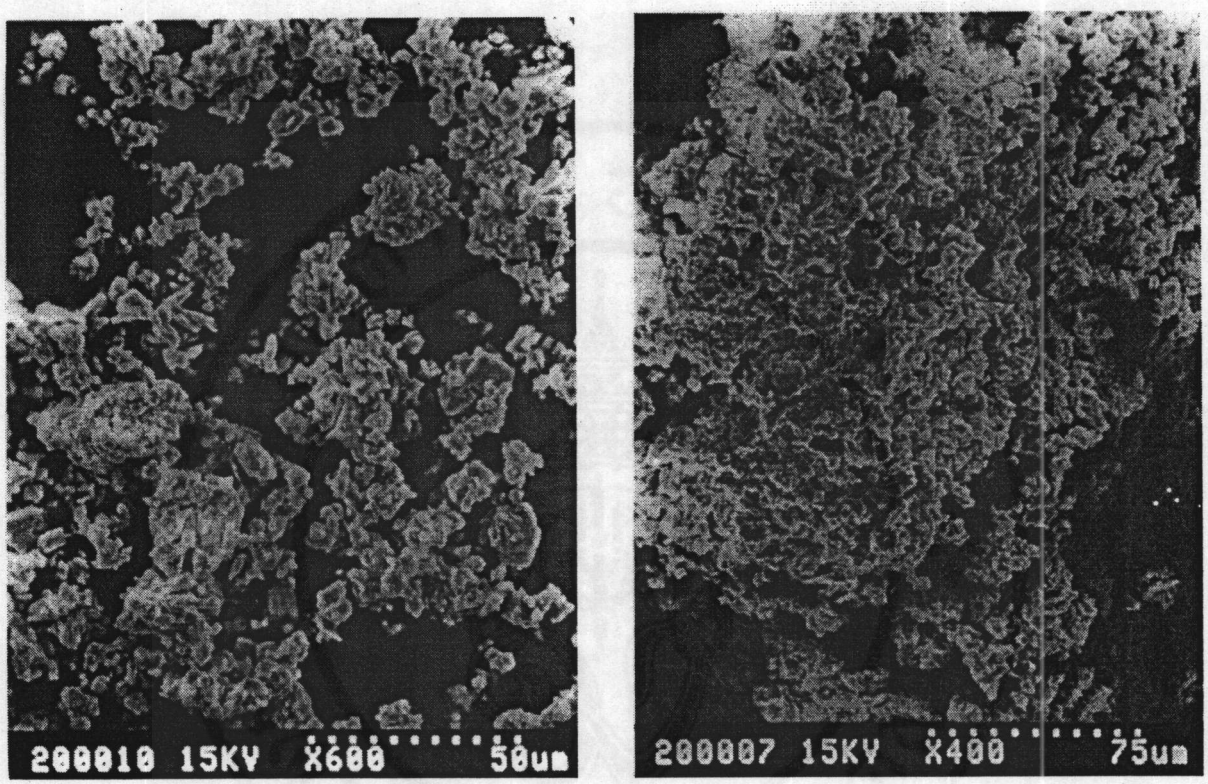

Figure 4.12 Scanning electron micrographs for ZNS

4.3 The Characterization of Zirconia, Prepared by SEG Method

ZNS was selected as a precursor in SEG method because zirconyl nitrate is cleaned and easily burned out when compared with zirconyl chloride [10]. In dispersion process, the magnetic agitator was generally used for generating droplet and homogenizing the immisible phases. Ultrasonic agitation known as a technique for decreasing agglomeration was applied in this study. Therefore, the effect of using ultrasonic was studied. This section consists of two parts. A first part is an investigation and characterization of zirconia, obtained by using both magnetic and ultrasonic agitations to generate droplets. The another is the result for zirconia synthesis without using ultrasonic in agitation process.

4.3.1 Zirconia Preparation using Ultrasonic and Magnetic Agitators

Infrared spectra of zirconia at various calcine temperatures are shown in Figure 4.13. Two broad absorption bands, at ~3400 cm^{-1} and ~1630 cm^{-1} were assigned for hydroxyl and coordinated water, respectively. The presence of Zr-O mode at ~740 cm^{-1} was determined monoclinic phase [26]. Therefore the identification of zirconia phase was predicted by the Zr-O mode. The vibrational band of the monoclinic phase appeared firstly at 500°C. The Infrared vibration band for zirconia powder, calcined at 1350°C presented a Zr-O mode of monoclinic characteristic peak, it was probably due to the complete formation of monoclinic phase.

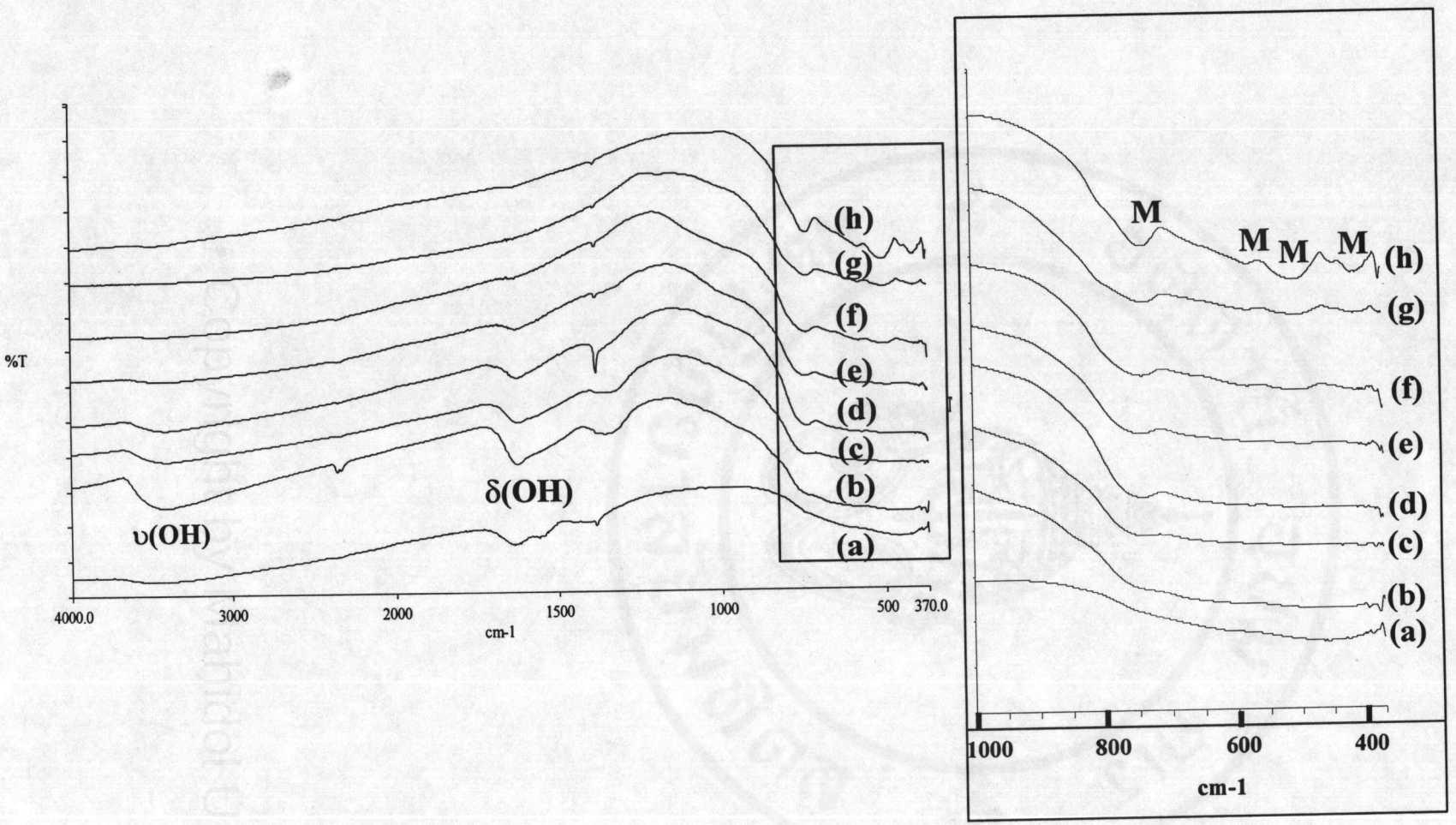

Figure 4.13 Infrared spectra for ZrO_2 at different calcine temperatures (a) 300°C (b) 400°C (c) 500°C (d) 600°C (e) 800°C (f) 1000°C (g) 1200°C and (h) 1350°C

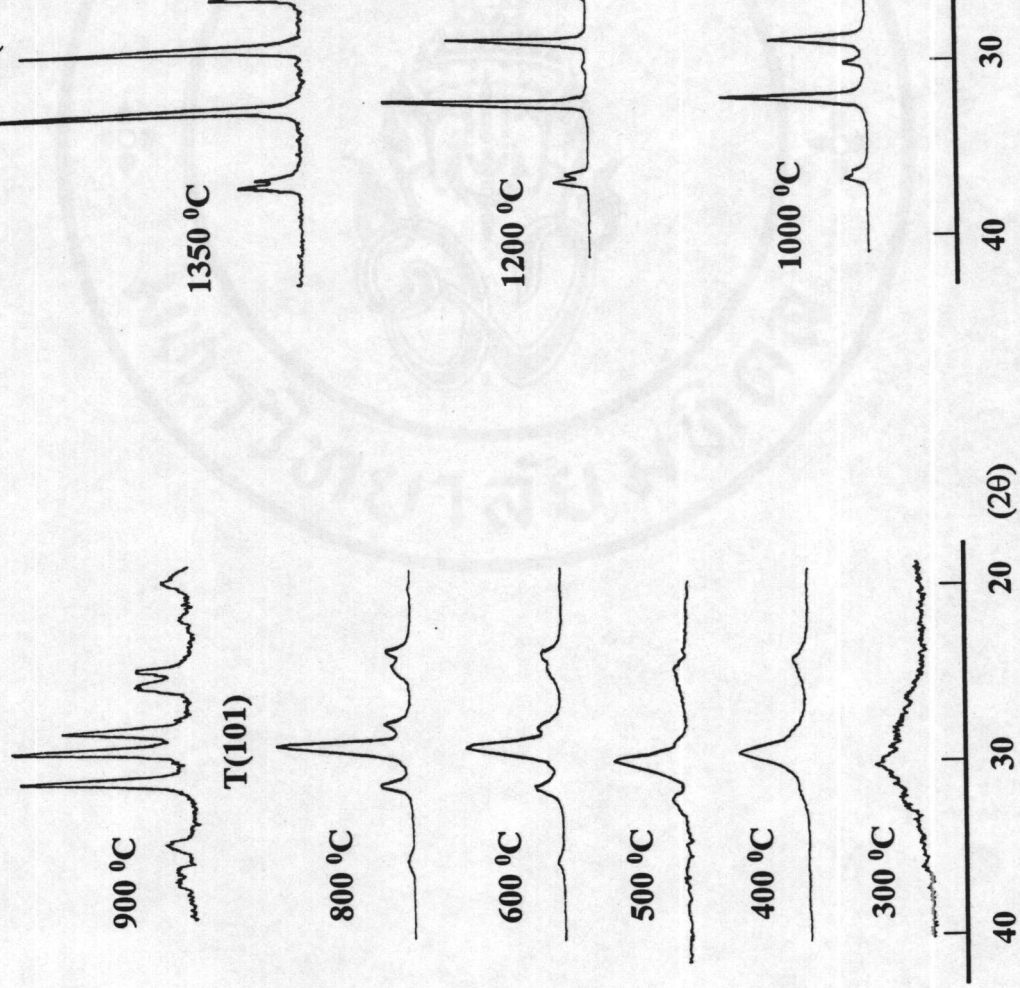

Figure 4.14 XRD patterns for ZrO_2 powder at different calcine temperatures

The XRD patterns for ZrO_2 powder, at different calcined temperatures, are shown in Figure 4.14. Percentage volumes of tetragonal phase and lattice parameter were analyzed using the equations in Section 2.3.1. The crystal size was estimated using the Scherrer equation. Results could determined from intensities of line (111) and ($\bar{1}11$) of monoclinic ZrO_2, and line (101) of tetragonal ZrO_2. These results of zirconia were summarized in Table 4.5.

Table 4.5 Summary results of ZrO_2 at different calcined temperatures

Sample code	Calcine temperature (°C)	% Volume fraction of t-ZrO_2	Particle size, t-ZrO_2 (nm)	Particle size, m-ZrO_2 (nm)
$3ZrO_2$	300	-	-	-
$4ZrO_2$	400	100	8.387	-
$5ZrO_2$	500	80.17	10.399	7.602
$6ZrO_2$	600	78.95	11.731	10.682
$8ZrO_2$	800	69.20	15.901	16.179
$9ZrO_2$	900	37.00	21.168	20.060
$10ZrO_2$	1000	8.85	44.780	27.92
$12ZrO_2$	1200	1.17	-	50.328
$13.5ZrO_2$	1350	0.00	-	59.757

t-ZrO_2 = tetragonal phase, m-ZrO_2 = monoclinic phase

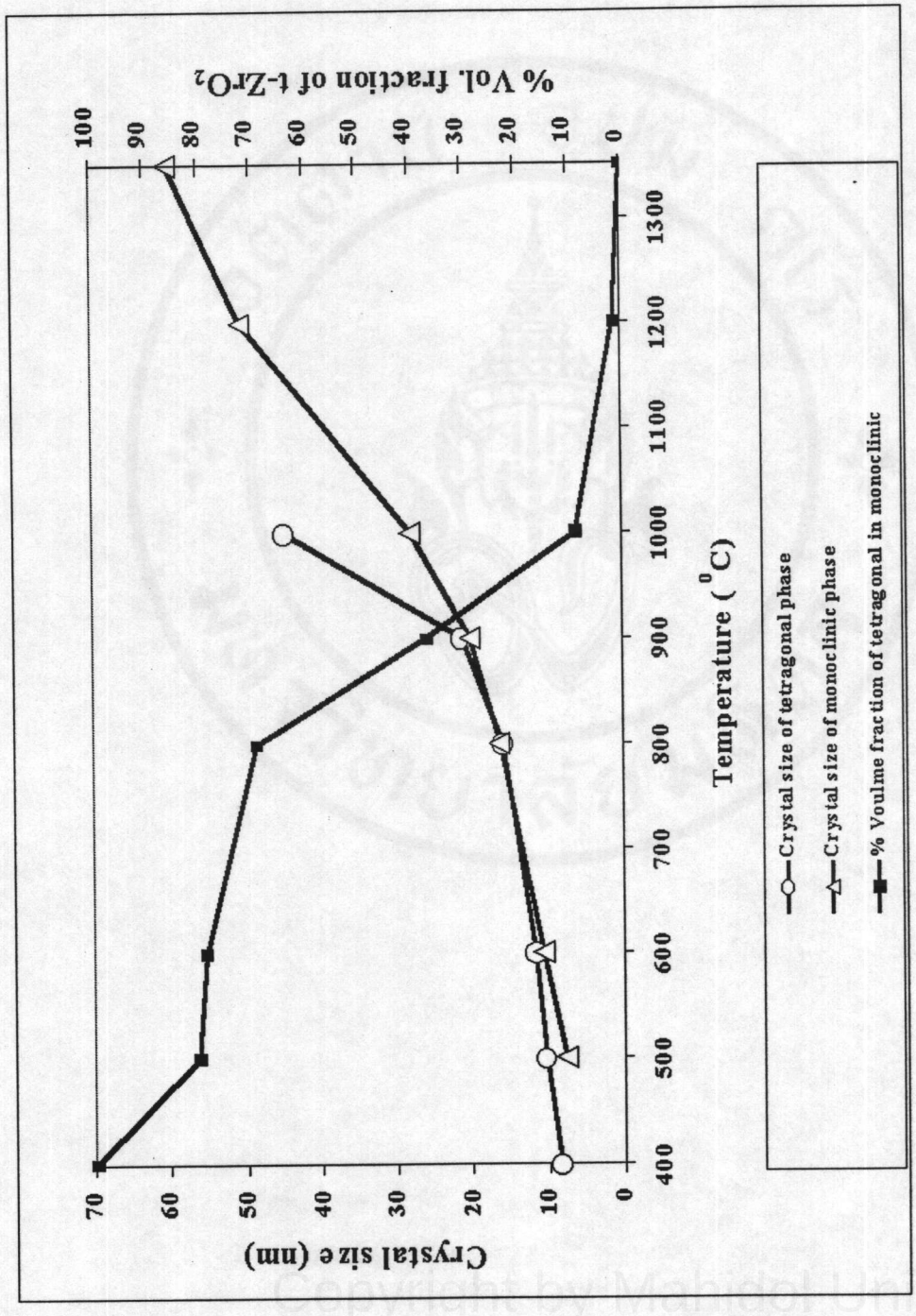

Figure 4.15 Relative % volume fraction of tetragonal zirconia and thermal evolution of tetragonal and monoclinic zirconia crystal size with temperature.

According to Figure 4.15, zirconia was amorphous up to 400 °C that identified the metastable tetragonal phase. The mixture of metastable tetragonal and monoclinic ZrO_2 found between 500°C and 1200°C. Finally calcined ZrO_2 powder at 1350 °C shown only monoclinic phase. The phase transition results agreed with the infrared result. The crystal size, which was estimated using the Scherer equation, shown the evolution of crystal size with temperature. The tetragonal crystal size did not significantly change with temperature in the region 400-900°C. The monoclinic crystal size at 500°C was slightly smaller than the tetragonal, and increased slowly with increasing temperature. However, at 1000 -1200°C a faster growth of tetragonal and monoclinic crystal was observed. This phenomenon could be explained the higher temperature caused compression of small powder and agglomerate to large particle [3].

The occurrence of metastable tetragonal phase was not well understood at this time. Several factors were probably involved [21,22].

(i) Influence of the particle size

On the basis of the lower value of the surface energy in the tetragonal phase (γ_t) in relation to the monoclinic phase (γ_m). Garvie [19] considered that in order to stabilize the tetragonal phase at low temperature the following equation should be satisfied.

$$(G_t - G_m) + S_t\gamma_t - S_m\gamma_m \leq 0$$

Where G is the molar free energy in single crystals, γ is the surface energy, and S is the surface area. Garvie suggested that the particle size for stabilizing the tetragonal phase must be ≤ 30 nm.

(ii) Influence of the structural similarities

Livage et al. [20], after a complete study by X-ray and neutron diffraction on amorphous ZrO_2, found that the interatomic Zr-Zr and Zr-O distances were similar to corresponding ones in the tetragonal structure (Figure 4.16).

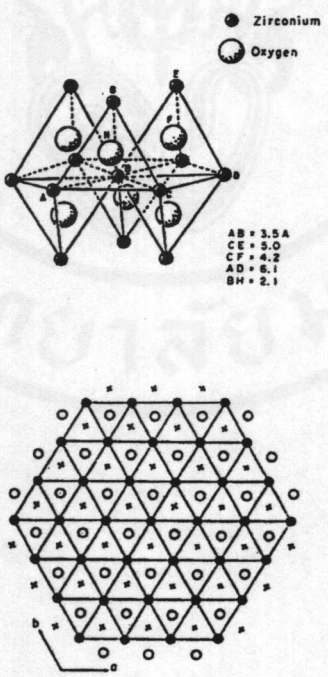

(a)

(b)

Figure 4.16 Models for tetragonal and amorphous zirconia (a) Representation of tetragonal zirconia. The Zr plane represented are the (111) planes of a fluorine-type cell. (b) Suggesested model for amorphous zirconia structure. ● = Zr atoms; ○ = oxygen atoms situated above the Zr plane; X = oxygen atoms situated under the Zr plane [20]

(iii) Stabilization produced by lattice stain

Mitshuashi et al. (24) claimed that domain boundaries inhibit the t → m transformation; the existence of single-domain tetragonal ZrO_2 was explained by the absence of an active nucleation site.

The thermal process and crystallization behaviors of the ZrO_2 powder were investigated by using DSC methods as shown in Figure 4.17. The endothermic region was found in the range between 50 and 150°C and it could be attributed to the organic burnout and nitrate decomposition. The exothermic band about 350 °C could be related to the beginning of crystallization [21], This result is agreed well with the XRD results in Figure 4.14.

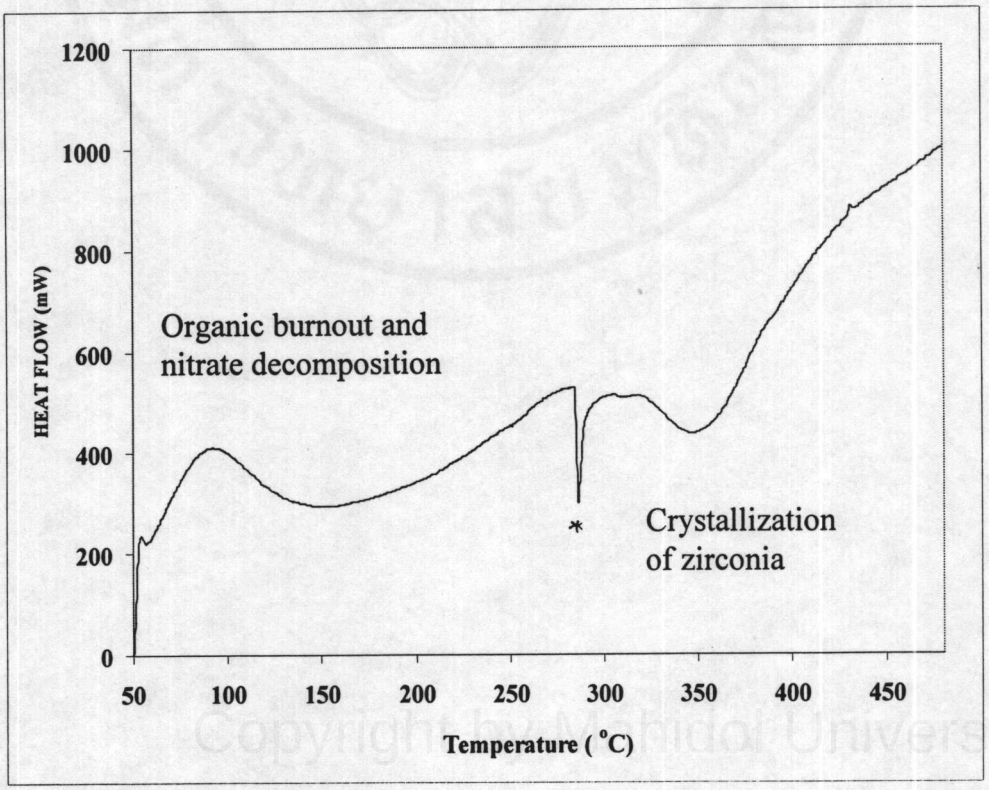

* Instrumental defect

Figure 4.17 DSC thermogram for ZrO_2 prepared by SEG method

In Figure 4.18 shows a particle size distribution of zirconia powder measured by Laser particle size analysis instrument. The ranges of size were 0.4 – 60 μm and average size was 11.18 μm.

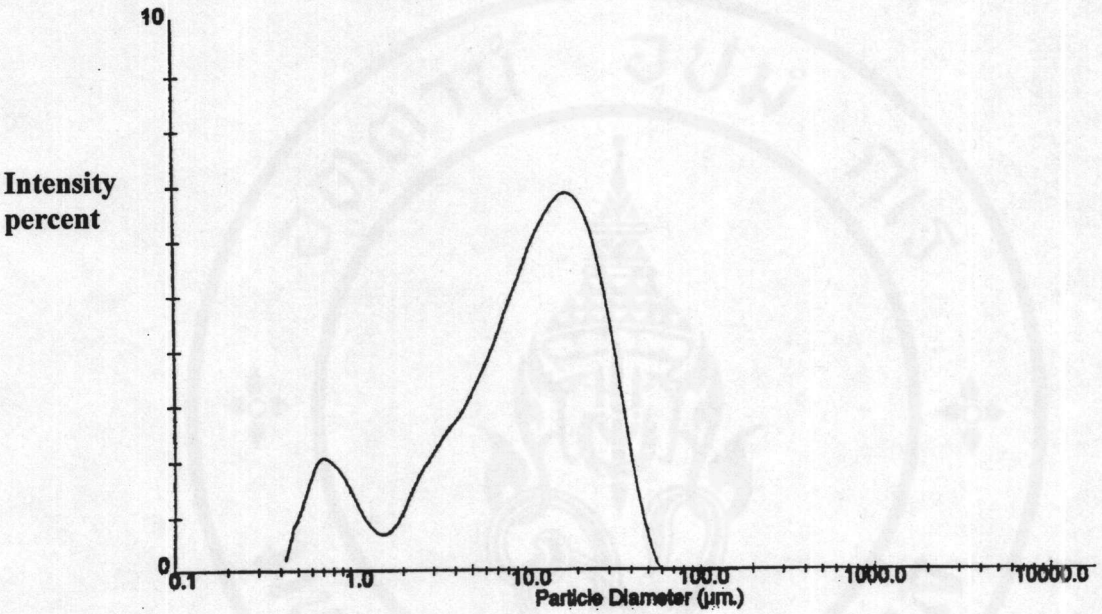

Figure 4.18 Particle size distribution of zirconia particles

The morphology of the particles was investigated by TEM and SEM. It was found that the polyhedral or spherical shapes of the prepared powder were observed in Figure 4.19. TEM micrographs demonstrated the evidence that the aggregated particle of zirconia composed of nanometre-size crystals, which they were loose, attached together in Figure 4.20. TEM and SEM micrographs shown also the change of the crystal size and morphology of zirconia under the difference calcination temperatures. When elevated temperature the fine particles possibly contacted with each other, and finally each particle was agglomerated corresponding to XRD data. This observation could be concluded that the crystal size mainly depended on the calcine temperature.

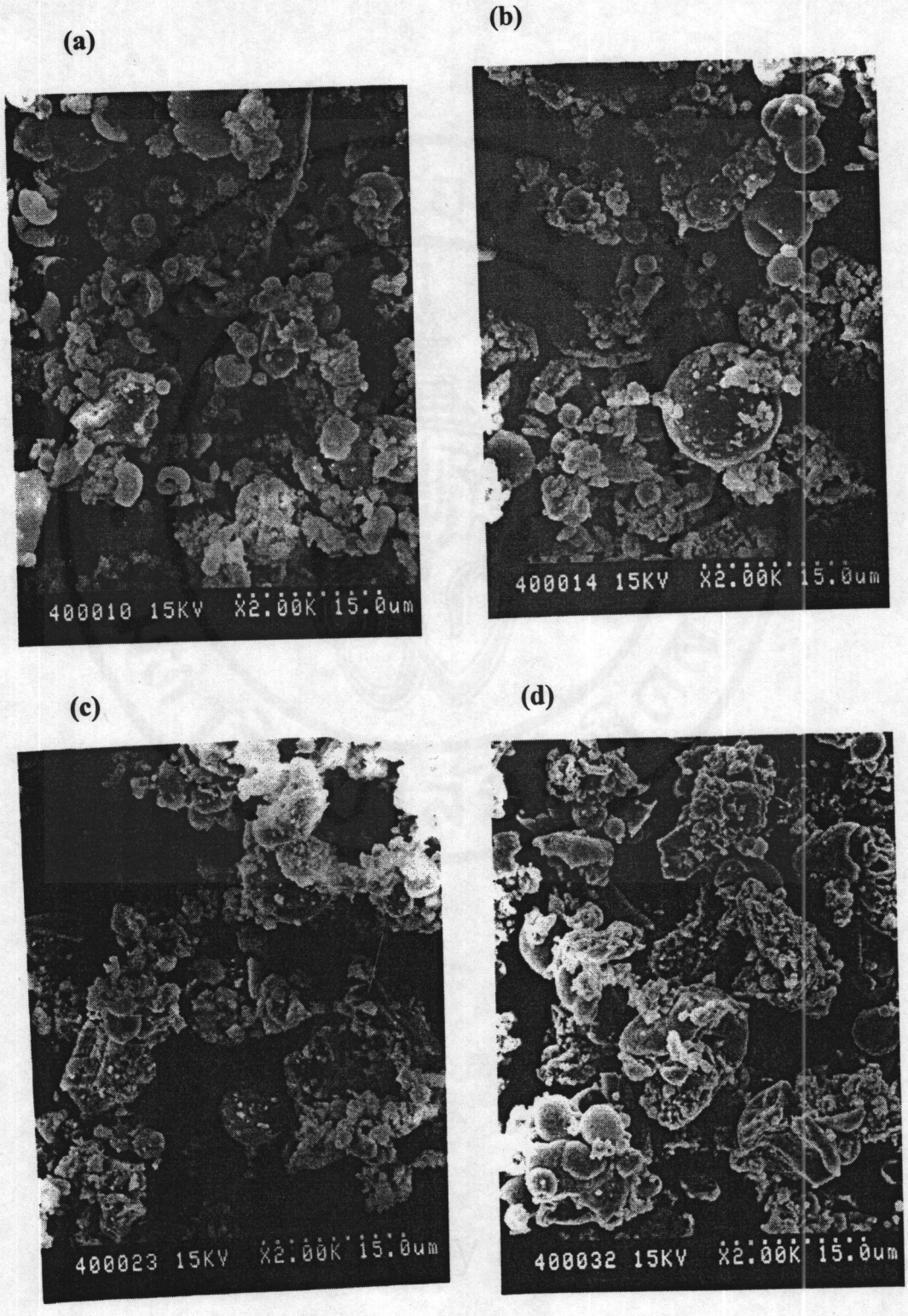

Figure 4.19 SEM micrographs for ZrO_2 at different calcine temperatures (a) 400°C (b) 600°C (c) 800°C and (d) 1000°C

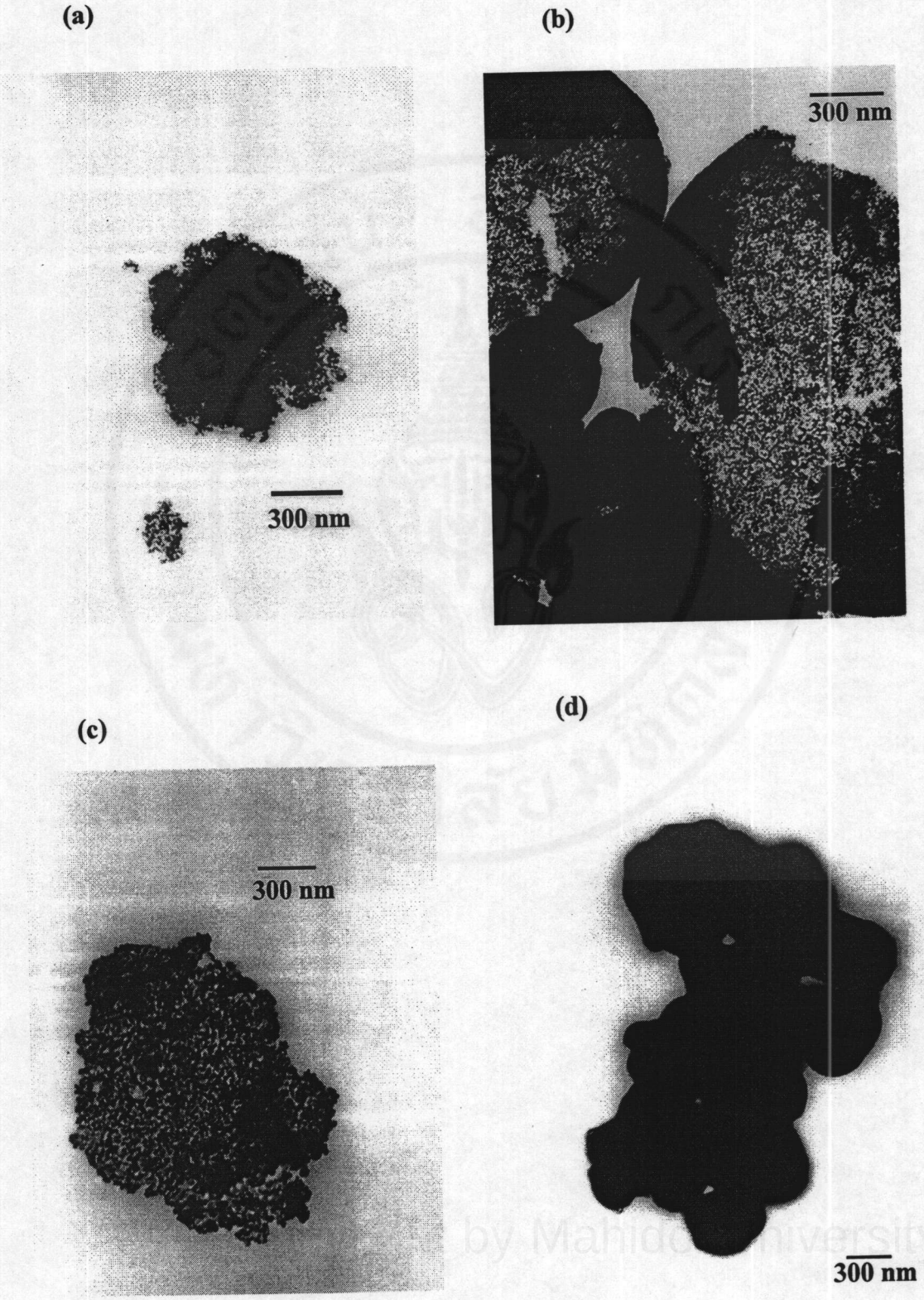

Figure 4.20 TEM micrographs for ZrO_2 at different calcine temperatures (a) 400°C (b) 500°C (c) 600°C and (d) 1000°C

4.3.2 Zirconia Preparation using Stirrer Only and Effect of Agitation

Discussion

In 1995 Gao at el. [36] prepared the stabilized zirconia powder by emulsion method, using only magnetic agitation for homogeneous dispersion. Therefore, only magnetic agitation should be required in zirconia powder preparation. This section shows the result of preparation ZrO_2 by SEG, which using a magnetic agitation only, and these results were compared with the results obtained by using ultrasonic agitation in Section 4.3.1.

The effect of two agitated processes, namely magnetic agitation (s-process) and a combination of magnetic and ultrasonic agitation (su-process) shown some different results. The particle size of s-process was smaller than su-process at same calcine temperature. Besides, the particle size, obtained via s-process shown a slight change with increasing temperature between 600-1000 °C. These results are summarized in Table 4.6.

Table 4.6 The comparison XRD data, crystal size and % volume fraction of tetragonal zirconia, prepared by using ultrasonic agitation and magnetic agitation only.

Calcine tempeature (°C)	crystal size, nm				% Volume fraction tetragonal phase	
	su-process		s-process		su-process	s-process
	Tetragonal	monoclinic	tetragonal	monoclinic		
1000	44.78	27.927	17.40	17.33	8.85	50.0
800	15.90	16.18	12.57	-	69.20	100.0
600	11.73	10.682	9.87	-	78.95	100.0
400	8.387	-	-	-	100.00	-

su-process : magnetic and ultrasonic agitation

s-process : ultrasonic agitator

The results in Table 4.6 indicate that the zirconia products from s-process were more stable than su-process.

Infrared spectra (Figure 4.22) of absorption band at ~ 1000 cm^{-1} was assigned to a bridge of O-H mode. This band appeared indistinctly in su-process, it might be an indicator that the particles agglomerated due to hydrogen bonding of water molecules.

The morphology of zirconia for s-process shown a main spherical particle and a minor polyhedral shape as shown in Figure 4.23. This result similarly appeared with the product via su-process.

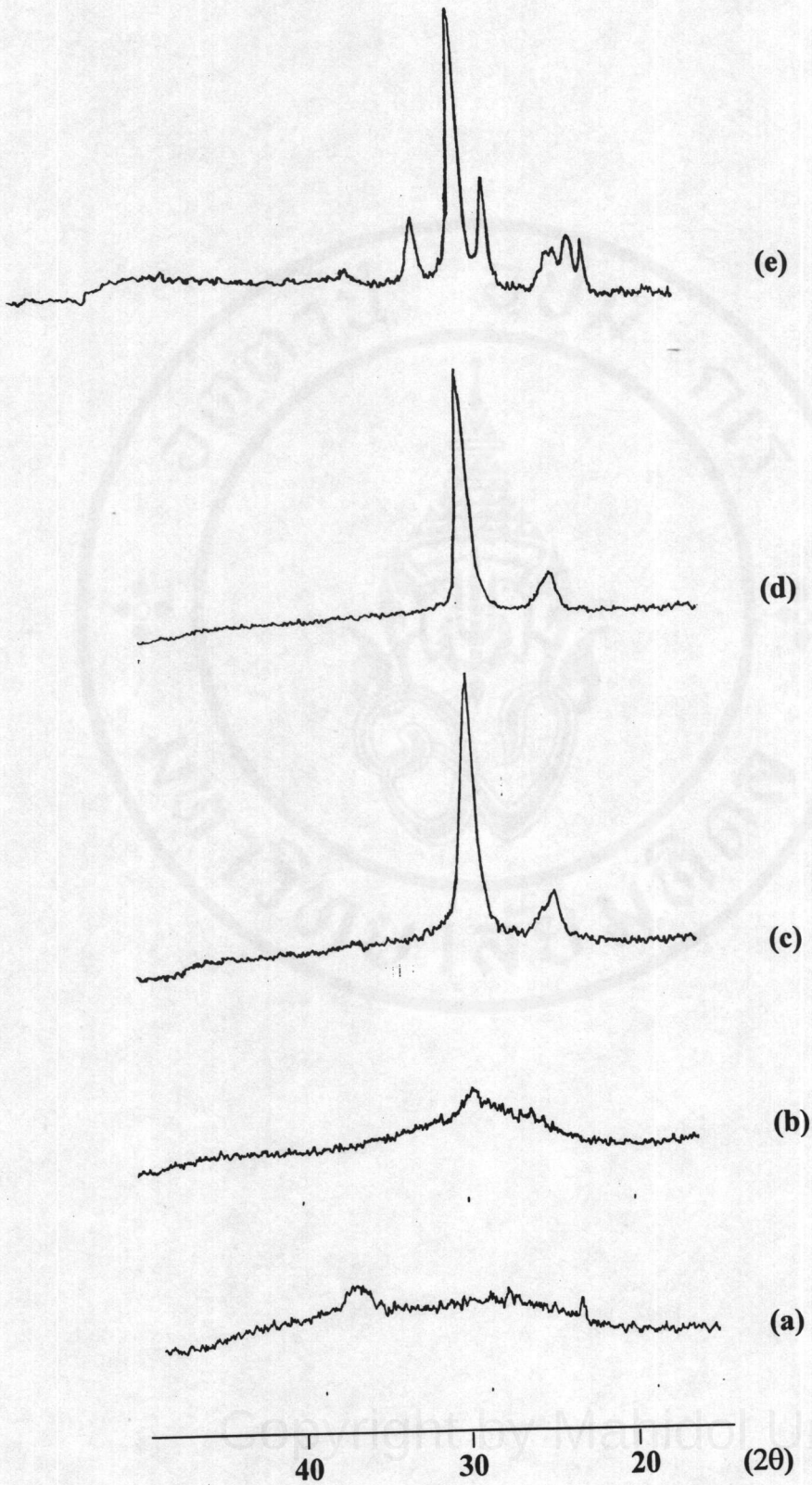

Figure 4.21 XRD patterns for ZrO_2 using only magnetic agitator at different calcine temperatures (a) 140°C, (b) 400°C, (c) 600°C, (d) 800°C and (e) 1000°C

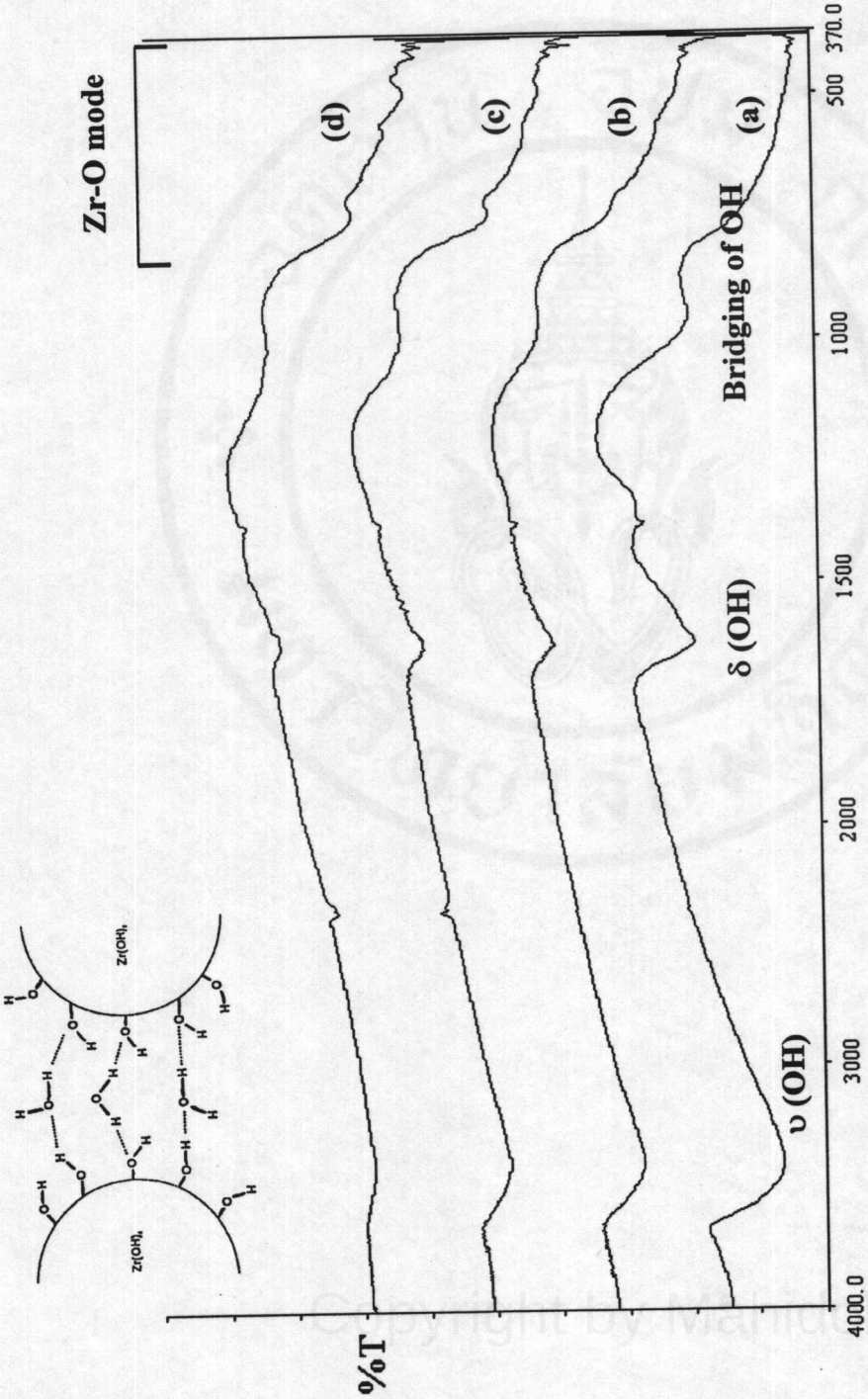

Figure 4.22 Infrared spectra for zirconia using only magnetic agitator at different calcine temperatures (a) 400°C (b) 600°C (c) 800°C and (d) 1000°C

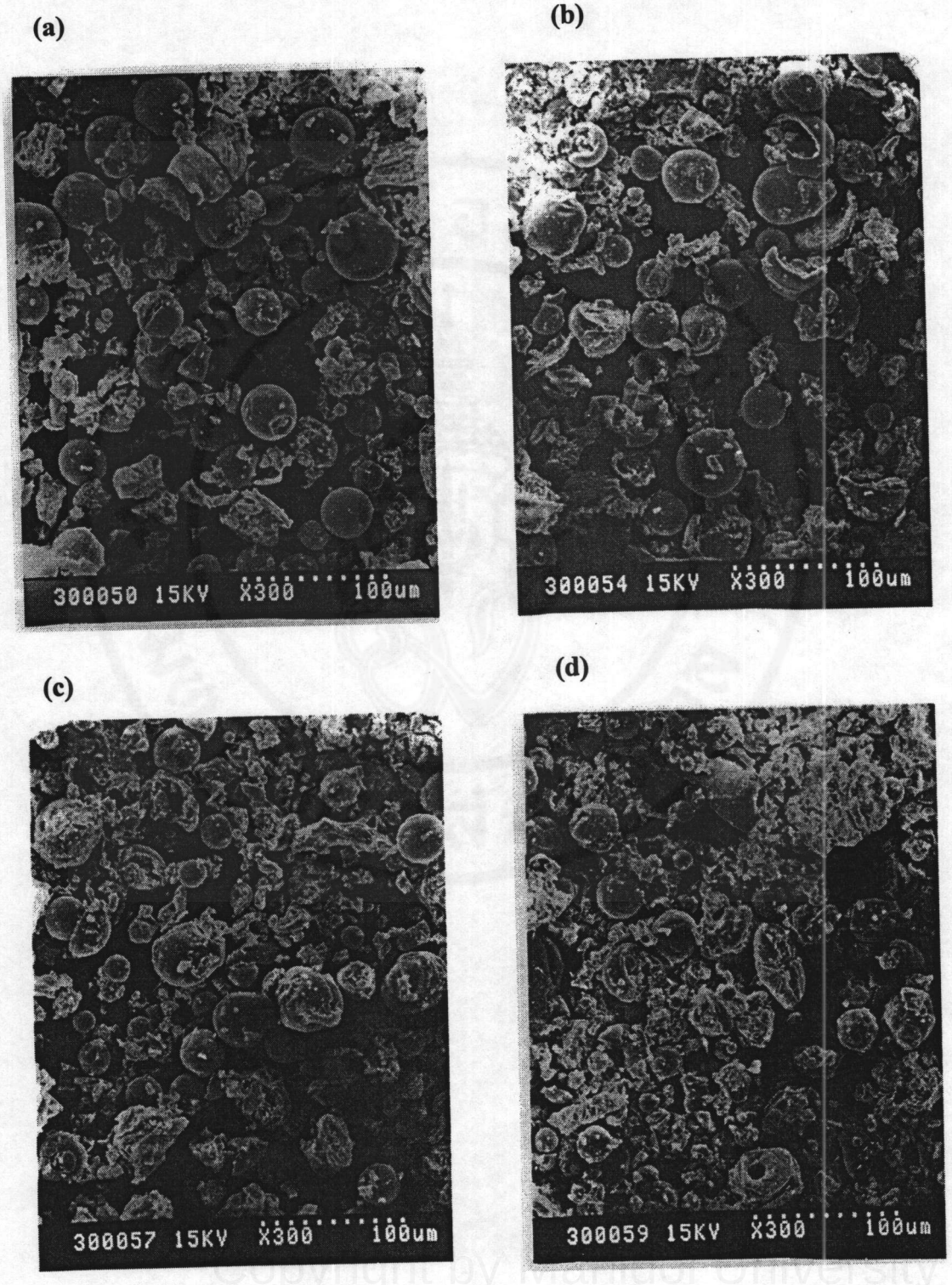

Figure 4.23 Scaning electron micrographs for ZrO_2 using only magnetic agitator at different calcine temperatures (a) 400°C (b) 600°C (c) 800°C and (d) 1000°C

4.4 Vanadium Doped Zirconia, V/ZrO_2

The preparation V/ZrO_2 synthesis pathway was modified from SEG method by adding NH_4VO_3 in solution of zirconyl nitrate. Only simple magnetic agitator was used in this preparation. Furthermore the effect of vanadium content and calcine temperature were investigated. In Figure 4.24 is the infrared spectra results of as-prepared V/ZrO_2, which various vanadium contents were shown. They exhibited that as- prepared V/ZrO_2 contained the functional group of NH_4, NO_3 and Tween 80. Furthermore, infrared spectra of V/ZrO_2 were shown in Figure 4.25 and 4.26, they consisted of spectra that various content of vanadium and temperature. The absorption band at ~1000 $cm^{-1}$and ~800 cm^{-1} appeared distinctly for high vanadia content and high calcine temperature. However, at low calcine temperatures (400°C and 600°C), the bands did not appeared. These bands were compared with spectrum of V_2O_5, the band at 1020 cm^{-1} was indicated to the V=O stretching vibration, and at 818 cm^{-1} the coupled vibration between V=O and V-O-V were assigned [59]. It was attributed that the existence of the crystalline vanadium oxide in zirconia support, and interaction between vanadium with zirconia caused the shift of wavenumber. The absorption band at ~740 cm^{-1} was a dominant Zr-O mode of ZrO_2 monoclinic phase, which could be identified the existence of monoclinic phase. The monoclinic phase appeared only at 800 and 1000°C calcine temperature. This results shown that phase transition of zirconia support was changed faster than zirconia. Some functional group observed at low calcine and low vanadium content, consisted of 3 bands of water modes (~3400, ~ 1610 and ~1000 cm^{-1}).

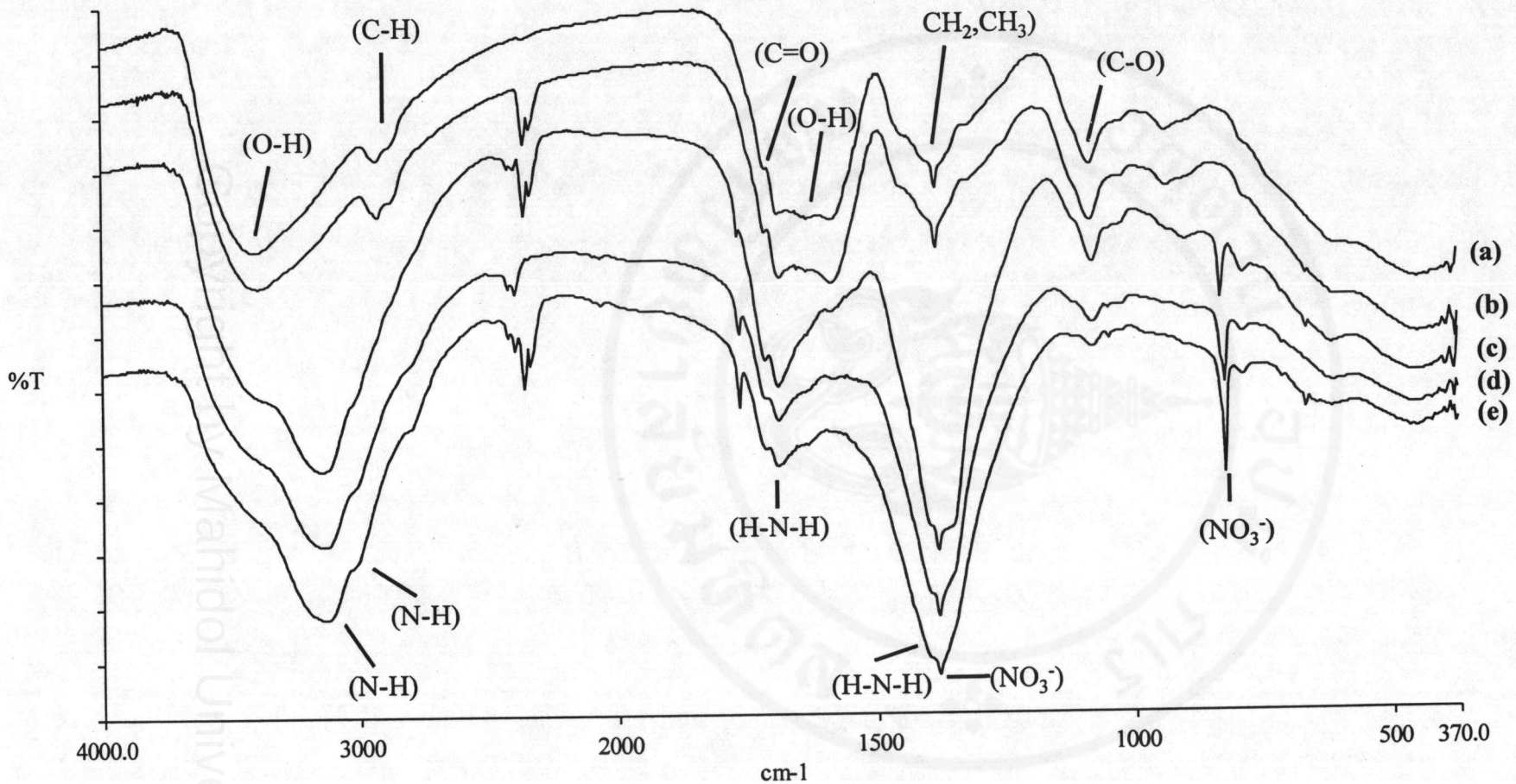

Figure 2.24 Infrared spectra for as-prepared V/ZrO_2 at different vanadium contents (a) 0%V (b) 1%V (c) 5%V (d) 10%V and (e) 15%V

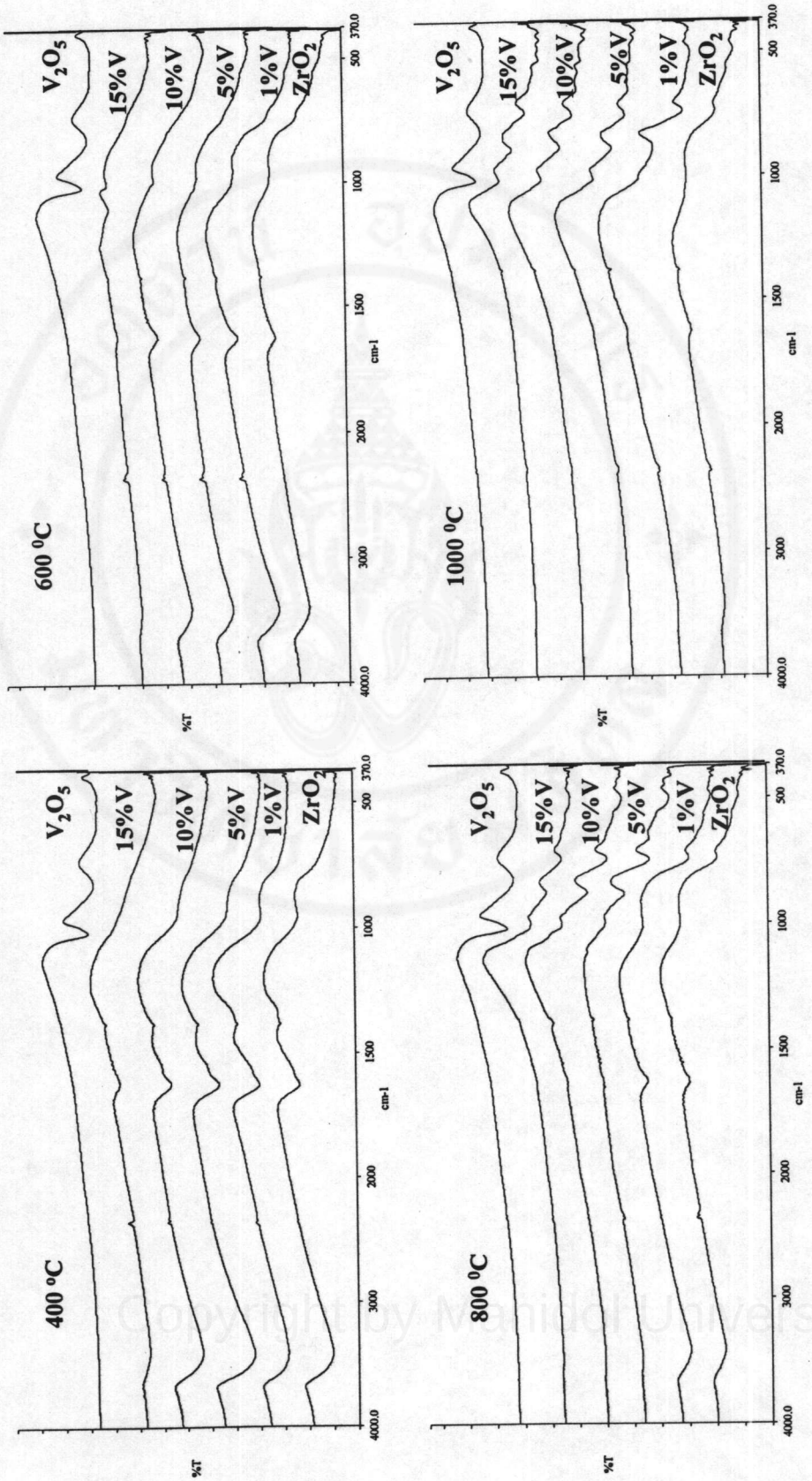

Figure 4.25 Infrared spectra for V/ZrO_2 at different calcine temperatures, compared with weigh percent of vanadium

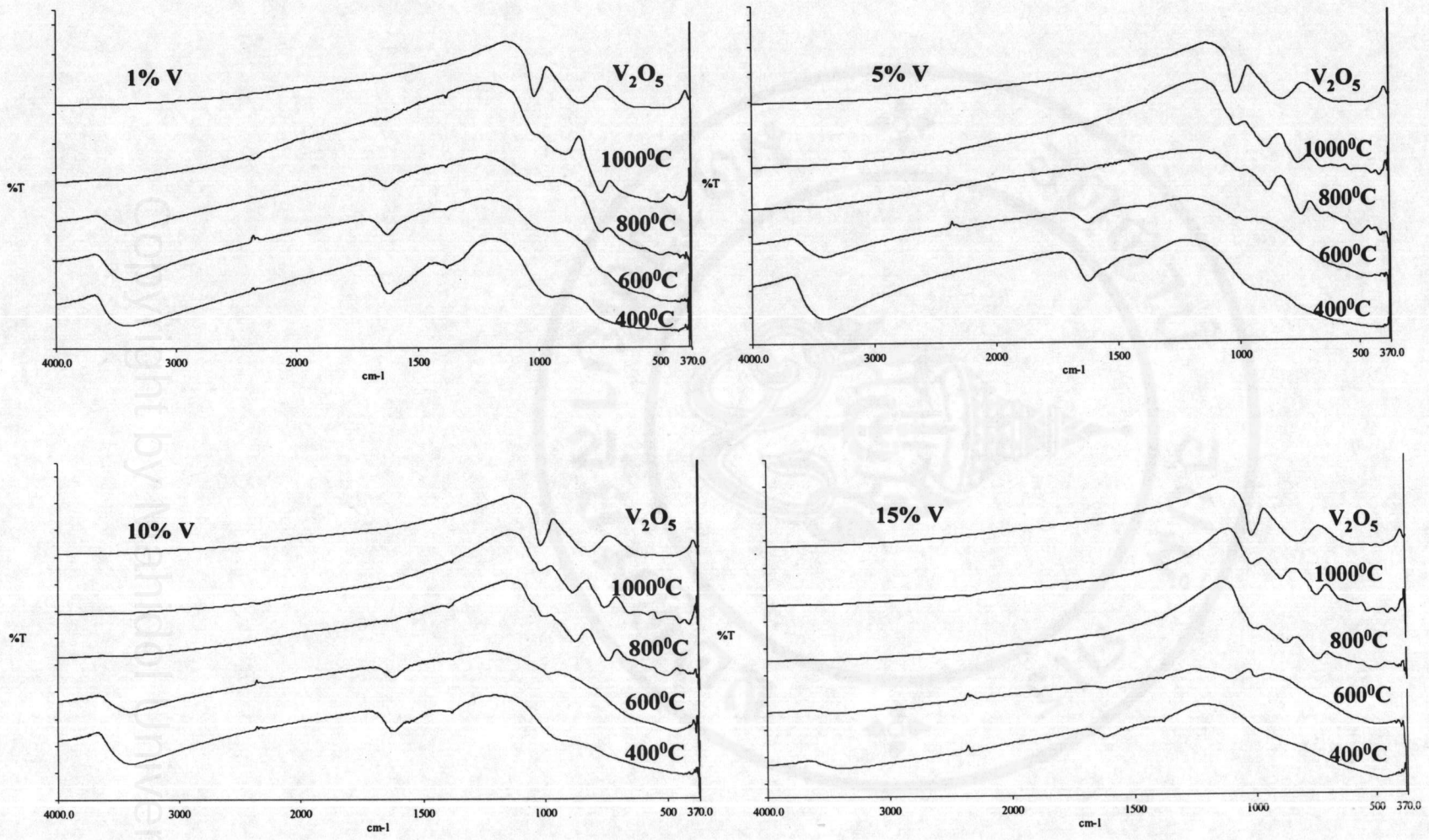

Figure 4.26 Temperature dependent infrared spectra of V/ZrO_2 at different weigh percent of vanadium

Figure 4.27 shows XRD patterns of V/ZrO_2 powders at different calcine temperatures and vanadium content. At drying the powder at 140 °C, diffraction peaks at 2θ = 22.4, 28.8, 32.8, 38.2 and 40.1 were detected, those peaks were possibly produced as NH_4NO_3 crystal [11]. V/ZrO_2 particles were still an amorphous state, until 400 °C, very broad peaks obtained from V/ZrO_2, also no NH_4NO_3 peak was detected due to decomposition. When the calcine temperature increased at 600°C, the peaks appeared only tetragonal phase. At 800 and 1000 °C calcine temperature, peak modified from tetragonal to monoclinic phase, respectively.

Table 4.7 Summary on phase transition for V/ZrO_2

Temperature, °C	0% V	1% V	5% V	10% V	15% V
1000	T + M	M + T*	M	M	M
800	T	T	M	M	M
600	T	T	T	T	T
400	A	A	A	A	A + T
140	A	A + C*	A + C	A + C	A + C

A = Amorphous; T = Tetragonal; M = Monoclinic; C Ammonium nitrate, * = trace

The crystalline structure at different weigh % of vanadium and calcine temperature was summarized in Table 4.7. V/ZrO_2 had a tetragonal phase and the mixture of the tetragonal and monoclinic phase at 600-1000 °C, respectively. However, in the case of vanadia in supported zirconia, the crystalline structures of sample were different from ZrO_2, which the phase transition changed higher by 200°C in $15V/ZrO_2$ than pure ZrO_2. The crystal size of V/ZrO_2 was summarized in Table 4.8.

Table 4.8 Summary on crystal size (nm) for V/ZrO_2

Temperature, °C	0% V	1% V	5% V	10% V	15% V
1000	[17.33]	[61.64]	[52.02]	[77.52]	[107.4]
	17.40	75.17			
800	12.57	13.71	[45.38]	[51.97]	[52.0]
600	9.87	10.80	10.55	10.54	16.77
400	-	-	-	-	10.56
140	-	-	-	-	-

Non parentheses: crystallite size of tetragonal phase

Parentheses: crystallite size of monoclinic phase

The effect of increasing temperature was proportion of zirconia crystal size. Furthermore, the elevated temperature caused phase transition corresponding to the result of infrared spectra. The above result was corresponding to sol-gel method [11], but opposite with impregnation method [12]. It is possibly to be a homogenous effect. However, effect of percentage vanadia content in zirconia support caused for increasing of crystallization of zirconia more than calcine temperature. This phenomenon explained the effect of interaction between vanadium and zirconia support.

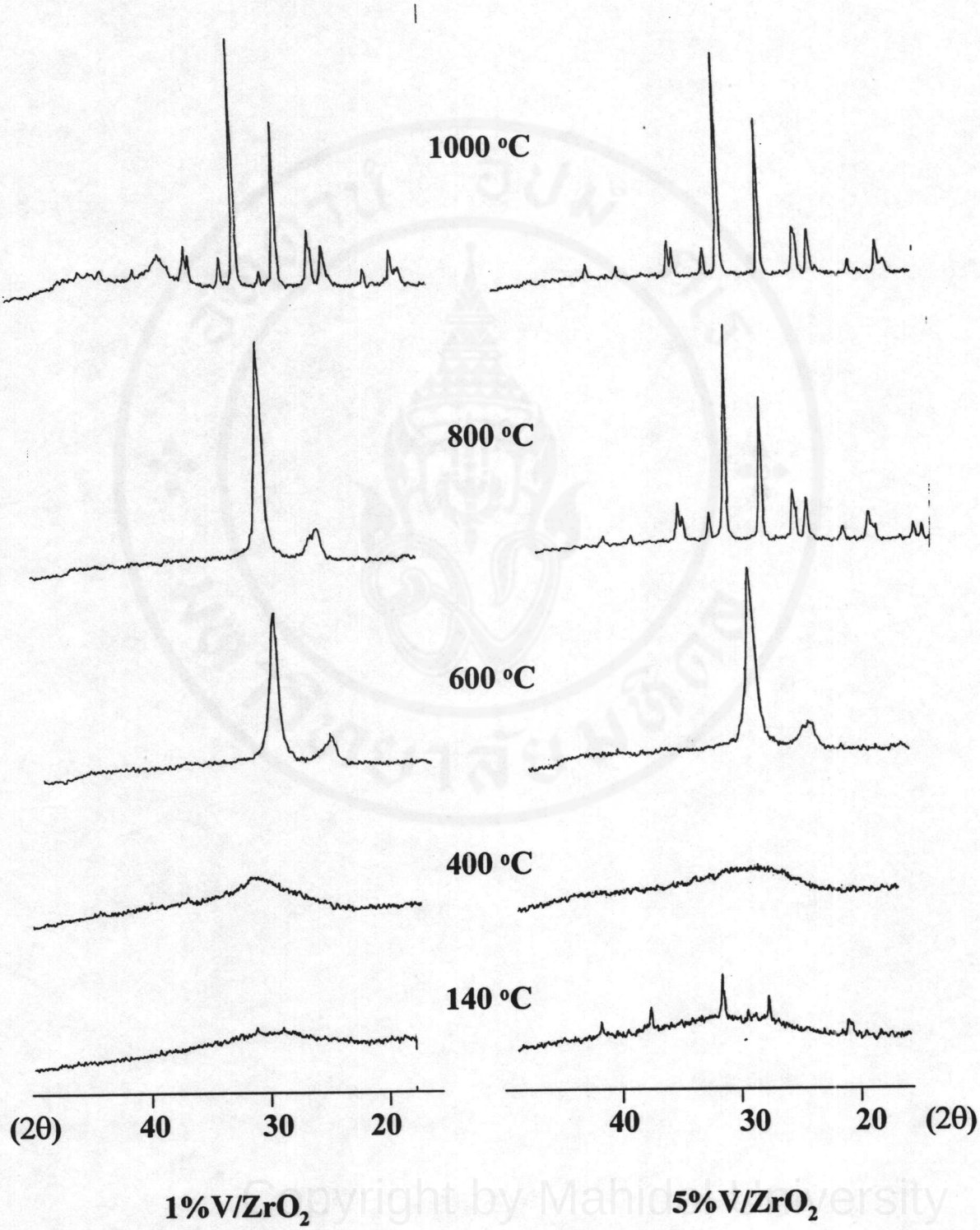

Figure 4.27 XRD patterns for ZrO_2 powder at different calcine temperatures.

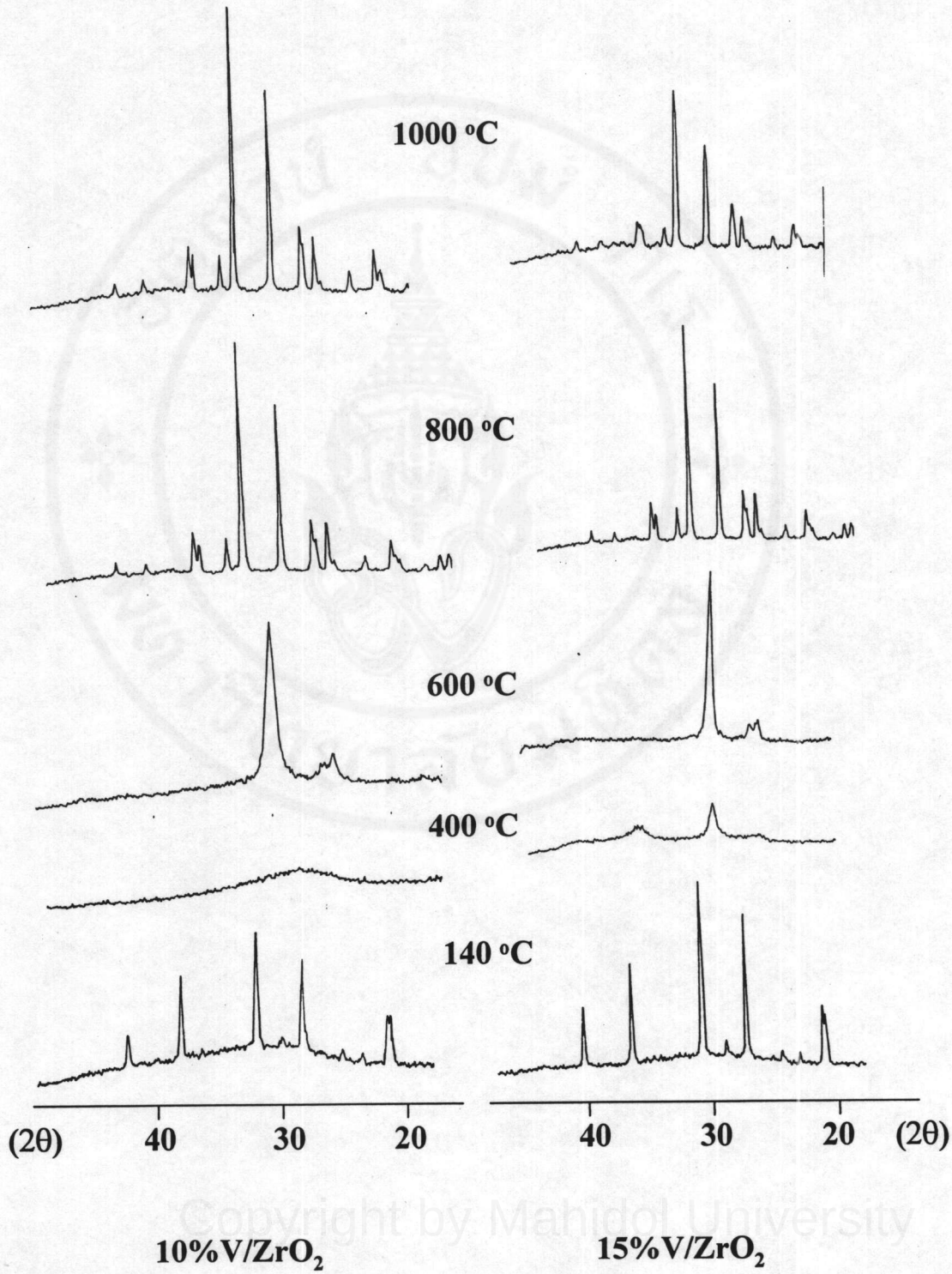

Figure 4.27 XRD patterns for ZrO_2 powder at different calcine temperatures.

(Continues)

The particles of ZrO_2 were the spherical shape, without vanadium content. However, the contained vanadium appeared polyhedron shape which vanadiun affected dissconstruct spherical shape. The needle crystal type on zirconia support appeared, when high vanadia content and calcine temperature increased as shown in Figure 4.28 and 4.29. This result was explained by Sohn et al. [12], due to vanadium oxide content excess on the surface of ZrO_2, and low dissolvable vanadia when high temperature. This effect could see distinctly at about 1000 and 800 cm^{-1} bands of infrared spectra.

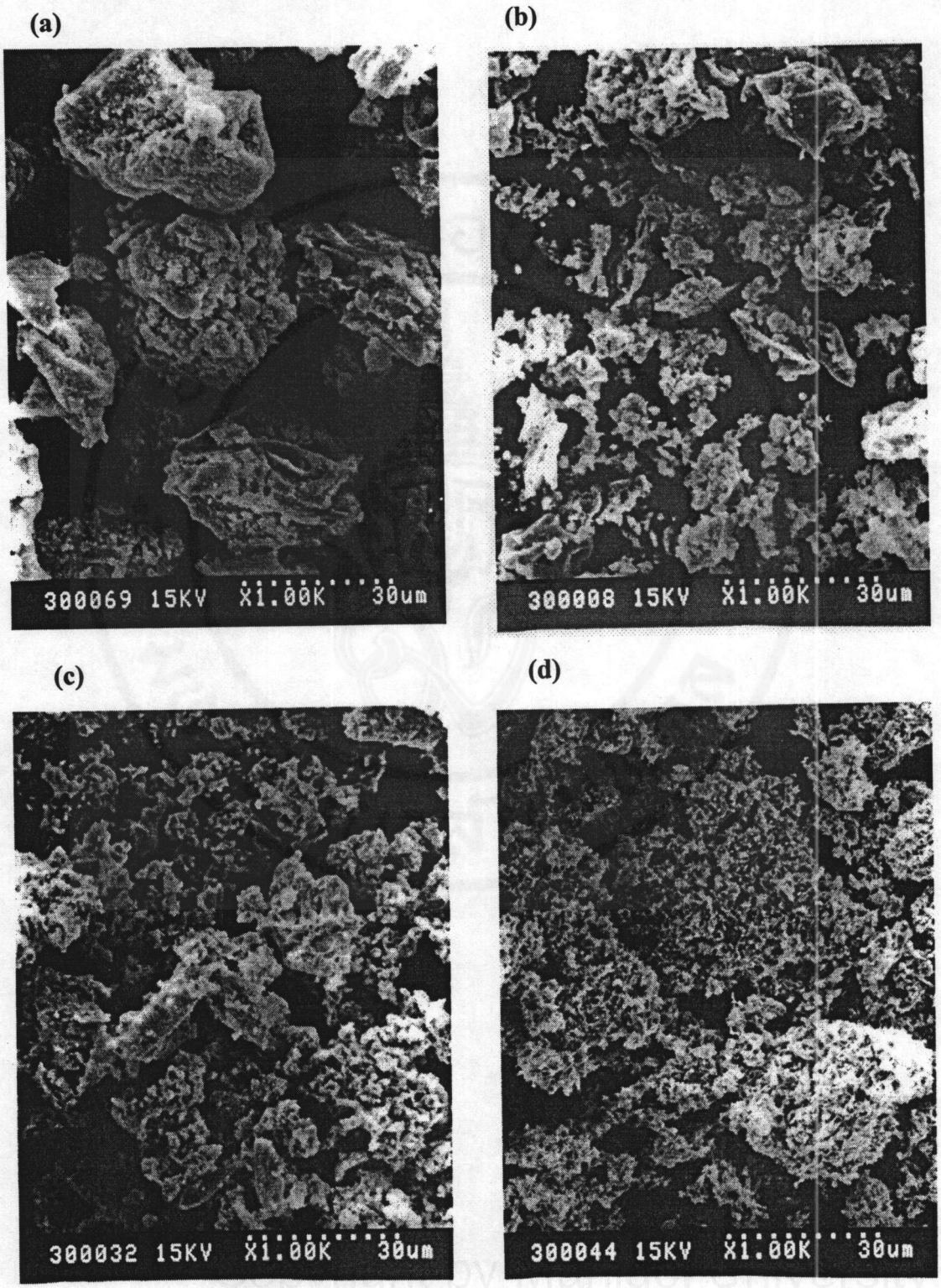

Figure 4.28 Scanning electron micrographs for 10V/ZrO_2 at different calcine temperatures(a) 400°C (b) 600°C (c) 800°C and (d) 1000°C

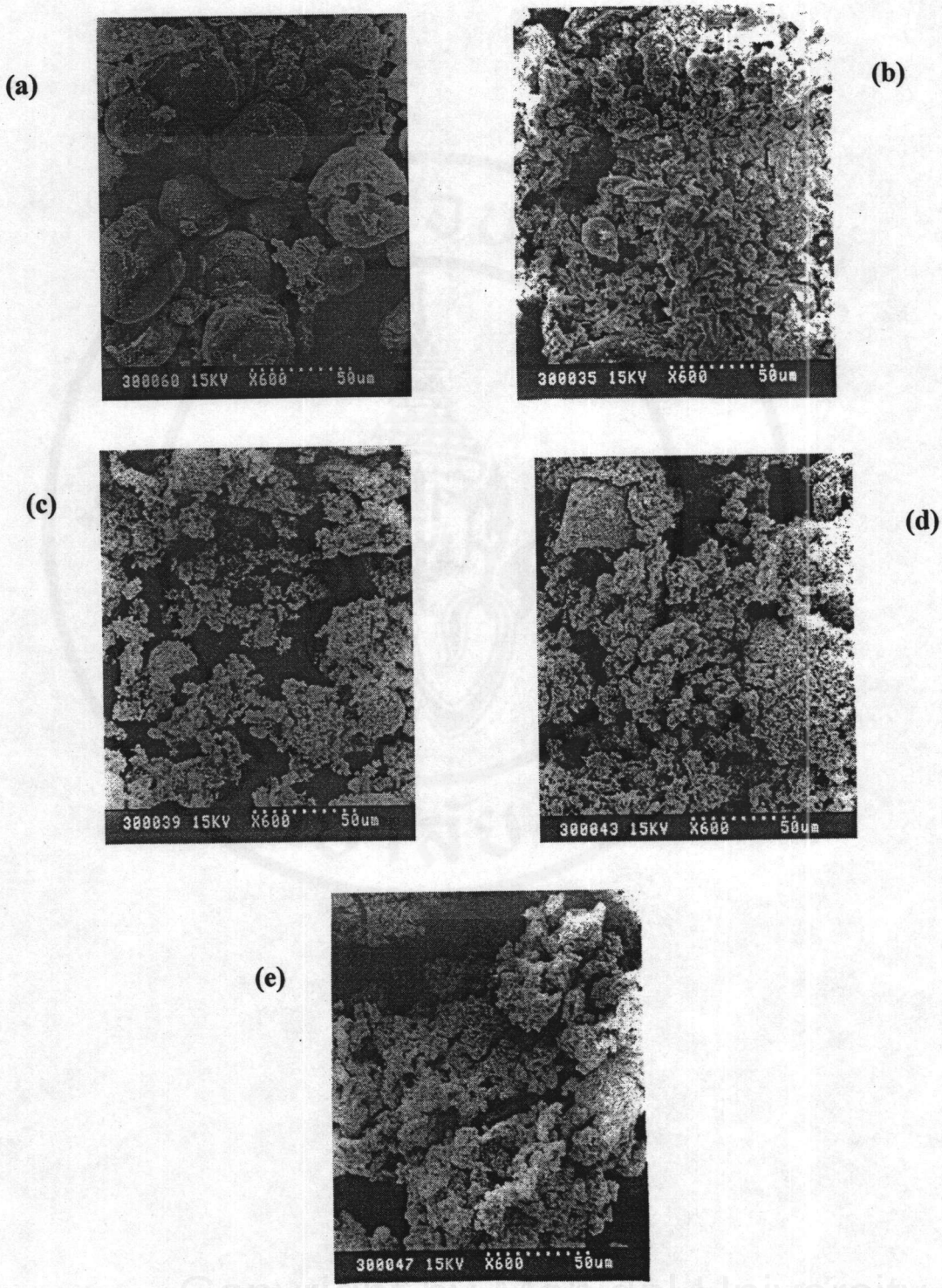

Figure 4.29 Scanning electron micrographs for V/ZrO_2 at 1000°C calcine temperature (a) 0%V (b) 1%V (c) 5%V (d) 10%V and (e) 15%V

4.5 Suggestion of Future Work

According to the results in thesis, many steps in Sol-Emulsion-Gel method could be modified for furthers studies such as

i) The less toxic and suitable solvents should replace for xylene.

ii) More careful and systematic studies on quantification of $NH_3(g)$ in reaction vessel should be preformed.

iii) Type of surfactant and method of agitation should be reconsiderd in relate to the designed ZrO_2 products.

iv) For the real applications, the zirconia products should be characterized in more details and tested for more specific applications.

CHAPTER V

CONCLUSION

The routes of ultrafine zirconia, ZrO2 and vanadium oxide supported zirconia, V/ZrO2 preparation can be summarized as the following: (1) The zircon mineral, Thai zircon sand was treated by alkali hydrolysis (2) zirconyl intermediate compounds namely, zirconyl hydroxide, zirconyl chloride and zirconyl nitrate were successfully prepared and characterized. (3) The SEG method has been developed for zirconia preparation by using ZNS as precursor. (4) The application of modified SEG method was demonstrated by the preparation of V/ZrO_2.

Zirconium raw material, zirconia and its related products were characterized by means of FT-IR, XRD, DSC, SEM and TEM techniques.

1. Thai zircon sand, raw material exhibited a ditetragonal dipyramid shape and its lattice parameters were a_0 = 6.6407 Å, c_0 = 6.1290Å. The distortion in crystal parameters, referred to the data from JCPDS was observed, due to impurity in nature zircon lattice or defect of crystal. These explanations were confirmed by qualitative ICP-MS results. The average crystal size was about 746 μm in length and 82 μm in width.

2. ZCS was prepared from Thai zircon and characterized by several techniques. ZCS was identified as $ZrOCl_2.6H_2O$. The morphology of ZCS crystal showed the needle form and crystal size was about 80 μm in length. By heat treatment water and HCl were eliminated and zirconia crystallization were found at about 467°C. ZNS was possibly $ZrO(NO_3)_2.2H_2O$ and was an agglomerate particle. Thermograms showed the loss of evaporate water and HNO_3 between 80 and 270 °C, and crystallization at about 474°C.

3. ZrO_2 was successfully obtained from ZNS precursor by SEG method. The phase transition, crystallization and morphology were investigated. Phase transition of zirconia shown existence amorphous at room temperature and transition to metastable tetragonal and monoclinic phases, when increasing calcine temperature. Existence of metastable caused by the effect of small particle and similarity of amorphous with tetragonal structure. A crystal size was increased with corresponding to the increment of calcine temperature. This phenomenon was explained that the elevate agglomerate of small particle to large particles, when higher temperature. From SEM and TEM results, a polyhedral or spherical shape of zirconia particle consists of an aggregate nanosize particle were notified. Effect of using ultrasonic agitator, losing agglomeration and less stability of zirconia were observed.

4. Modified SEG method by adding NH_4VO_3 in ZNS solution was applied for the preparation of V/ZrO_2. The influence of vanadium content and calcine temperatures were investigated. When temperature increased, phase of zirconia support transformed from amorphous phase, metastable tetragonal and finally

monoclinic, in similar manners as found for zirconia result. Anyhow, the early transition from tetragonal to monoclinic phase of doped zirconia was observed at lower temperature due to the increasing of vanadium contents. The crystallization of vanadium oxide exhibits its needle form on surface of zirconia at high temperature and vanadium content.

REFERENCES

1. MEL Chemicals Group, MELCHEMICAL NIKKEI-MEL;1999 Available from: http://www.zrchem.com [Accessed 1999 Dec 12]
2. Vincenzini P, editor. Fundamental of ceramic chasing. Cambridge: Elsever Applied Science; 1991.
3. Jastrzebski ZD. The nature and properties of engineers materials. 3rd ed. NY: John Wiley&Songs; 1987.
4. Chapter3 synthesis and processing of ferroelectric PZT powders, ceramic and films 1-18 Available from: http://www.fimg. bham.ac.uk/bosu/phd/3-1.htm. [Accessed 1999 Nov 10]
5. Data and statistics section, Technical and planning division, Department of mineral resources, Mineral Statistics of Thailand;1997-98.
6. MacDonald DJ, Guidotti RA, Henry FG, Method for producing zirconyl sulfate Solution from zircon sand, Bureau of mines, Report of investigations 8718.
7. Choi HS. Preparation of pure zirconyl compounds from zircon caustic frit. Transcations 1965;68:65-70.
8. Page CH, Bhattacharjee S, Thombare CH, Varadarajan V, Chatterjee AK. Experiences of extracting zirconia from Indian zircon sand and its Characterization; In: Bannister MJ, editor. Ceramics adding the value 2nd vol. Melboure: CSIRG; 1992. p.1166-72.

9. Siri-upathum K, Tasana-udom M, Srichom K, Sangariyavanich A. Caustic treatment of Thai zircon sand. OAEP technical report 1991:1-160.

10. Ramamurthi SD, Xu Z, Payne D. Nanometer size ZrO_2 particles prepared by a sol-emulsion-gel method. J Am Ceram Soc 1990;73(9):2760-63.

11. Rojas-Cervantes ML, Lopez-Peinado AJ, Lopez-Gonzaler JD, Carrasco-Marin F. Preparation of V/ZrO_2 catalysts by the sol-gel method: physical and structural characterization. J Mater Sci 1996;3:437-44.

12. Sohn JR, Cho SG, Pae YI, Hayashi S. Characterization of vanadium oxide-zirconia catalyst. J Catal 1996;159:170-7.

13. Lakshmi LJ, Ju Z, Alyea EC. Synthesis, Characterization, and activity studies of vanadium supported on zirconia and phosphorus-modified zirconia. Langmuir 1999;15:3521-8.

14. Scharf, U, Schraml-Marth M, Wokaun A. Comparison of vanadia species on ZrO_2, TiO_2, SiO_2 and TiO_2/SiO_2 mixed oxides. J Chem Soc Faraday Trans 1991;87(19):3299-307.

15. Su SC, Bell AT. A study of the structure of vanadium oxide dispersed on zirconia. J Phys Chem 1998;102:7000-7.

16. Blumenthal WB. The chemical behavior of zirconium. NY: D. van nostrand; 1958.

17. Heuer AH, Hobbs LW. Science and technology of zirconia: Advances in ceramics 3rd vol. Ohio: America Ceramic Society; 1981.

18. Tani E, Yoshimura M, Somiya S. Formation of ultrafine tetragonal ZrO_2 powder under hydrothermal conditions. J Am Ceram Soc 1983;66(1):11-4.

19. Garvie RC. The occurrence of metastable tetragonal zirconia as a crystallite size effect., J Phys Chem 1965;69(4):1238-43.

20. Livage J, Doi K, Mazieres C. Nature and Thermal evolution of amorphous hydrated zirconia oxide. J Am Ceram Soc 1968;51(6):349-52.

21. Osendi MI, Moya JS, Serna CJ, Soria J. Metastability of tetragonal zirconia Powders. J Am Ceram Soc 1985;68(3):135-9.

22. Garvie RC. Stabilization of the tetragonal structure in zirconia micrecrystals. J Phys Chem 1978;82(2):218-24.

23. Ruh R, Rockett TJ. Proposed phase diagram for the system ZrO_2, J Am Ceram Soc 1970;53:360.

24. Mitshuhashi T, Ichihara M, Tatsuka V. Characterization and stabilization of metastable tetragonal ZrO_2. J Am Ceram Soc 1974;57(2):97-101.

25. Mazdiyani KS, Lynch CT, Smith JS. Metastable transition of zirconium oxide obtained from decomposition of alkoxides. J Am Ceram Soc 1966; 49(5):286-7.

26. Phillippi CM, Maziyasni KS. Infrared and Raman spectra of zirconia polymorphs. J Am Ceram Soc 1971;54(5):254-8.

27. Hannink RHJ, Porter JR, Marshall DB. Direct observation of cycled phase transformation in zirconia, J Am Ceram Soc 1986:C-116-9.

28. Keramidas VG, White WA. Raman scattering study of the crystallization and phase transitions of ZrO_2. J Am Ceram Soc 1974;57(1):22-4.

29. Katz G. X-ray diffraction powder pattern of metastable cubic ZrO_2. J Am Ceram Soc 1971:531.

30. McCullough JD, Trueblood KN. The crystal structure of baddeleyite (Monoclinic ZrO_2). Acta Cryst 1959;12:507-11.

31. Duwez P, Odell F, Brown FH. Stabilization of zirconia with calcia and magnesia.

J Am Ceram Soc 1952;35(5):107-13.

32. Piconi C, Maccauro G. Zirconia as a ceramic biomaterial. Biomaterials 1999; 20:1-25.

33. Tani E, Yoshimura M, Somiya S. Hydrothermal preparation of ultrafine monoclinic ZrO_2 powder. J Am Ceram Soc 1981:C-181.

34. Somiya S, Yamamoto N, Yanagida H. Science and technology of zirconia III, Advances in ceramic 24A Vol. The American Ceramic Society, Ohio:201-9.

35. Takehiki S, Shigemi O, Norkazu A, Joachim R. Micronized zirconia and method for production thereof. European patent 85109875. Aur 6, 1985.

36. Gao L, Oiao HC, Qiu HB, Yan DS. Preparation of ultrafine zirconia powder by emulsion method. J Eurp Ceram Soc 1995:6:373-376.

37. Qiu HB, Gao L, Qiao HC, Guo JK, Yan DS. Nanocrystalline zirconia powder processing through innovative wet-chemical methods. Namostructureal Materials 1995;6:373-6.

38. Kanai T, Rhine WE, Bowen HK. Preparation of $2ZrO_2.Yb_2O_3$ by emulsion techniques. Ceramic powder science II: A Ceramic Transcation. 1st vol.: 119-26.

39. Lee MH, Tai CY, Lu CH. Synthesis of spherical zirconia by precipitation between two water/oil emulsions. J Eur Ceram Soc 1999:2593-2603.

40. Xie Y. Preparation of ultrafine zirconia particle. J Am Ceram Soc 1999; 82(3): 768-70.

41. Zhang SC, Messing GL, Borden M. Synthesis of solid, spherical zirconia particles by spray pyrolysis. J Am Ceram Soc 1990; 73(1): 61-7.

42. Lukasiewicz SJ. Spray-drying ceramic powder. J Am Ceram Soc 1989; 72(4): 617-24.

43. Feng Z, Postula WS, Akgerman A, Anthony RG. Characterization of zirconia-based catalysts prepared by precipitation, calcination, and modified sol-gel methods. Ind Eng Chem Res 1995;34:78-82.

44. Pavlik RS, Klein LC, McCauley RA. Zirconia gels in concentrated NaOH, J Am Ceram Soc 1995;78(1):221-24.

45. Rivas PC, Martinez JA, Caracoche MC, Garcia AL. Perturbed-angular- correlation study of zirconia produced by the sol-gel method. J Am Ceram Soc 1995;78(5):1329-34.

46. Ward DA, Ko EI. Use of preformed sols in the sol-gel preparation of Zirconia. Langmuir 1995;11:369-72.

47. Berry LG, Mrose ME, Post B, Weiggmann S, McMurdie HF, McClune WF, editors. Powder diffraction file. . Pensylvania: Joint Committee on Powder Diffraction Standards (JCPDS);1976.

48. Bahr LS, Johnston B, editors. Collier 's Encyclopedia vol. 23. NY: Macmillian Educatinal;1992,

49. Klein C, Hurlbut CS. Manual of mineralogy 20th ed. John Wiley&Songs

50. Syme RWG, Lockwood DJ, KerrHJ. Raman spectrum of synthetic zircon ($ZrSiO_4$) and thorite ($ThSiO_4$). J Phys C: Solid State Phys 1977;12: 1335-48.

51. Elyntin VP, Parlav YA, Leriv BE, Alekscer EM. Product of feroalloys 2nd ed. Jerusalem: SMONSON; 1961.

52. Lustman B, Frank Kerze JR, editors. The metallurgy of zirconium. Michigan:

Edwards Brothers; 1955.

53. Lepla M, Cockburn JG, Bird J, Thorpe 's dictornary of applied chemistry 4th ed. 1962.

54. .Linsen BG, Fortuir JMH, Okkerse C, Steggerder JJ. Physical and chemical aspects of adsorbents and catalysts.London;1970.

55. Cotton FA, Wilkinson G. Advanced inorganic chemistry 3rd ed. Taipei: John Wiley&Songs; 1974.

56. Kirk RE, Othmer DF, editors. Encyclopedia of chemical technology 15th vol. NY: Mack; 1956.

57. Wambach J, Baiker A, Wokaum A. CO_2 hydrogenation over metal/zirconia Catalysts. Phys Chem Chem Phys 1999;1:5071-80.

58. Belomestnykh P, Skrigan EA, Rozhdestvenkaya NN, Isagulyants GV. Formation of an active surface on oxide systems containing vanadium used for dehydrogenation of hydrocarbons in the presence of hydrogen acceptors. 439-42.

59. Sanati M, Andersson A, Wallenberg LR, Rebenstorf B. Zirconia-supported vanadium oxide catalysts for ammoxidation and oxidation of toluene: A characterization and activity study. Appl Catal A:General 1993;106: 51-72.

60. Bergen, Risbud. Introduction to phase equilibrium in ceramics. BER;16-8.

61. Readey MJ, Lee RR, Halloran JW, Heuer AH. Processing and sintering of ultrafine MgO-ZrO_2 and (MgO, Y_2O_3)-ZrO_2 powders. J Am Ceram Soc 1990:73(6); 499-503.

62. Heuer AH, Claussen N, Kriven WM, Ruhle M. Stability of tetragonal ZrO_2

particles in ceramic matrices. J Am Ceram Soc,1982:65(12);642-50.

63. Claussen N. Stree-induced transformation of tretragonal ZrO_2 particles in ceramic matrices. J Am Ceram Soc;61(1-2):85-6.

64. Kostorz G, editor. High-Tech ceramics viewpoints and perspectives. CA: Academic;1989.

65. Vincenzini P. Fundamentals of ceramic engineering. Cambridge: Elsevier Science;1991.

66. Jones RW. Fundamental principles of sol-gel technology. London: The Institute of Metals;1989.

67. McWhan DB, Lundgren G. The crystal structures of some zirconium hydroxide salt. Acta Cryst 1963;16:A36.

68. Chattopadhyay AK, Mittal KL, editors, Surfactants in solution: Surfactant science series 64th vol.. NY:Arcel Dekker; 1996.

69. Becher P. Emulsions: theory and practice 2nd ed. NY: Reinhold; 1957.

70. Stein HN, editor. The preparation of dispersions in liquids, surfactant science series 58th vol. NY: Arcel Dekker;1996.

71. Ichinose N, editor. Introduction to fine ceramics applications in engineering. England: John Wiley&Sons;1987.

72. Weast RC. Handbook of chemical and physical, 58th ed. Florida: CRC Press; 1977-8.

73. Clint JH. Surface aggregation, London: Blackie&songs;1992.

74. Bentley F, Smithson LD, Rozek AL. Infrared Spectra and characteristic frequencies ~700- ~300 cm^{-1}. USA: Wiley & Sons;1968.

75. . Powers DA, Gray HB. Characterization of the thermal dehydration of zirconia

oxide halide octahydrates. Inorg Chem1973;12(12):2721 –26.

76. Phillippi CM, Mazdiyani KS. Infrared and Raman spectra of zirconia polymorphs. J Am Ceram Soc 1971;54(5):254-8.

77. Alexandor LE. X-ray diffraction methods 2nd ed. USA: John Wiley&Sons; 1968.

78. Stefanic G, Music S, Grzeta B, Popovic S, Sekulic A. Influence of pH on the stability of low temperature t-ZrO_2. J Phys Chem Solids 1998;59[6-7]: 879-85 .

79. Weat AR. Solid state chemistry and its applications. Singapore: John Wiley & Songs; 1984.

80. Toraya H, Yashimwra M, Somiya S. Calibration curve for quantitative analysis of monoclinic-tetragonal ZrO_2 system by X-ray diffraction. J Am Ceram Soc: C-119.

81. Addision CC, Gatehouse BM. The infrared spectra of anhydrous transition- metal nitrates.1959:613-6.

82. Herman A, Szymanski, editor. Progress in infrared spectra 1st vol. Plenan;1961.

83. Field BO, Hardy CJ. Volatile and anhydrous nitrato-complexes of metals: Preparation by the use of dinitrogen pentoxide, and measurement of infrared spectra. 1963:4428-34

84. Wing M, Callahan KP. Characterization of metal-oxygen bridge systems, Inorg Chem 1969;(4):871-74.

85. Schugar HJ, Rossman GR, Barraclough CG, Gray HB. Electronic Structure of oxo-bridged iron(III) dimers. J Am Chem Soc 1972;94(8):2682-90.

86. Morrison RT, Boyd RD. Organic Chemistry 3rd ed. New Delhi: Prentice-Hall of India Private;1978.

87. Prinetto F, Ghiotti G, Occhiuzzi M, Indorina V. Characterization of oxidized surface phases on VO_x/ZrO_2 catalysts. J Phys Chem B 1998;102: 10316-25.

88. Hench LL, Gould EW. Characterization of ceramic NY: Marcel Dekker;1971.

89. Griffith WP. Raman studies on rock-forming minerals. Part II Orthosilicates and cyclosilicates. J Chem Soc (A) 1969;1372-77.

90. Dawson P, Hargreare MM, Wilkinson GR. The vibrational spectrum of zircon ($ZrSiO_4$). J Phys C: Solid Sate Phys 1971;4:240-56.

91. Clearfield A, Vaughan P. The Crystal Structure of zirconyl chloride octahydrate and zirconyl bromide octahydrate. Acta Cryst 1956;555-8.

92. Mak TC. Refinement of the crystal structure of zirconyl chloride octahydrate. Canadian J Chem 1968;46:3491-7.

93. Spasibenko TP, Goroshchchenko. Investigation of the hydrates of zirconium oxide chloride. Russ J Inorg Chem 1969;14(6):757-9.

94. Spasibenko TP, Kobycheva AS. Zirconium oxide chloride hydrates, Russ J Inorg Chem 1970;15(2):181-2.

BIOGRAHY

NANE Mr. Tanakorn Ratana

DATE OF BIRTH 29 June 1974

PLACE OF BIRTH Yala, Thailand

INSTITUTIONS ATTENDED

Prince of Songkla University, 1993 - 1996:

Bachelor of Science (1st class honor)

(Chemistry)

Mahidol University, 1997 - 1999:

Master of Science

(Applied Analytical and Inorganic Chemistry)

RESEARCH GRANT

Recipient of Development and Promotion of Science and Technology talent (DPST) project from The Institute for the Promotion of Teaching Science and Technology in the year 1997-1999.